NASA TECHNICAL TRANSLATION

NASA TT F-553

NASA TT F-553

LIGHT SCATTERING IN THE ATMOSPHERE, PART 2

by A. I. Ivanov, G. Sh. Livshits, V. Ye. Pavlov, B. T. Tashenov, and Ya. A. Teyfel'

"Nauka" Press, Alma Ata, 1968

NATIONAL AERONAUTICS AND SPACE ADMINISTRATION • WASHINGTON, D. C. • NOVEMBER 196

LIGHT SCATTERING IN THE ATMOSPHERE, PART 2

By A. I. Ivanov, G. Sh. Livshits, V. Ye. Pavlov,
B. T. Tashenov, and Ya. A. Teyfel'

Translation of "Rasseyaniye Sveta v Atmosfere, Chast' 2"
"Nauka" Press, Alma Ata, 1968

NATIONAL AERONAUTICS AND SPACE ADMINISTRATION

For sale by the Clearinghouse for Federal Scientific and Technical Information
Springfield, Virginia 22151 – CFSTI price $3.00

TABLE OF CONTENTS

Foreword 2

Chapter 1. THE DIRECT PROBLEM
1. Scattered Light of the Clear, Daytime Sky (review) 4
2. Results of Measurements 11
3. Comparison with Theory 14

Chapter 2. FUNDAMENTAL OPTICAL PARAMETERS OF THE ATMOSPHERE
1. Scattering Functions 31
2. Optical Thickness. Atmosphere Stability 46
3. Properties of the Aerosol Scattering Function, Interrelationship of Certain Parameters, and Pure Absorption in Aerosols 51

Chapter 3. THE POSSIBILITIES OF SOLVING THE REVERSE PROBLEM FROM OBSERVATIONS OF THE BRIGHTNESS AND POLARIZATION OF THE CLEAR, DAYTIME SKY
1. General Properties of the Atmosphere Aerosol 64
2. Light Scattering and the Atmosphere Aerosol 68
3. Deviations from the Theoretical Model 73
4. Results of Measurements at Small Angular Distances from the Sun 78
5. Brightness and Light Polarization of the Daytime Sky at Large Angular Distances from the Sun and the Size Distribution of the Atmosphere Aerosol 91

Conclusion 95

References 96

Appendix 101

FOREWORD

This paper is the second part of a monograph published in 1965 [33]. /3* The first book primarily contained the results of investigations of a straightforward problem—the determination of the radiation field of a realistic atmosphere. The investigative method and the results of a determination of the fundamental atmospheric optical parameters, presented in the first part, permitted formulating a question concerning a more rigorous solution of the direct problem and carrying out studies of the possibility of solving the reverse problem—the determination of the size spectrum of an atmosphere aerosol from observations of scattered light intensity and polarization.

The analysis of the solution of the direct problem is continued in the first chapter of the present monograph. Data from spectral observations of the sky brightness and polarization are presented; an attempt is made to interpret these data with the aid of present-day theoretical calculations.

The results of studies of the fundamental optical parameters are presented in the second chapter. The material presented is derived entirely from direct observational data.

The possibilities of solving the reverse problem—the determination of the aerosol spectrum from observations of sky light brightness and polarization—are analyzed in the third chapter, and the first results of these investigations are given.

This monograph describes the data from research conducted in the atmospheric optics department of the Astrophysical Institute, Academy of Science Kazakh SSR. Overall editing was performed by G. Sh. Livshits.

The authors wish to express their sincere gratitude of Professor G. V. Rozenberg for valuable critical comments made during the review of the manuscript.

*Numbers in the margin indicate pagination in the foreign text.

SYMBOLS USED FOR THE MOST FREQUENTLY ENCOUNTERED QUANTITIES

τ - vertical optical thickness of the atmosphere,

p - transmission coefficient,

P - degree of polarization,

B - sky brightness,

$f(\varphi)$ and $\mu(\varphi)$ - scattering indicatrices,

πS - spectral solar constant,

T - turbidity factor.

The quantities enumerated refer to monochromatic light. We omit, as a rule, the index λ (wavelength). The other indices, which appear when it is necessary to emphasize a difference between quantities being discussed, hav the following meanings:

1 - a quantity resulting from 1-st order scattering, /4

2 - a quantity resulting from multiple scattering,

q - a quantity resulting from light scattering from the earth,

n - a quantity resulting from pure absorption,

b - a "Bouguer" quantity,

R - a molecular ("Rayleigh") quantity,

D - an aerosol quantity,

h - a quantity related to haze.

Optical parameters of the polydisperse aerosol:

r - particle radius,

r_1 and r_2 - lower and upper radius limits of particles of the polydisperse aerosol,

ν^* - exponent in Junge's formula.

Angular quantities and atmosphere masses:

$Z_\odot$ - distance to sun, at zenith,

$m_\odot$ - atmosphere mass in sun direction,

Z - zenith distance to observed point of the sky,

m - atmosphere mass in direction of observed point of the sky,

φ - angular distance from sun (scattering angle).

LIGHT SCATTERING IN THE ATMOSPHERE. PART 2.

A. I. Ivanov, G. Sh. Livshits, V. Ye. Pavlov,
B. T. Tashenov, and Ya. A. Teyfel'

ABSTRACT: The results of spectrophotometric studies of the brightness and polarization of the daytime sky, the scattering function and other optical parameters of the atmosphere are contained in this monograph. Observations are compared with recent theoretical calculations. The paper is devoted to direct and indirect approaches to the problem of light scattering in the earth's atmosphere.

The monograph consists of three chapters. A review of work on sky brightness is given in Chapter 1; data from direct observations and the result of comparing these data with theory are presented. Methods are proposed for calculating sky brightness and polarization with aerosol microstructure and multiple scattering taken into account. Results of the calculations agree with the data from direct measurements, which have been made in the visual and ultraviolet spectral regions by various authors.

In Chapter 2 the results of measurements of the scattering functions, the angular and spectral dependence of these functions, data on their variations and interrelationship, as well as the results of studies of atmosphere stability and transmittance, scattering functions and optical thickness (total, aerosol and haze) are presented. Pure absorption in aerosols has been studied, and, on the basis of the established properties of the aerosol scattering function, a formula is derived that interrelates a number of parameters of the earth's atmosphere.

The reverse problem—determination of the aerosol spectrum from optical observations of the sky—is considered in Chapter 3. The results of investigations of the spectrum of the large particle size fraction of the aerosol are presented; the role of Aitken particles is evaluated; the deviations from theoretical models of an aerosol with a Junge distribution of particle sizes are shown. The fundamental difficulties in solving the reverse problem from observations of sky brightness at large angular distances from the sun are indicated.

This book is intended for meteorologists, astrophysicists, geophysicists and other specialists whose work involves problems of light scattering in the earth's atmosphere.

CHAPTER 1 /5

THE DIRECT PROBLEM

1. Scattered Light of the Clear, Daytime Sky (review)

The radiation of the daytime sky has attracted the attention of specialists in the most varied fields of science. Theoretical and experimental investigations, aimed at explaining the observed phenomena of sky brightness and polarization, from the beginning have fallen outside the realm of atmospheric optics problems and have led to development in other important directions, for example, spectroscopy, the study of light displacement and scattering by matter, etc.

In this brief review it is impossible to discuss, in detail, the history of the problem, as well as the effect of studies of daylight sky radiation on other fields of science, which have been covered in detail in, for example [1]. It is our purpose to consider studies of the clear daytime sky carried out in the last decade.

The brightness and polarization of the light of the cloudless daytime sky are determined by the scattering characteristics of solar rays in the earth's atmosphere and depend on many factors. In addition to the scattering of direct solar rays (1-st order scattering), multiple scattering and scattering of the radiation, reflected from the earth's surface, occur. The light is polarized during each elementary act of scattering, and as it propagates, the light is attenuated not only because of scattering but also because of absorption.

The atmosphere is spherical, and a plane model can only serve to approximate reality. The amount and direction of the light reflected from the earth depend on the photometric properties of the underlying surface. The character of the light scattering in the atmosphere is determined by its optically active medium, which consists of two basic components—gaseous and aerosol. The gaseous component is distinguished by the presence of absorption bands characteristic of water vapor molecules, ozone, oxygen and other constituents. The aerosol component is basically characterized by a pronounced scattering property. In view of this, a study of the aerosol is of primary interest. Variations of sky brightness are primarily associated with the variability of the aerosol component. The optical parameters of the aerosol are determined by the physical characteristics of its particles: their size, shape, structure, spatial orientation, refractive index. The atmosphere contains a polydisperse aerosol, and the /6
particle distribution acquires an important significance. The sky brightness, determined by all the above-mentioned parameters, varies as a function of the sun distance at zenith ($Z_\odot$), the zenith (Z) and angular (φ) distances of the observed point of the sky, the light wavelength (λ) and the energy distribution in the solar spectrum (the spectral solar constant πS_λ).

There is no exact theory that takes account of the factors enumerated above. Individual analyses are based on models that do not entirely represent all the actual properties of the atmosphere. Rayleigh [2] developed the first theory for the brightness and polarization of the cloudless, daytime sky. Its major deficiencies are well known: Rayleigh ignored multiple scattering and the effect of aerosols. As a result of the work of S. Chandrasekar [3], Z. Sekera [4] and

other authors, it was possible to solve the problem for a purely gaseous ("Rayleigh") atmosphere with multiple scattering taken into account. The tables of Chandrasekar and Elbert [5] and, in particular, of Coulson, Dave and Sekera [6], in which computations are given for a wide choice of parameters, can serve as some basis for interpreting the complex processes resulting from multiple scattering and light reflection from the underlying surface. The theoretical analyses, recently developed by Dave and other authors, are intended to take account of the effect of molecular anisotropy [7], light reflection from the underlying surface [8], pure absorption [9], etc.

Moreover, since the aerosol plays a significant role in the sky radiation, very serious attention has been given to studies of the optical properties of this very important atmosphere component ever since the theory of light scattering by large particles, developed by Love [10] and Mie [11], appeared. After electronic computers became available, calculations were made of the optical parameters of aerosol particles with different size, shape, refractive index and other physical properties. The results of investigations of light scattering by haze particles have been reported in the monographs of K. S. Shifrin [12] and Van de Hulst [13].

Of greatest interest are calculations of the optical parameters of a polydisperse aerosol. Tables [14], containing data for particles with a refractive index of $m = 1.5$ and with a Junge-type of size distribution: $\frac{dn}{d \lg r} = \frac{c}{r^{\nu^*}}$ (dn is the number of particles in the logarithm radius interval d lg r; c and ν^* are constants), have recently been published. More extensive computations, performed by K. S. Shifrin and I. L. Zel'manovich [15], should soon be published as four volumes of tables*. These volumes should contain calculations for a polydisperse aerosol with the diverse structure that is typical of the earth's atmosphere.

A number of papers have been devoted to studying the dependence of the optical parameters of a polydisperse aerosol on the refractive index [16, 17], pure absorption [18], the ratio between the coarse and fine particle fractions [16]. L. Foitzik has recently carried out calculations for the case of a Gaussian type of particle size distribution [19].

A rigorous theory must take account of a polydisperse aerosol as well as multiple scattering. The aerosol scattering function, unlike the Rayleigh, is drastically elongated "forward". In a theory, that accounts for multiple scattering, the effect of aerosols can be indicated by specifying an asymmetric scattering function. The most important work in this area has been done by V. A. Ambartsumyan [20], V. V. Sobolev [21] and Ye. S. Kuznetsov [22]. The theoretical analyses of these authors permit determining numerical solutions of the transport equation for the earth's atmosphere. The most complete data tables are contained in papers of the Institute of the Physics of the Atmosphere [IFA], Academy of Science, USSR [23, 24] and also in [25]. V. V. Sobolev and co-workers investigated light scattering for a spherical atmosphere [26]. /7

*The first volume has been published [15].

At the present time some authors are using the following method of calculation. First order scattering is computed separately for different models of a polydisperse aerosol. Multiple and Rayleigh scattering is determined with the aid of the analyses of Coulson, Dave and Sekera [6], performed for a Rayleigh atmosphere. By summing the components, one can find an approximate value not only for the total brightness but also the degree of sky polarization and can ascertain the effects due to multiple scattering. A series of recently published papers have been devoted to these questions [27, 28].

The qualitative picture of the brightness distribution over a cloudless daytime sky is well known. In the visible region, the brightness is observed to increase from zenith to horizon and as one approaches the sun. Quantitative measurements were begun in the XVII century by Saussure, and systematic observations —in 1898 by Ch. Jensen [29]. Dorno [30], who made brightness and polarization observations over a period of several years, contributed a great deal. In spite of the fact that nearly fifty years have passed since then, Dorno's measurements are still used in textbooks. A large amount of similar work was frequently not interpreted at all. By citing only the results of brightness observations, and in particular—day skylight, many authors limited themselves to a description of this model or that, without any attempts to provide a general picture. Only a few investigations were an exception. The paper of V.A. Krat [31], published in 1946, is of particular interest. Devoted to the problem of the visibility of ground features from an airplane, it contains a large number of direct observations and theoretical results concerning the optical properties of the atmosphere.

In 1957, Ye. V. Pyaskovskaya-Fesenkova published a monograph devoted entirely to the brightness of the daytime, cloudless sky [32]. The result of this work is the derivation of a large number of relationships for the scattering of light. It was established that the optical properties of the earth's atmosphere often possess astonishing stability under the widest variety of conditions and are amenable to reliable interpertation. Eight years later, the first part of the present monograph was published [33], and it was also devoted entirely to sky brightness. Both works were done at the Astrophysics Institute AN KazSSR (AFI) in the atmospheric optics department where sky brightness and polarization observations have been carried out for about 20 years. The works of other authors, associated with studies of the clear daytime sky, were published in the form of papers dealing only with particular aspects of the problem, or were discussed in individual chapters of monographs devoted to radiative [34], twilight [55] and other investigations, and also to the optical properties of the atmosphere layer near the ground [92]. /8

More and more interest in direct observations of the sky brightness and polarization is evident each year. In addition to the studies carried out up to the present time at the AFI, which were mentioned above, measurements of the scattered light intensity are included in the program of complex investigations of the radiation field being carried on at the Leningrad State University [36, 37]. In the USA, a group of visibility laboratory researchers are making systematic measurements of the background brightness of natural objects (in particular, sky brightness) under different illumination conditions [38]. Photometric measurements of the daytime sky have covered a wide variety of locales,

including India [39], Africa [40] and other geographical areas. Recently these observations have aimed at verifying theory and at solving the reverse problem—the determination of the size distribution of aerosols; this will be discussed in detail below.

A large number of sky brightness observations have been performed in the solar almucantar. The brightness indicatrices, obtained in this region of the sky $\mu(\varphi)$, permit determining the scattering functions relating to the entire atmosphere height [32, 33, 41]. The mean relative indicatrices, determined in the visual and in the near infrared regions of the spectrum, are shown in Fig. 1. Some numerical data were presented in Part 1 of this monograph [33].

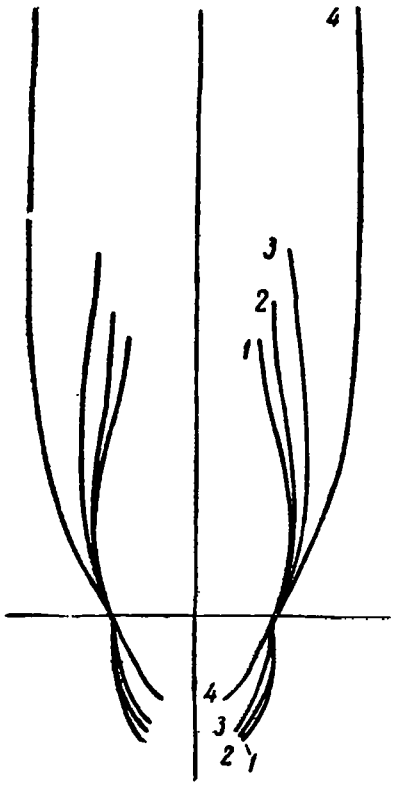

Figure 1. Average Relative Brightness Indicatrices: 1—λ= 0.476 μm; 2—λ = 0.546 μm; 3—λ = 0.625 μm; 4—λ = 0.940 μm.

The indicatrix $\mu(\varphi)$, derived from data of the sky brightness observations in the solar almucantar, is weighted with secondary effects. At the present time, however, a number of methods exist for isolating the scattering indicatrix $\mu_1(\varphi)$, excluding the effect of multiple scattering and of light reflection from the underlying surface. The function $\mu_1(\varphi)$ characterizes the scattering power of the entire atmosphere thickness as a whole [32, 33]. We note that since the lower layers of the atmosphere make the largest contribution to the sky brightness, the aerosol function $\mu_D(\varphi)$ gives the characteristic of an aerosol distributed up to an altitude of 5.6 km. The elongation of the indicatrix can vary appreciably, both from day to day as well as during a given day, with the degree of asymmetry increasing with an increase in wavelength. Several authors [32, 42] have directed their attention to the inconsistency between this fact and theoretical results. Thus, all calculations for Junge aerosol models lead to the conclusion that the elongation of the indicatrix should decrease with an increase in wavelength. This discrepancy, however, is only an apparent one. Observed indicatrices $\mu(\varphi)$ are influenced by Rayleigh and multiple scattering, which increase drastically at shorter wavelengths, so that the backward portion of the indicatrix increases. As will be shown below (Chapter 2 of this paper), observations at small scattering angles agree with the results of theoretical analyses.

To illustrate the order of magnitude of the sky brightness and its variation as a function of one factor or another, let us cite some numbers [34]. In summertime for an optical thickness of about 0.15, the sky brightness at $Z_\odot = 60°$ /9

and $\varphi=60°$, expressed in units of $S_\lambda/2$ (πS_λ is the solar constant), is equal to $\sim$0.15. With an increase in τ, the brightness, in a first approximation, increases approximately proportional to $_1\tau$ and its variation with wavelength is determined by the dependence of the optical thickness on λ. The brightness increases with a decrease in φ and when $\varphi\approx2°$ it can be two or more orders of magnitude greater than at $\varphi=60°$. For angles $\varphi>60°$ the sky brightness decreases smoothly up to angles of $\varphi=90-110°$. A minimum is observed in this interval, and then a small increase in brightness is frequently observed with an increase in φ. The general representation of the angular distribution gives the brightness indicatrix (see Chapter 2). The brightness increase from zenith of horizon usually does not exceed one order of magnitude. With a change in the sun zenith distance from $Z_\odot=30°$ and $Z_\odot=75°$, the sky brightness in the visible region at zenith decreases by about a factor of 2. Table 1, which contains data on the sky brightness for different parameters, is provided for orientation and to illustrate the order of magnitude. (More detailed data both for the visible as well as for the ultraviolet spectral regions are presented in the following paragraphs.)

It should be noted that until now very few direct measurements have been made at different altitudes in the free atmosphere. Investigations (see bibliography of [24]), previously carried out, were sporadic in nature and have largely become obsolete. New data, measured from aircraft [44], rockets [45] and from satellites [46], indicate the vast role played by the aerosol. The importance of such measurements is clearly obvious. Thus, even the few results of measurements, made recently, forced us to reject some incorrect ideas, concerning, in particular, the relative increase in Rayleigh scattering in the upper layers of the atmosphere.

Numerous observations of sky polarization have made it possible to establish a number of fundamental relationships and to recognize some points with characteristic polarization properties. The degree of polarization varies from zero (in particular, the neutral points of Arago, Brewster, Babinet) to a maximum, amounting to nearly 90% in individual cases. The attention to many authors was focused on these special (with respect to polarization) points. It has been established that the location of the Babinet and Brewster neutral points, relative to the sun, varies within the limits from 12 to 30°, depending on the wavelength and meteorological conditions. Sometimes a deviation of the neutral points from the solar vertical was observed [29, 47, 48]. The polarization maximum lies in the solar vertical at an angle distance of about 90° from the sun. Its location shifts by 3—5°, depending on various conditions. The relation of the polarization to the transmittance and the albedo of the underlying surface has been mentioned. The last factor exerts a particularly strong influence. Horizontal inhomogeneity of the underlying surface can lead not only to a change in the degree of polarization but also to a rotation of the polarization plane [49].

The number of polarization measurements has increased drastically in recent years. They have been made in regions with vastly different climatic conditions: in Germany, southern Italy, Greenland. The results of these measurements are discussed in [50]. G. V. Rozenberg and co-workers [51, 52], Ye. V. Pyaskovskaya-Fesenkova [53-56], D. G. Stamov [57] and others have investigated sky polarization and the relation of the observed polarization (both its degree and its plane of orientation) to different factors. The basic features of the polarization pattern of the sky have been described in considerable detail

(see, for example, [35, 58]), and there is no reason to repeat them here. Let us only note the following: in spite of the fact that polarization studies were begun 150 years ago, after Arago's discovery, new effects are still being detected through direct observations. This can be illustrated by the data obtained quite recently [59]. They indicate that up to now a false notion existed concerning the presence of one point with maximum polarization, located in the solar vertical. /10

Speaking of polarization measurements, the attempts to detect elliptical polarization should be noted. Daytime skylight was found to be elliptically unpolarized, within the limits of experimental error [52, 60]. Thus, in order to characterize the radiation field of the daytime sky it is sufficient to specify the the three Stokes parameters [1], characterizing the intensity, degree and position of the polarization plane.

Obviously, the value of investigations and conclusions based solely on observational data, is extremely limited. More significant results were obtained through the joint use of observations and theory.

Comparison of theory with observations is not a simple problem, and frequently the comparison attempts do not withstand critical review. In view of this, different methods have come to be used, which enable one to exclude the effect of one or another factor that is difficult to take into account. For a satisfactory agreement with observations, it is sufficient to introduce into the theory the actual values of the following four quantities: 1) total optical thickness, 2) scattering function, 3) albedo of the underlying surface, 4) optical thickness for pure absorption [33].

An analysis of the observations on the basis of theoretical calculations led to a clarification of the role of the major factors determining the character of light scattering in the atmosphere and made it possible find methods for taking them into account. It has been established that tha altitude variation of the scattering function cannot be taken into account in the solar almucantar. Sky brightness is determined by the integrated indicatrix, relating to the entire thickness, independently of the altitude distribution of localized scattering functions [33]. The earth's curvature can be taken into account by replacing the secants of the zenith distances in the sky brightness formula with the atmosphere masses [32]. The brightness, produced by multiple scattering for a spherical earth, can be calculated with satisfactory accuracy from a plane model. Secondary fluorescent radiation plays a minor role. Attempts to detect the effect by comparing the daytime and lunar sky showed that this radiation, if it exists, cannot exceed 5-6% [33]. D. Nokson and R. Goody [61], using a more precise and original method, detected a fluorescent radiation amounting to 2-3% of the total sky brightness.

Calculations of sky brightness, made for different models, distinguished by different aerosol composition, are analyzed in [62]; and the effect of multiple scattering is discussed. Just as one should expect, the greater the number of coarse particles in the polydisperse aerosol composition, the greater the angular intensity gradient, especially at small angular distances from the sun. The role of multiple scattering increases with a decrease in the solar altitude, an increase in the angular distance from the sun, a decrease in wavelength and an increase in the number of fine particles. Multiple scattering, even with an albedo equal to zero, can sometimes double the sky brightness value produced by 1-st order scattering.

Molecular and multiple scattering, as a rule, play the biggest role in the ultraviolet region on a clear day. The aerosol exerts an effect only at extremely small angular distances from the sun. /11

The aerosol plays the biggest scattering role in the very near infarared region [33]; a significant absorption of radiation by water vapor is observed. In the transmission windows in the IR region one can confine himself to a first-order calculation of the purely aerosol scattering for a very crude correction factor, making it possible to take multiple effects into account. However, the appreciable contribution of reflected radiation must be taken into account. In the water vapor absorption bands the sky brightness decreases sharply. There are few data from direct observations in this spectral region [63]. Of the theoretical investigations, one can recommend [15], and of the reviews—[65].

In addition to studying the scattered light intensity, considerable continuing attention has been devoted to theoretical and experimental polarization studies. Of most interest in the question concerning the connection between the polarization characteristics of the sky and the atmosphere aerosol. First, I. Soret [66], and then F. Ahlgrimm [67] and J.J. Tichanowsky [68], showed how important it is to take account of multiple scattering. After formulation of the transport equation into matrix form [3, 69] and appropriate calculations [5, 6], it became clear that multiple scattering and light reflection from the underlying surface play a tremendous role.

However, there is not doubt whatsoever that the polarization varies with variations in the aerosol. Several authors have observed a correlation between the degree of polarization and the atmosphere transmittance ([35, 70] and others). Finally, attempts are still continuing to determine the aerosol distribution from data of measurements of the degree of polarization [71, 72].

Of interest is the attempt of T. Gehrels [73] to determine the role of the different components of scattered radiation in the polarization pattern of the sky. Comparing theory with observations, T. Gehrels concluded that the departure from 100% maximum polarization, which can be expected with simple Rayleigh scattering, is caused by polarization produced by multiple scattering (6%), by molecular anisotropy (6%), by light reflection from the earth's surface (5%) and by the aerosol (8%). These numbers, relating to a somewhat special case, are obviously approximate.

In spite of the large number of measurements, thus far there is an insufficient amount of direct observational data to permit a detailed analysis of the question of solving the reverse problem in different spectral regions (in particular, in the ultraviolet), expecially in terms of the sky polarization characteristics.

2. Results of Measurements

We will present the results of direct measurements of the sky spectral brightness, made at the Astrophysics Institute AN KazSSR (AFI). They can be used in those problems where knowledge of the daytime cloudless sky background is required. The inadequacy of such brightness measurements in absolute units with the simultaneous determination of the optical thickness—one

of the fundamental optical parameters of the atmosphere—has been indicated in the review section. Performing such studies had the following purpose:

1. To provide tables of the absolute brightness at different points of the sky for an isophot plot, determining the actual value of the optical thickness. /12

2. To perform detailed spectral measurements of the sky brightness at small angular distances from the sun, where brightness variations are especially large.

3. To develop basic relationships in the observed sky brightness pattern.

4. To compare observational data with theory in order to answer the question concerning the possibility of satisfactorily solving the direct problem both for the brightness and the polarization of the daytime sky.

Measurements in the visible portion of the spectrum were made at intervals of $\Delta\Psi=45°$ (Ψ is the azimuth angle, measured from the solar vertical) and vertical intervals of $\Delta Z=15°$ for the following wavelengths: $\lambda=$ 0.691, 0.650, 0.593, 0.553, 0.495, 0.447, and 0.404 μm.

The formula for determining the brightness value has the form

$$B_\lambda = \frac{n_0}{n_s}\frac{A_\lambda}{\pi}\pi S_{0\lambda}\, p_\lambda^{m_\odot}\frac{r_0^2}{r^2}, \qquad (1.1)$$

where B_λ - spectral sky brightness in W/cm^2-sterad-μm;

n_0 and n_s - instrument readings from the sky point being observed and from the screen, respectively;

A_λ - spectral albedo of gypsum screen;

$\pi S_{0\lambda}$ - spectral solar constant, taken from the data of [77];

p_λ - spectral transmittance of the atmosphere;

$m_\odot$ - atmosphere mass in direction toward sun;

$\frac{r_0^2}{r^2}$ - correction term that takes account of the seasonal variation of the distance of the earth from the sun.

Table 1, a, b is provided as an example, illustrating the sky brightness value. The brightnesses for only half the sky are given in the table since they were symmetrical with respect to the solar vertical (except for the large zenith distances of $Z=75°$, where the inhomogeneity of the underlying surface probably exerted an influence). /13

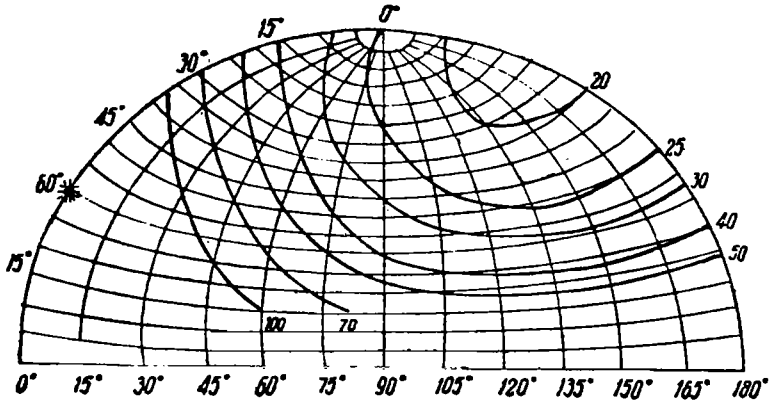

Figure 2. Observed Isophots of Clear Daytime Sky for $z_{\odot} = 61°$, $\lambda = 0.553\,\mu m$, $p_b = 0.82$, $q = 0.2$ (Aug. 27, 1965, a.m.). The Values Plotted are B(W/cm^2-sterad-μm) x 10^4.

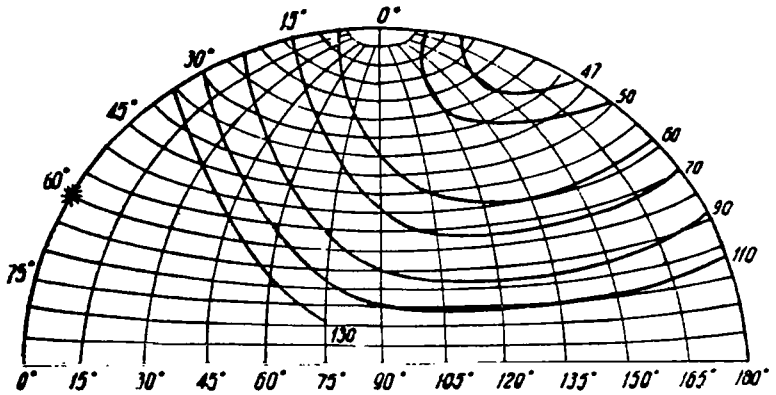

Figure 3. Observed Isophots of Clear Daytime Sky for $z_{\odot} = 58.7°$, $p_b = 0.66 \pm 0.01$, $\lambda = 0.404\,\mu m$, $q = 0.1$ (Aug. 27, 1965, a.m.). The Values Plotted are B (W/cm^2-sterad-μm) x 10^4.

Typical behavior of the brightness in different almucantars and verticals is shown in Figs. 2 and 3. A brightness increase with an increase in Z (from zenith to the horizon) and a brightness decrease with an increase in the azimuth angle Ψ (as one goes away from the sun) are observed. In the individual curves one can observe a brightness minimum that is caused by the specific form of the scattering function (minimum scattering in the directions $\varphi \approx 90°$). Theoretical analyses also yield the same brightness behavior [23, 24].

The angular distances Δ between the minimum brightness point and the sun and the zenith distances Z of this point are listed in Table I for different $z_{\odot}$ and λ.

TABLE I. Location of Minimum Brightness Points

27. VIII 1965, a. m.				14. IX 1965, a. m.				16. VIII 1965, a. m.			
$Z^\circ_\odot$	Δ°	Z°	λ (μm)	$Z^\circ_\odot$	Δ°	Z°	λ (μm)	$Z^\circ_\odot$	Δ°	Z°	λ (μm)
72,5	85	12,5	0.404	72,4	87,4	15,0	0.447	67,1	82,1	15,0	0.404
65,8	86	20,2	»	65,7	82,2	16,5	»	59,6	81,6	22,0	»
58,7	81	22,3	»	56,1	81,1	25,0	»	48,7	75,7	27,0	»
78,0	93	20,0	0.691	76,6	92,0	15,4	0.691	72,5	92,5	20,0	0.691
70,4	95	20,6	»	69,6	89,0	19,4	»	62,1	87,1	25,0	»
63,3	90	26,7	»	60,0	85,0	25,0	»	54,2	84,2	30,0	»

Note: Commas represent decimal points.

From the table it is seen that:

1. The distance between the minimum brightness point and the sun varies within the interval from 76—98°.

2. As the sun rises, Δ decreases and Z (the zenith distance for the minimum brightness point) increases, i.e., the point "sets."

3. The quantity Δ changes as a function of λ. The greater λ, the greater Δ.

Observations in the ultraviolet region were made with an electrophotometer with a silver light filter and an FEU-27 photomultiplier (Fig. 4). Brightness measurement data in absolute units are listed in Table 1. It should be noted that because of multiple scattering, which comes to play a dominant role in the total sky brightness in the UV-region in comparison with the primary event, the isophots become even more symmetrical with respect to the scattering angle $\varphi = 90°$. /14

Special attention has been given to the region of small angular distances from the sun. Separate observations were made of the sky spectral brightness (visible region) at scattering angles of $\varphi = 2, 4, 6, 8$ to 10°. Figure 5 illustrates an example of typical isophots. Listed in Table 2, a, b are measurement data for several days in units of 10^{-3} cal-cm^{-2}-min^{-1}-μm^{-1} for different sun positions and different values of the turbidity factor.

3. Comparison with Theory /17

In the first part of this work [33], a comparison was made between the results of observations and theory, and it was shown which of the principal parameters must be taken into consideration for a satisfactory agreement between theory and observations. Having more complete direct observational data, one can attempt to interpret the basic relationships and characteristics of the details in the brightness distribution over the sky, and can then proceed to an analysis of the more subtle effects, for example, the effect of polarization of scattered light, and can also ascertain the possibility of solving the direct problem with respect to the polarization characteristics of the radiation field.

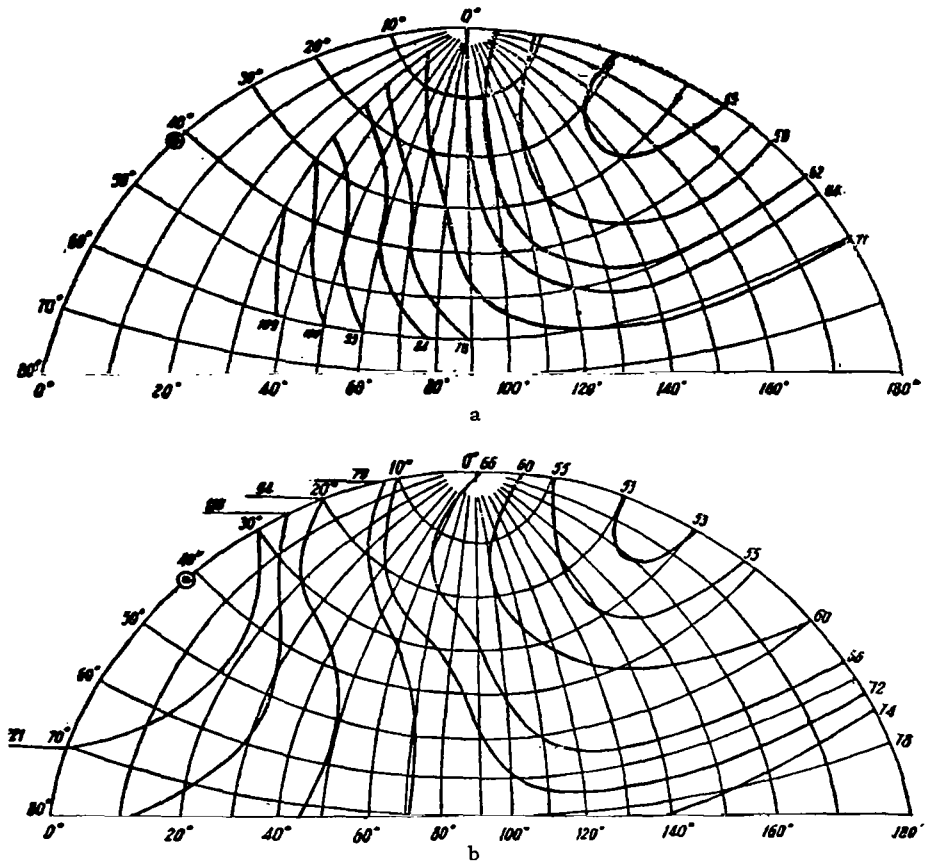

Figure 4. Observed Isophots of Daytime Sky in 0.34 μm Spectral Region for $Z_{\odot} = 41°$: a) June 12, 1964, a.m., $p_b = 0.48$; b) July 30, 1965, a.m., $p_b = 0.49$. The Values Plotted are B (W/cm^2-sterad-μm) x 10^4.

Some of the disagreement of observations with theory and certain errors in the latter are revealed in such a detailed comparison. Thus, the increase of Δ with an increase in λ, established from sky brightness observations (see also [78]), does not agree with data from theoretical analyses [23, 24], which can be explained by the fact that more symmetrical indicatrices are employed in them for the smaller optical thickness values (which corresponds to an increase in wavelength).

From the results, listed in Table 1a, one can trace the variation of the sky color. Listed in Table II are the ratios B ($\tau = 0.4$): B ($\tau = 0.2$) for $Z_{\odot} = 60°$, obtained from our observations (a), from the data of [33] (b), and from [23, 24] (c).

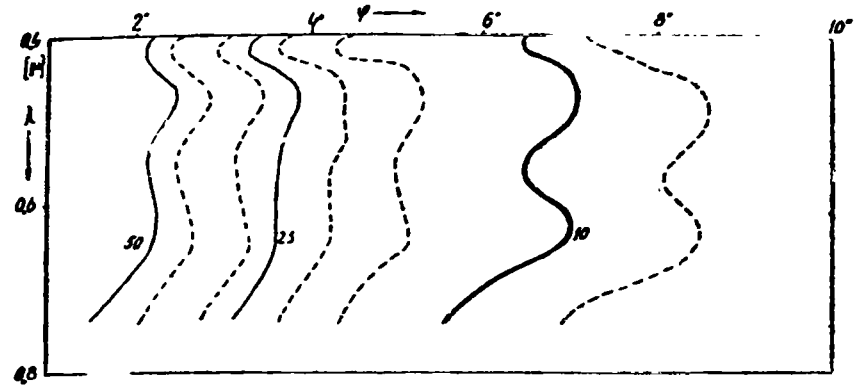

a

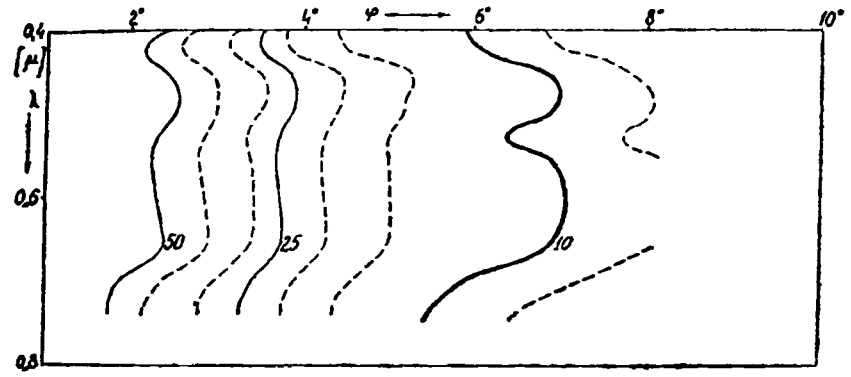

b

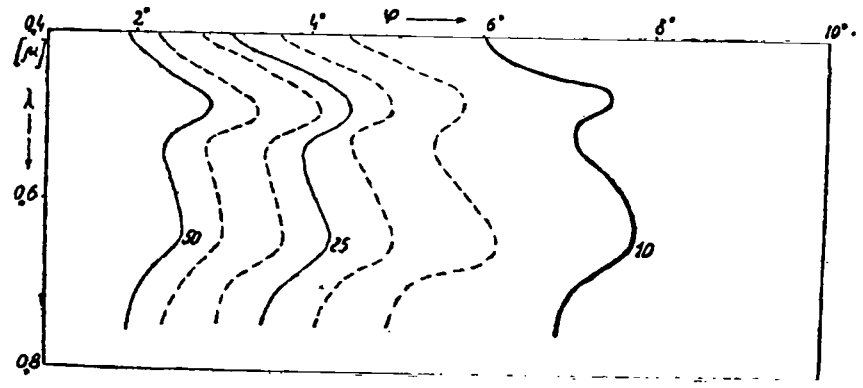

c

Figure 5. Isophots of Daytime Sky in Solar Almucantar at Small φ: Data From Autumn-Summer Observations (a, b, c).

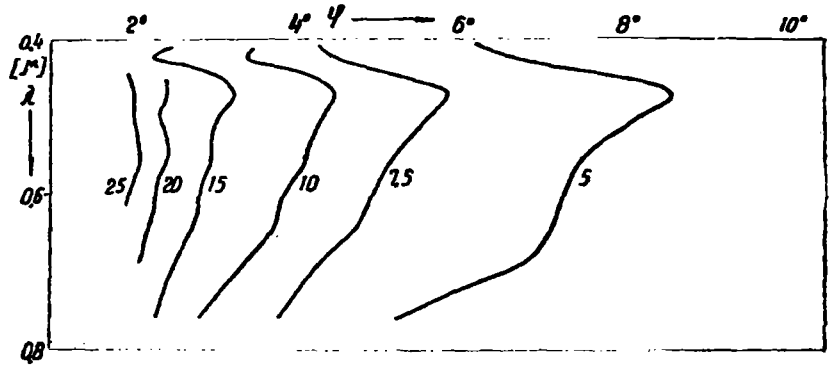

d

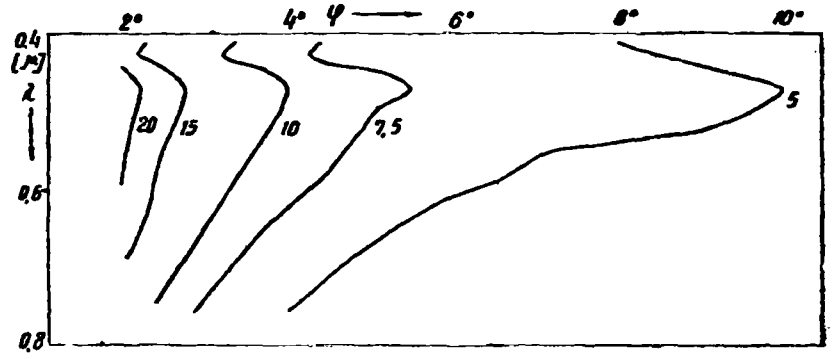

e

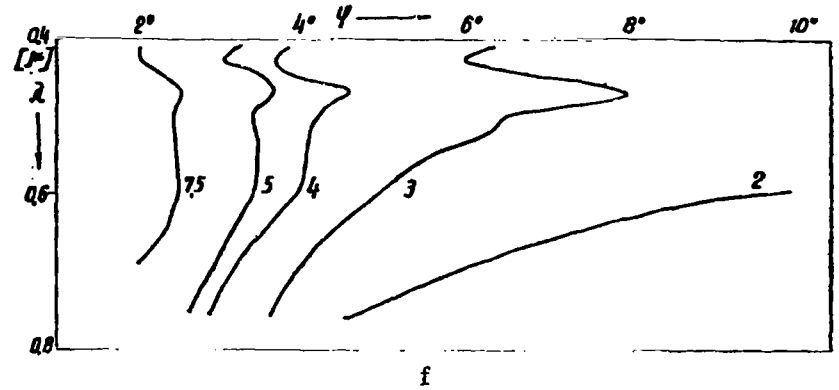

f

Figure 5. Isophots of Daytime Sky in Solar Almucantar at Small φ: Data From Winter Observations (d, e, f).

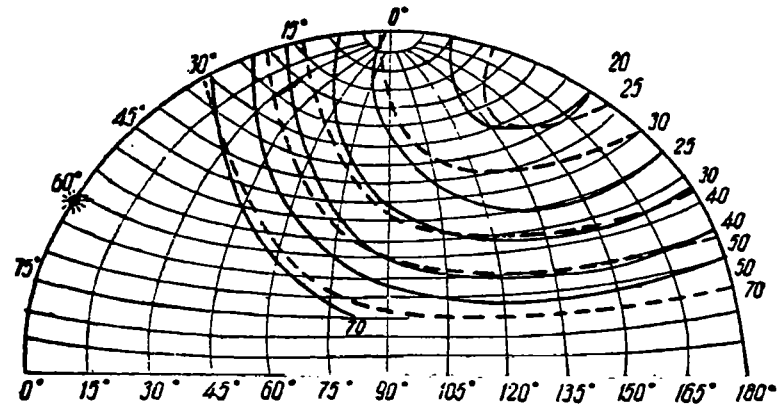

Figure 6. Observed (solid lines) Isophots of Clear Daytime Sky for $z_{\odot}=61°$, $\lambda=0.553$ μm, $p_b = 0.82$, $q = 0.2$ (Aug. 27, 1965, a.m.) and Theoretical (dashed) for $z_{\odot}=60°$, $\tau= 0.20$, $q = 0.2$, Indicatrix VI, Without Radiation Absorption by Ozone. The Values Plotted are B (W/cm^2-sterad-μm) x 10^4.

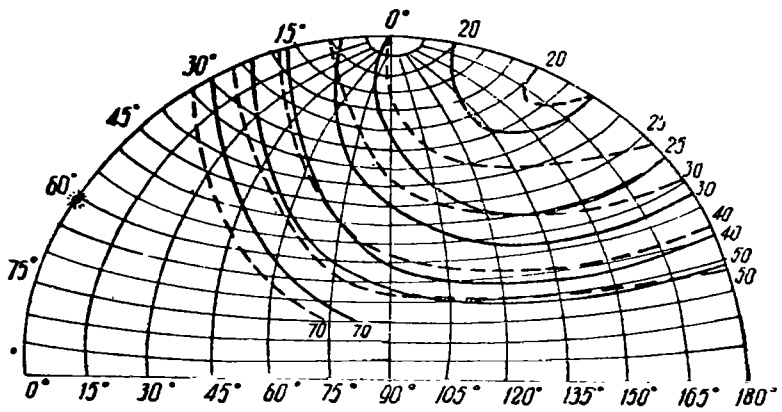

Figure 7. Observed (solid lines) and Theoretical (dashed) Isophots of Clear Daytime Sky. The Parameters are the Same as in Fig. 6, but Light Absorption by Ozone is Taken into Account for the Theoretical Data.

The isophots of a clear sky, plotted from observational data and the results of theoretical analyses [23, 24], are shown in Fig. 6; shown in Fig. 7 are the results of measurement for the same parameters as in Fig. 6; however, the theoretical data have been adjusted for ozone absorption by the method developed in Part 1 of this work [33]. The introduction of this correction brought the analytical results appreciably closer to the observed brightness values.

The theoretical [23, 24] and observed isophots for an atmosphere with different parameters are shown in Fig. 8. Here, one can observe an incongruity in the shape of the isophots and an appreciable difference in the brightness values. This difference cannot be associated with ozone absorption (it is small in this region of the spectrum) nor with a possible error in choosing the local albedo. It is the result of an inconsistency between the scattering function, assumed in the calculations, and that which is actually observed.

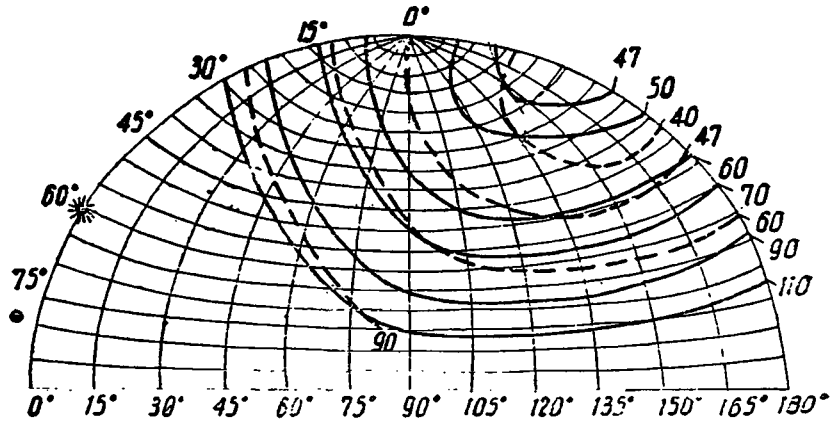

Figure 8. Observed (solid lines) Isophots of Clear Daytime Sky for $z_{\odot} = 58.7°$, $p_b = 0.66 \pm 0.01$, $\lambda = 0.404\ \mu m$, $q = 0.1$ (Aug. 27, 1965, a.m.) and Theoretical (dashed) for $z_{\odot} = 60°$, $\tau = 0.4$, $q = 0.1$, Indicatrix VI. The Values Plotted are B (W/cm^2-sterad-μm) x 10^4.

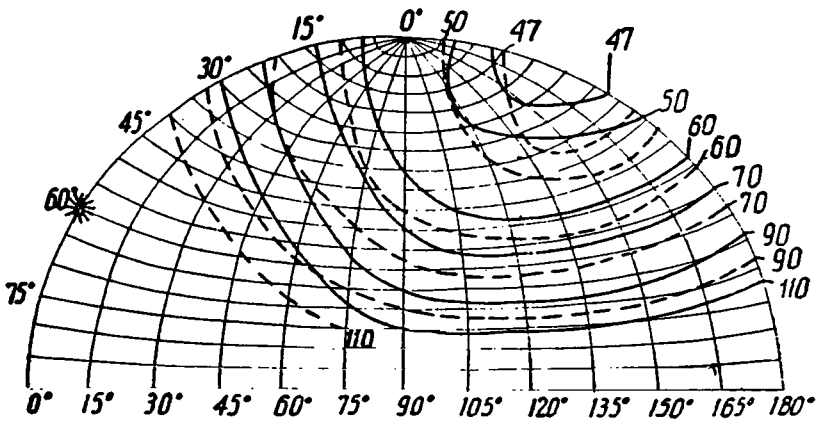

Figure 9. Observed (solid lines) Isophots of Clear Daytime Sky for $z_{\odot} = 58.7°$, $p_b = 0.66 \pm 0.01$, $\lambda = 0.404\ \mu m$, $q = 0.1$ (Aug. 27, 1965, a.m.) and Theoretical (dashed) for $z_{\odot} = 60°$, $\tau = 0.4$ $q = 0.1$. The Values Plotted are B (W/cm^2-sterad-μm) x 10^4.

The isophots, observed (solid lines) and plotted on the basis of the data of [33] (for the same atmosphere parameters as in Fig. 8), are presented in Fig. 9. The agreement in isophot shape and in brightness values is noticeably better because the actually observed wavelength dependence of the shape of the scattering indicatrix is taken into consideration in the calculations in [33].

Let us consider the question of whether it is possible, without recourse to direct measurements, to specify the shape of the scattering function in order to derive the actual brightness distribution over the sky. /19

TABLE II. Variation of "Color" Ratios

Z°	a					b					c				
	Ψ°														
	0	45	90	135	180	0	45	90	135	180	0	45	90	135	180
0	2,20	2,20	2,20	2,20	2,20	1,88	1,88	1,88	1,88	1,88	1,54	1,54	1,54	1,54	1,54
15	2,03	2,11	2,23	2,37	2,37	1,82	1,80	1,84	1,88	1,89	1,72	1,67	1,50	1,39	1,39
30	1,63	1,92	2,24	2,44	2,44	1,77	1,80	1,88	1,89	1,88	1,80	1,74	1,44	1,38	1,38
45	—	1,72	2,19	2,43	2,51	1,57	1,75	1,84	1,83	1,84	1,88	1,75	1,36	1,07	1,23
60	—	1,59	2,03	2,32	2,32	—	1,57	1,74	1,75	1,68	1,82	1,69	1,24	1,12	1,18
75	—	1,32	1,56	1,91	1,89	1,32	1,46	1,48	1,53	1,51	1,60	1,50	1,11	0,95	1,05

Note: Commas represent decimal points.

Let us first examine the solar almucantar region. As is known [32], the spectral sky brightness in the solar almucantar for first order scattering can be expressed by the formula

$$B_1(\varphi, \lambda) = \pi S_\lambda \mu_1(\varphi, \lambda) p^{m_\odot} m_\odot, \tag{1.2}$$

where p is the atmosphere transmission coefficient, φ is the scattering angle, $m_\odot$ is the atmosphere mass in the direction toward the sun, and $\mu_1(\varphi, \lambda)$ is the absolute scattering function. Let us represent the last quantity as the sum of Rayleigh and aerosol components

$$\mu_1(\varphi, \lambda) = \mu_R(\varphi, \lambda) + \mu_D(\varphi, \lambda). \tag{1.3}$$

The absolute Rayleigh scattering indicatrix can be calculated from the formula

$$\mu_R(\varphi, \lambda) = \frac{3}{16\pi} \tau_R (1 + \cos^2 \varphi), \tag{1.4}$$ /20

where τ_R is the Rayleigh optical thickness. We represent the aerosol scattering

indicatrix in the form

$$\mu_D(\lambda, \varphi) = \tau_D k f_D(\varphi, \lambda), \tag{1.5}$$

where τ_D is the aerosol optical thickness for scattering, $f_D(\varphi)$ is the relative scattering function. We assume that a so-called normal [50] Junge particle size distribution exists in the atmosphere:

$$\frac{dn(r)}{d \lg r} = cr^{-\nu^*}, \tag{1.6}$$

in which $\nu^* = 3$ and the limiting values of the radii r_1 and r_2 are 0.04×10^4 and 10.0×10^4 cm.

The aerosol scattering indicatrix $f_D(\varphi, \lambda)$, normalized for the condition $f_D(90°) = 1$, is listed in Table III for a particle refractive index of m = 1.5 and a wavelength of $\lambda = 0.55$ μm.

TABLE III. Relative Polydisperse Indicatrix for "Normal" Junge Distribution

$\varphi°$	0	5	10	20	30
f_D	28,4	65,6	38,6	20,6	12,2
$\varphi°$	40	50	60	70	80
f_D	7,44	4,64	2,97	1,97	1,37
$\varphi°$	90	100	110	120	130
f_D	1,00	0,781	0,663	0,614	0,625
$\varphi°$	140	150	160	170	180
f_D	0,699	0,871	1,20	1,35	1,74

Note: Commas represent decimal points.

The coefficient k is equal to 1/45. The shape of the aerosol scattering indicatrix for a "normal" Junge particle size distribution changes slightly with wavelength in the visible portion of the spectrum. For some problems one can assume $f_D(\varphi)$ is independent of λ. In this case, the asymmetry of the scattering indicatrix $\mu_1(\varphi, \lambda)$ as a function of wavelength will be determined by the ratio of the values of τ_R and τ_D for each specific day of observations. Since the quantity τ_R increases significantly more rapidly than τ_D, with a decrease in wavelength and consequently, with an increase in optical thickness, then the asymmetry of the scattering indicatrix $\mu_1(\varphi, \lambda)$ will decrease with a decrease in wavelength.

Calculations of multiple scattering and light reflection from the underlying surface can be accomplished with the aid of the above-mentioned tables [23, 24] with appropriate interpolation when necessary.

Let us consider how well the results of direct observations agree with theoretical calculations of sky brightness, made under the assumption of a "normal" Junge particle size distribution. When calculations are made using the tables of [23, 24], it is adequate to determine experimentally the values of the Bouguer optical thickness τ_b, the optical absorption thickness τ_π (in the visible region—in the Chappuis band) and the albedo of the underlying surface q. A correct comparison of calculations and direct observational data is possible only when the experimental errors involved in determining these quantities are carefully taken into account. /21

The error in determining the optical thickness of the atmosphere by the Bouguer method is the most significant. Thus, if the atmosphere transmission coefficient p_b is 0.90 and is measured with an accuracy of 1%, then the relative error in determining the Bouguer optical thickness $\tau_b = \ln p_b$ will be about 10 %. The accuracy of the aerosol optical thickness determination $\tau_D = \tau_b - \tau_R - \tau_\pi$ will be even less .

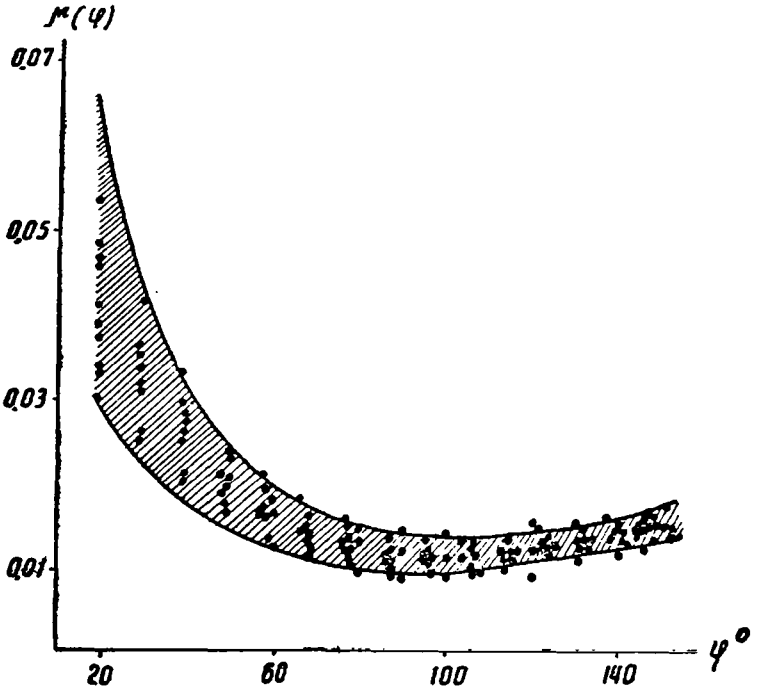

Figure 10. Comparison of Experimental Values of $\mu(\varphi)$ (points) with Data from Theory (shaded area) for λ=0.542 μm.

*The estimates given here refer to a clear, optically stable day.

Shown in Figs. 10 and 11 are values of

$$\mu(\varphi) = -\frac{B(\varphi)}{\pi S_\lambda p^{m_\odot} m_\odot}, \qquad (1.7)$$

determined from direct observations of the sky brightness in the solar almucantar for scattering angles of $\varphi \geqslant 20°$ (points). The maximum day-to-day variations of the atmosphere transmission coefficient in the green region of the spectrum (λ = 0.542μm) did not exceed 2.5%, and in the red (λ = 0.634μm)—1.5%. The solid lines define the upper and lower limits of the theoretical values of $\mu(\varphi)$, caused by errors in the determination of τ_b and τ_π; the limits were calculated under the assumption of a "normal" Junge size distribution of atmospheric aerosols. Multiple scattering of the light was taken into account with the aid of the tables of [23, 24]. Average data for the spectral albedo of a grassy surface were used for the underlying surface. /22

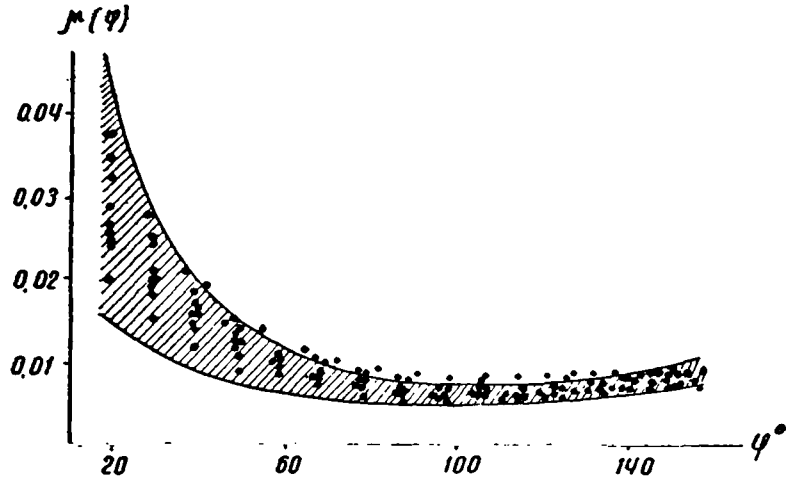

Figure 11. Comparison of Experimental Values of $\mu(\varphi)$ with Data from Theory for $\lambda = 0.63$ μm.

Analogous sky brightness calculations were made for different zenith distances Z and azimuth angles Ψ; the results of the calculations are listed in Table 3. The upper and lower lines give the limits within which the calculated brightness lies and the middle line contains the experimental data.

As seen from Figs. 10, 11 and Table 3, the observational results agree quite well with the results of theoretical calculations.

An analogous method of calculating the brightness distribution over the daytime sky can be used with success for the ultraviolet portion of the spectrum. Since the asymmetry of the scattering function $\mu_1(\varphi)$ in the ultraviolet region of the

spectrum due to the influence of Rayleigh scattering is significantly less than in the visible, in calculations of multiple light scattering it is more suitable to use the tables of [6], calculated under the assumption of a Rayleigh indicatrix.

Calculations of the angular dependence of the quantity $\mu(\varphi)$ and direct measurement data in the solar almucantar are shown in Fig. 12 for two summer days of observations with a silver light filter ($\lambda_{eff} = 0.34\ \mu m$). The albedo of the underlying surface was assumed to be equal to zero in the ultraviolet portion of the spectrum. The difference between theoretical and observational data does not exceed 10%. Approximately the same differences are observed when the results of measurements and of theoretical calculations of sky brightness for different zenith distances Z and azimuth angles Ψ are compared (Table 4).

Thus, at scattering angles of $\varphi > 10-20°$ the direct problem—calculation of the brightness distribution over the daytime sky—can be solved with sufficient accuracy in the visible and ultraviolet spectral regions for a given shape of the aerosol indicatrix corresponding to a "normal" Junge-type of size distribution for atmospheric aerosols. /23

Let us proceed to a consideration of the possibility of solving the direct problem at small scattering angles.

We have utilized the calculations of E. deBary and K. Bullrich [80]. By using data from their previous papers [81, 82, 83], the authors of [80] calculated the sky brightness for two values of the Junge exponent $\nu = 2.5$ and $\nu = 4.0$ and two aerosol models (the particle radii lie within the interval from $r_1 = 0.04$ to $r_2 = 10\ \mu m$ and from $r_1 = 0.04$ to $r_2 = 3\ \mu m$). Calculations were also carried out by Linke [84] for two values of the turbidity factor ($T_1 = 2$ and $T_2 = 6$), defined by the formula /24

$$T_\lambda = \frac{\tau_R(0,55) + \tau_D(0,55)}{\tau_R(0,55)}, \qquad (1.8)$$

in which τ_R (0,55) and τ_D (0.55) are the Rayleigh and aerosol optical thicknesses for a for a wavelength of $\lambda = 0.55\ \mu m$. The atmosphere is treated as a mixture of a gaseous medium (Rayleigh scattering) and an aerosol. The height H_D of the uniform aerosol atmosphere is assumed equal to 1.25 km.

Simultaneously with observations of the sky brightness in the visible portion of the spectrum at small distances from the sun (see preceding paragraph), measurements were made of the spectral transmission and stability of the atmosphere and, thus, one could determine the turbidity factor T, measure the intensity in absolute units and represent the result in a form analogous to the theoretical isophots in units of 10^{-3} cal-cm^{-2}-min^{-1}-lm^{-1} [75].

Comparing observations with theory, one can draw the following conclusions. First of all it is quite obvious that the aerosol distribution in all our measurements

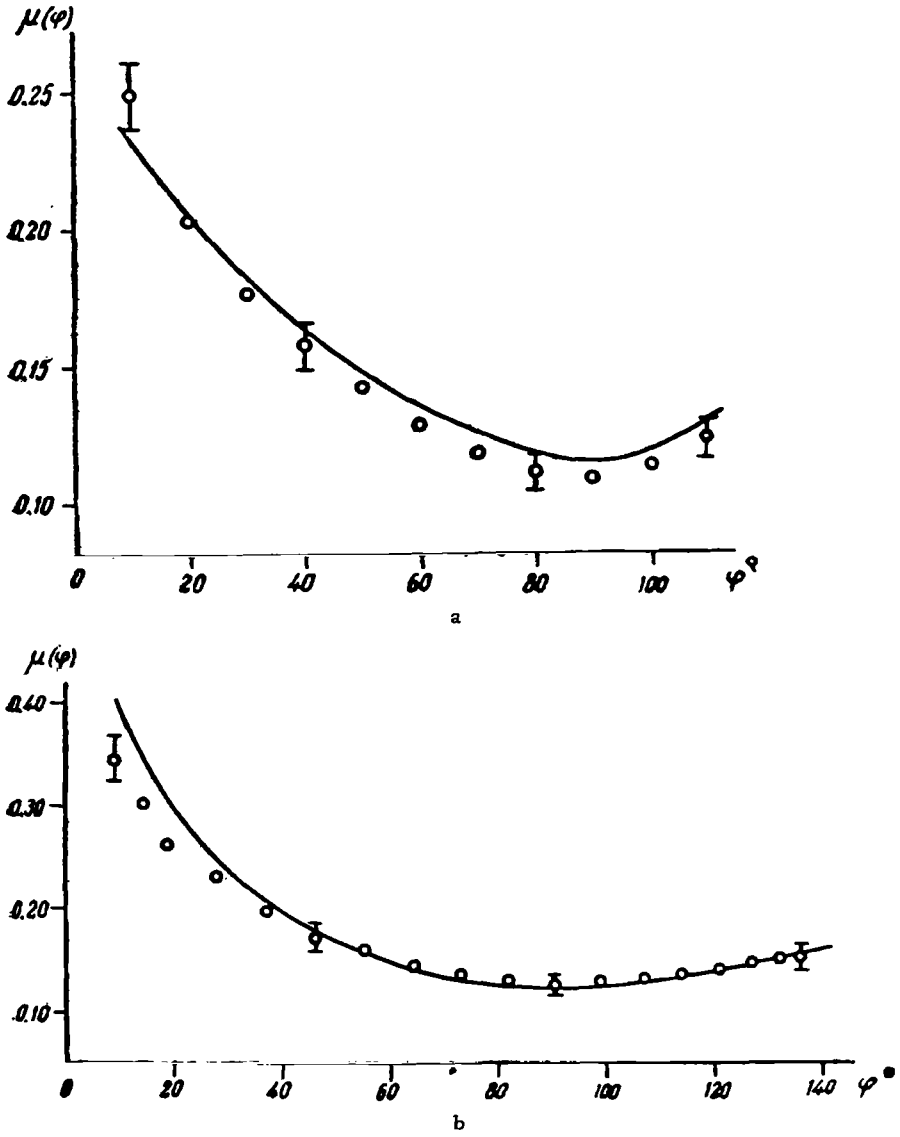

Figure 12. Comparison of Experimental Values of $\mu(\varphi)$ (circles) with Data from Theory (solid line) in 0.34 μm Spectral Region: a) July 12, 1964, a.m., $m_{\odot} = 2.30$, $p_b = 0.48$; b) Sept. 7, 1964, a.m., $m_{\odot} = 2.64$, $p_b = 0.43$.

can be characterized by a value of the exponent ν^* that is closer to 2.5 than to 4 (see Figs. 13 and 14). The differences in the shape of the isophots, determined from observations (during which a broad and shallow band spectrum is observed near $\lambda \approx 0.5$ μm) and from calculations for $\nu^* = 2.5$, should be noted. Under other conditions, however, drastic deviations from the average value of ν^* can be

observed. The solution of the direct problem for the aureole zone cannot correspond well with the actual situation.

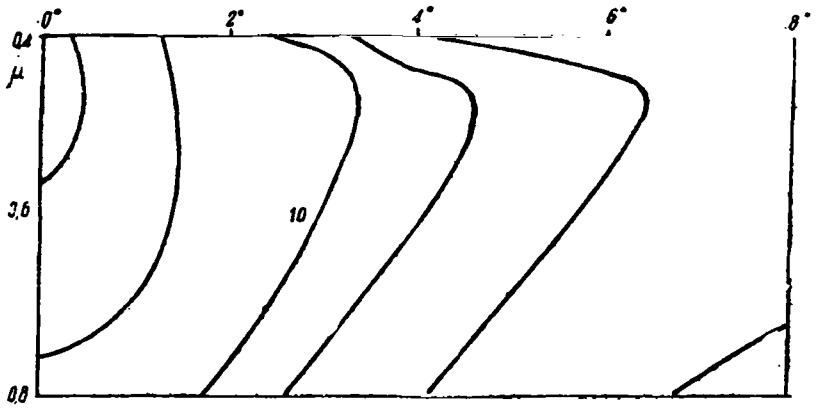

Figure 13. Theoretical Isophots of Daytime Sky in Solar Almucantar [62], Calculated in Units of 10^{-3} cal-cm^{-2}-min^{-1}-μm, $T=2$, $\nu^*=2.5$, $Z_\odot=45°$. The Curves are Plotted for the Intervals 2.5-5.0-7.5-10.0, etc.

Let us now consider solving the direct problem with respect to the polarization characteristics of the daytime sky light.

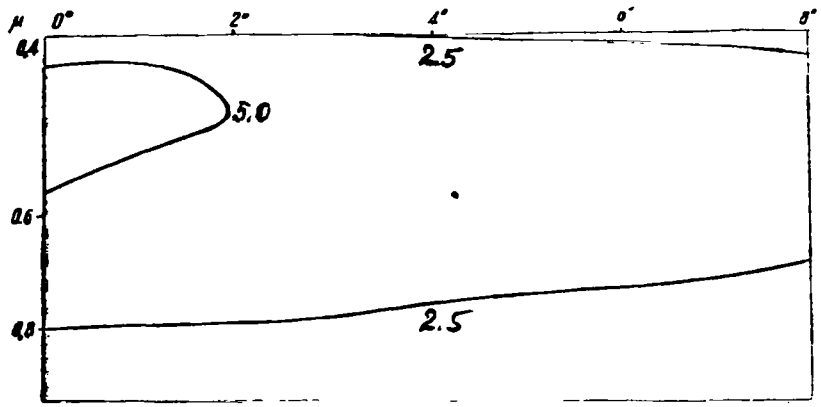

Figure 14. The Same as in Fig. 13 but for $\nu^* = 4$ and $Z_\odot = 70°$. Lower Curve Corresponds to 2.5 Units, Upper—5.0.

Attempts are now being made to reconstruct the polarization pattern of the daytime sky with the inclusion of theoretical calculations of the polarization components of the scattering functions for a molecular atmosphere and for

different aerosol models. Thus, E. de Bary [27, 28] proposed the following analysis scheme. The polarization components of the scattered radiation are computed separately and then combined: a) for Rayleigh scattering with a Rayleigh optical thickness τ_R from the tables of [6] with multiple light scattering taken into account; b) for aerosol scattering with an aerosol optical thickness τ_D from the tables of [14] with only first order scattering taken into account; c) for multiple scattering, caused by the presence of an aerosol. The last quantity is determined from the tables of [6] as the difference of the components produced by all scattering for τ_D (first order + multiple) and by first order scattering for τ_D under the assumption that multiple light scattering processes can be described by the Rayleigh model. The second component—the first act of aerosol scattering—was computed under the assumption of a Junge particle size distribution [27]. The tables of [14] contain calculations of the polarization components of the scattering functions for models characterized by ν^* values, equal to 2.5, 3 and 4, and by different particle radii limits. The refractive index is taken equal to 1.5. /25

Certain objections can be raised with respect to the described method proposed by E. de Bary [27]. In the multiple light scattering calculations, reciprocal illumination by the aerosol and gas components of the atmosphere is ignored. This deficiency can, however, be eliminated in the following manner. Using the symbols employed in [27, 28], we write the formula for the degree of light polarization in the form

$$P = \frac{F_1 - F_2}{F_1 + F_2}, \tag{1.9}$$

where

$$F_i = f_i PSR\,\tau_R + f_i PSD\,\tau_D + [f_i MSR(\tau_R + \tau_D) - \\ - f_i PSR(\tau_R + \tau_D)];\ (i = 1, 2). \tag{1.10}$$

The indices 1 and 2 refer to the mutually perpendicular polarization components of the scattering functions f_i; PS and MS designate primary scattering and multiple scattering, respectively; the indices R and D refer to the Rayleigh and aersol components of the atmosphere; the symbols τ_D, τ_R and $\tau_D + \tau_R$ mean that the calculations are made for the aerosol, Rayleigh and total optical thicknesses, The quantity of $f_i PSR\tau_D$ is calculated from the known Rayleigh formula with the anisotropy of air molecules taken into account; $f_i PSR\tau_R$ is determined from the tables of [14]. The quantity of $f_i MSR(\tau_R+\tau_D)$ is found from the tables of [6], and $f_i PSR(\tau_R+\tau_D)$—from the Rayleigh formula without molecular anisotropy taken into account.

Thus, Eq. (1.10) enables one to calculate primary scattering exactly, and multiple scattering—approximately. Since calculations of multiple scattering are made for an optical thickness of $\tau = \tau_D + \tau_R$, then reciprocal illumination by

the molecular and aerosol components of the atmosphere is thereby taken into consideration in an approximate fashion.

Let us illustrate the advantage of Eq. (1.10), compared with E. de Bary's method, in calculating the degree of polarization. Observational data and calculations of the degree of polarization under the assumption of a "normal" Junge particle size distribution, taken from [27], are shown in Fig. 15, along with the results of calculations based on use of Eq. (1.10). Just as one should expect, taking account of the reciprocal illumination by the molecular and aerosol components and, to a lesser extent, taking account of molecular anisotropy led to a decrease in the theoretical value of the degree of polarization and to better agreement with observed results.

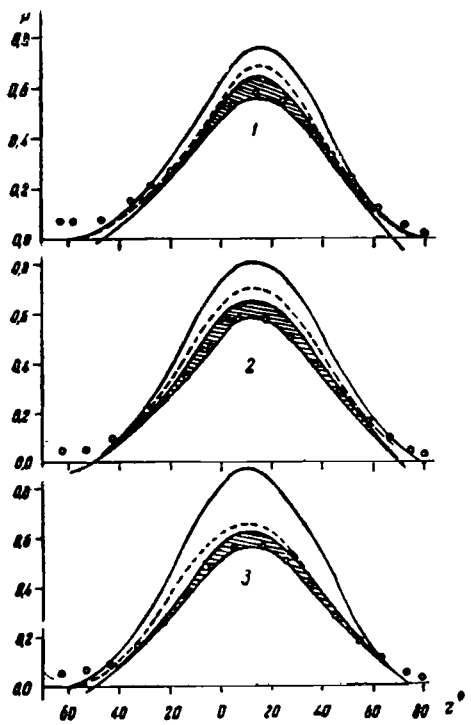

Figure 15. Observed (points) and Theoretical (shaded region) Values of the Degree of Polarization in the Solar Vertical. Boundaries of the Region are Determined by Albedo Values of 0 and 0.25. Theoretical Calculations [27] are Depicted by Solid and Dashed Lines: 1—λ= 0.65 lm; 2—λ= 0.55 μm; 3—λ=0.40 μm.

Below, we will restrict ourselves, in interpreting the observational results, to cases when the turbidity factor $T_{\lambda=0.55}$ does not exceed 2 in the λ= 0.55 μm region, which is equivalent to conditions of fairly high atmospheric transmission. (With higher atmosphere turbidity the method of taking account of the effect of multiple light scattering under the assumption of a Rayleigh atmosphere can obviously introduce significant errors).

Plotted in Fig. 16 are data from spectral measurements of the maximum degree of polarization in the solar vertical for three zenith sun distances, made by P. N. Boyko under summer conditions in the vicinity of the Astrophysics Institute AN KazSSR with the aid of a spectro-electrophotometer [76]. Also given here are the results of calculations of the maximum degree of polarization for an underlying surface albedo of q = 0 and q = 0.25. As seen from the figure, the theoretical values of the maximum degree of polarization agree well with observational data.

The relative amount of radiation, /27
scattered by the aerosol, is generally decreased significantly by diffusion flow with a decrease in wavelength. In the ultraviolet region of the spectrum at an angular distance of φ=90° from the sun, the contribution of the component $f_i PSD_{\tau_D}$ in f_i (1.10) is negligibly small, so that the following formula can be used in calculations of the polarization components:

$$F_i = f_i PSR\tau_R + [f_i MSR(\tau_R + \tau_D) - f_i PSR(\tau_R + \tau_D)];\ (i = 1.2). \qquad (1.11)$$

This relation will be valid not only for the solar vertical but also for the solar almucantar since in the vicinity of $\varphi = 90^\circ$ multiple scattering, as noted by J. Dave [85], only slightly alters the position of the polarization plane.

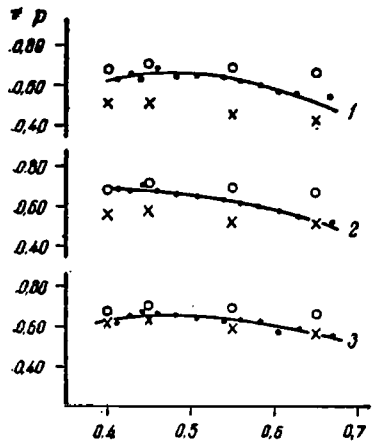

Figure 16. Maximum Polarization of Sky Light in Solar Vertical: 1) $Z_\odot = 50°$; 2) $Z_\odot = 64°$; 3) $Z_\odot = 77°$. Points—Observational Data, Circles and Crosses—Results of Theoretical Calculations for Albedos of 0 and 0.25.

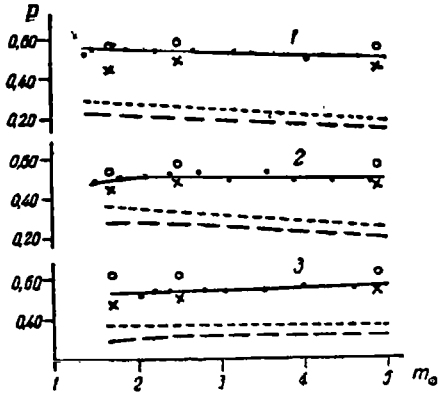

Figure 17. Maximum Polarization of Sky Light in 0.34 lm Spectral Region in Almucantar (1 and 2) and in Solar Vertical (3): 1) Aug. 6, 1965, a.m., $p_b = 0.479$; 2) June 4, 1965, a.m., $p_b = 0.484$; 3) Sept. 11, 1965, a.m., $p_b = 0.481$. Points—Observational Data, Circles and Crosses—Results of Theoretical Calculations for Albedos of 0 and 0.25. Beta of Theoretical Calculations for Albedos of 0 and 0.25, without Polarization of Multiply Scattering Light taken into Account, are Represented by Fine and Coarse Dashed Lines.

The results of calculations and observational data on the maximum degree of polarization in the ultraviolet portion of the spectrum are presented in Fig. 17 for the solar vertical (3) and the almucantar (1 and 2). From this figure it is seen that the observational data fall between the theoretical values of the degree of polarization calculated for underlying surface albedos of 0 and 0.25.

Neglecting the polarization effects of multiple light scattering leads to a significant difference between the theoretical and observed values of the degree of polarization. The results of calculations of the maximum degree of polarization in the ultraviolet portion of the spectrum, made under the assumption that multiply scattered light is not polarized, are represented by the dashed lines in Fig. 17: the long dashes correspond to an albedo value of q = 0.25,

the short—to q = 0; the theoretical values of P are nearly twice as small as the actual values.

The observational results, represented above, and their comparison with theory allow one to draw the following conclusions. /28

The direct problem can be solved with an accuracy that is satisfactory for most practical problems, both in the ultraviolet and in the visible regions of the spectrum for a large portion of the sky($\varphi > 10—20°$). The only exception is the region near the aureole zone ($\varphi > 10—20°$). Here, large deviations of the actual brightness values from their values for the average atmosphere model are possible.

The proposed method for calculating sky polarization enables one to determine, for clear days the degree of sky polarization with an error that is less than the error produced by the normal errors in determining the optical thickness and localized albedo.

Chapter 2

FUNDAMENTAL OPTICAL PARAMETERS OF THE ATMOSPHERE /29

1. Scattering Functions

Before presenting the results of scattering function measurements, let us discuss the definitions and symbols adopted in this paper in order to eliminate certain ambiguities that occasionally arise because of differences in terminology.

Sky brightness observations in the solar almucantar enable one to determine the scattering indicatrix (we denote it by $\mu(\varphi)$), relating to the total atmosphere height and influenced by the effect of multiple scattering [32]. We will also call it the "absolute brightness indicatrix." Formally, the function $\mu(\varphi)$ is defined by the appropriate formula:

$$\mu(\varphi) = \frac{B}{\pi S p^m m},$$

derived with only primary scattering taken into account. If the sky brightness B_1, produced by primary scattering, is determined then the function

$$\mu_1(\varphi) = \frac{B_1}{\pi S p^m m} \tag{2.1}$$

represents the scattering indicatrix, calculated over the entire atmosphere height [32, 33]. And if the latter has a completely defined physical meaning (see [33]), then the indicatrix $\mu(\varphi)$ only gives a representation of the observed sky brightness, weighted by all the secondary effects. Although the "pure" scattering indicatrix $\mu_1(\varphi)$, is undoubtedly of most interest, the function $\mu(\varphi)$ has always attracted attention not only because existing methods [32, 33, 41] allow one to isolate the primary indicatrix from it but also because of its interrelationship with other parameters, and also because of the possibility of investigating, by means of it, the role of different factors in the radiation of the daytime sky.

Therefore, being observational material, let us first of all present data concerning the function $\mu(\varphi)$ and its most characteristic features.

Speaking of the scattering indicatrix $\mu_1(\varphi)$, let us mention two facts. First, /30
since it is calculated over the entire height, for a model of a homogeneous atmosphere one can write

$$\mu_1(\varphi) = \mu' H, \tag{2.2}$$

where μ' is the scattering function calculated per unit volume (this elementary

volume has a height equal to unity), and H is the height of the homogeneous atmosphere.

Second, the function $\mu_1(\varphi)$ consists of aerosol and Rayleigh components:

$$\mu_1(\varphi) = \mu_{1D}(\varphi) + \mu_{1R}(\varphi) \tag{2.3}$$

or, if this expression is written, in a manner similar to the foregoing, in terms of a function relating to a unit volume, we obtain

$$\mu_1(\varphi) = \mu'_D(\varphi) H_D + \mu'_R(\varphi) H_R. \tag{2.4}$$

The results of observations of the $\mu(\varphi)$ functions in the visible region of the spectrum are presented in Table 5.

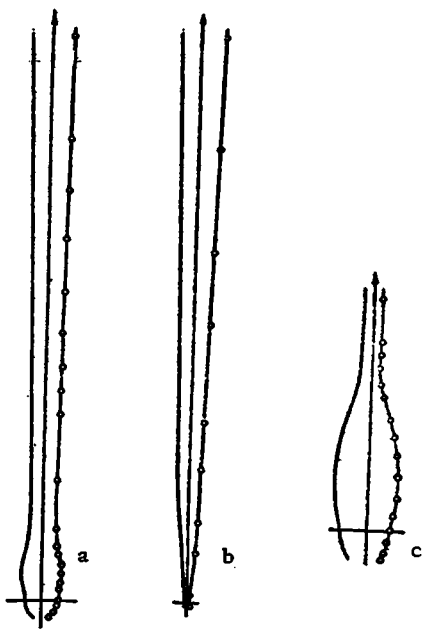

Figure 18. Absolute Brightness Indicatrices $\mu(\varphi)$: a) June 29, 1962, a.m., $\lambda = 0.450$ μm, $p_b = 0.77$; b) Sept. 17, 1962, a.m., $\lambda = 0.450$ μm, $p_b = 0.73$; c) Dec. 20, 1963, a.m., $\lambda = 0.542$ μm, $p_b = 0.87$.

Absolute brightness indicatrices, encompassing the region of small scattering angles ($2 \leqslant \varphi \leqslant 150$—$160°$), which were obtained with the aid of a photoelectric photometer with automatic recording [87] in the visible portion of the spectrum (arbitrary scale), are depicted in Fig. 18 in polar coordinates.

The meteorological conditions during the observations were quite different—from dense haze under summer conditions to an exceptionally clear winter atmosphere. As seen from the figure, the shape of the brightness indicatrix, especially at small φ (aureole), changes markedly from day to day. Thus, the ratio $\frac{\mu(2°)}{\mu(90°)}$ in the $\lambda = 0.542$ μm spectrum region can change by more than a factor of 15.

From the observations it follows that the asymmetry of the brightness indicatrix decreases with a decrease in wavelength [32, 88]. This is most noticeable when one compares the indicatrices in the visible and ultraviolet regions of the spectrum. Summer and winter relative indicatrices, normalized to the condition $\mu(90°) = 1$ in the 0.35 and 0.69 μm spectral regions, are presented in Fig. 19 as an example.

We will characterize the shape of the indicatrix $\mu(\varphi)$ by the ratio of the light fluxes scattered in the forward and backward hemispheres,

$$r = \frac{\int_0^{\pi/2} \mu(\varphi) \sin \varphi d\varphi}{\int_{\pi/2}^{\pi} \mu(\varphi) \sin \varphi d\varphi}. \qquad (2.5)$$

The values of r, obtained from observational data in different spectral regions, are listed in Table 4. /31

TABLE IV. Values of the Asymmetry Quantities r and r_1

Date	λ, μm	r	r_1
7. VI 1962, a. m.	0,634	1,86	2,83
•	0,542	1,42	2,10
•	0,450	1,33	1,89
29. VI 1962, a. m.	0,634	1,92	2,20
	0,542	1,65	1,88
	0,450	1,27	1,67
30. VI 1962, a. m.	0,634	1,88	2,02
	0,542	1,41	1,80
9. IX 1962, a. m.	0,634	2,00	2,69
•	0,542	1,83	2,38
•	0,450	1,35	1,77
17. IX 1962, a. m.	0,634	2,11	3,18
•	0,542	1,80	2,40
•	0,450	1,27	1,82

Note: Commas represent decimal points.

Let us introduce the optical thickness τ_0', defined by the formula:

$$\tau_0' = 2\pi \int_0^{\pi} \mu(\varphi) \sin \varphi \, d\varphi. \qquad (2.6)$$

Since the function $\mu(\varphi)$ is the scattering indicatrix, weighted by multiple scattering and light reflection from the underlying surface, then the quantity τ_0' is the optical thickness, modified by the above-mentioned effects. The concept of the quantity τ_0' was introduced by E. V. Pyaskovskaya-Fesenkova [32] and was found to be very convenient for treating a number of atmospheric light scattering problems.

As a rule, most researchers have measured indicatrices in the scattering angle interval $\varphi \geqslant 10°$, and sometimes—$\varphi \geqslant 15°$ [43] and to determine τ_0' they

extrapolate the quantity $\mu(\varphi)$ into the region of small scattering angles. It is usually assumed that the product $\mu(\varphi)\sin\varphi$ in the region $0° \leqslant \varphi \leqslant 10°$ is small, and the error in determining the form of $\mu(\varphi)=\mu(10°)=\text{const}$ through extrapolation is small. Measurements of the total brightness indicatrices made it possible to estimate the magnitude of this error [89]. It was found that in the visible portion of the spectrum, the values of τ_0 are reduced by 4-5% as a result of the extrapolation, and the error can amount to 10% only at high turbidities. In the ultraviolet portion of the spectrum this error is significantly less since the aureole around the sun decreases with a decrease in wavelength.

With an equivalent value of τ_0, all the absolute brightness indicatrices $\mu(\varphi)$, obtained through measurements of the sky brightness in the visible and ultraviolet spectral regions under summer and winter conditions, intersect near an angular distance from the sun ($\varphi=57°$), which can be used to interpret the observational results both for small and large atmosphere optical thickness [32, 33, 41].

Let us discuss the empirical formulas describing the atmosphere brightness indicatrix. According to the data of various authors [13, 90, 91], at small scattering angles ($0° \leqslant \varphi \leqslant 5—8°$) the indicatrix is quite well approximated by the Van de Hulst formula /33

$$\mu(\varphi) = A\varphi^{-q}. \tag{2.7}$$

The parameter q, characterizing the elongation of the indicatrix, can vary from 0.9 to 1.9 in the visible portion of the spectrum under summer conditions and amounts to about 1.5 on the average. At scattering angles of $2° \leqslant \varphi \leqslant 150—160°$, the indicatrix, on the whole, can be represented by the following relation [41]:

$$f(\varphi) = 1 + B(e^{-3\varphi} - 0.009) + Q\cos^2\varphi + Se^{-36\varphi}, \tag{2.8}$$

i.e., by the formula of V. A. Krat [42], to which is added an exponential term that takes account of the aureole around the sun. The parameter S can vary from 35 to 515 in the visible portion of the spectrum, depending on the meteorological conditions and the wavelength. The possible variations of the parameters B and Q have been discussed in Part 1 of this paper [33].

There are a number of methods [32, 33, 41], yielding quite similar results, for isolating the scattering indicatrix $\mu_1(\varphi)$. It is obviously necessary to take account of multiple scattering and light reflection from the underlying surface, as well as radiation absorption. In particular, if the scattering optical thickness is small ($\tau_1 \leqslant 0.2—0.3$) and the asymmetry of the indicatrix

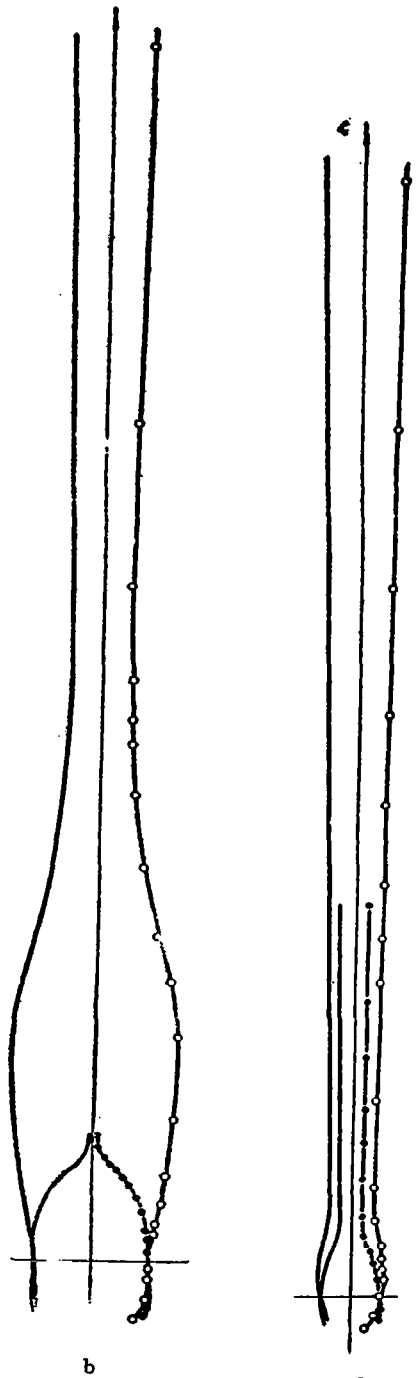

Figure 19. Relative Brightness Indicatrices in the Visible (0.634 lm—circles) and Ultraviolet (0.35 lm—points) Spectral Regions: a) June 30, 1962, a.m.; b) Dec. 19, 1963, a.m.

$$\Gamma_1 = \frac{\int_0^{\pi/2} \mu_1(\varphi) \sin\varphi d\varphi}{\int_{\pi/2}^{\pi} \mu_1(\varphi) \sin\varphi d\varphi} \qquad (2.9)$$

does not exceed 2.5-3, then multiple light scattering can be assumed to be independent of the scattering angle [79] and the method of E.V. Pyaskovskaya-Fesenkova can be used for isolating the quantity $\mu_1(\varphi)$ [32]:

$$\mu_1(\varphi) = \mu(\varphi) - \frac{\tau_a - \tau_b + \tau_\pi}{4\pi}. \qquad (2.10)$$

In this last expression the Bouguer optical thickness of the atmosphere is designated by τ_b; the optical thickness caused by light absorption alone is designated by τ_a.

It should be noted that it is very important to take account of radiation absorption by the gaseous component of the atmosphere. With a low spectral resolution, the major gaseous component of the atmosphere, markedly absorbing radiation throughout almost the entire visible portion of the spectrum, is atmospheric ozone, forming a fairly broad absorption band—from 0.44 to 0.75 μm with a maximum near 0.60μm. The question of light absorption by the atmosphere aerosol will be treated, to some extent, below. Beforehand, let us mention that in a mountainous locality, remote from industrial centers, the role of this factor is small.

Let us estimate the accuracy with which the absolute scattering indicatrix $\mu_1(\varphi)$ can be isolated from sky brightness observation data. We select the results of observations on those days when neglecting the azimuth effect of multiple scattering does not introduce a significant error (small τ_1 and slight indicatrix asymmetry). In this case, Eq. (2.10) can be used. We assume that the method of determining

$\mu_1(\varphi)$, by itself, is absolutely precise. Then the error in determining $\mu_1(\varphi)$ depend on the absolute values of the quantities, entering into the latter equation, and on the errors in their determination. If the quantity $\mu(\varphi)$ is measured with a relative error of 5%, the atmospheric transmission coefficient p (for mandatory control of the stability of its optical properties) —with an accuracy of 1% and the quantity τ_a—with an accuracy of 20-30%, then the error in determining the quantity $\mu_1(\varphi)$ even outside the absorption band varies within the limits from 5% at small values of φ to 20% at $\varphi \approx 90°$. /34

Since the effect of multiple scattering and light reflection from the underlying surface on the indicatrix is eliminated, its asymmetry increases. The data of Table 4, in which values of Γ and Γ_1, calculated from Eqs. (2.5) and (2.9) are listed, confirm this. Nevertheless, the general character of the wavelength dependence of the quantity Γ_1 remains the same as before: the indicatrix asymmetry decreases with a decrease in wavelength. Thus, multiple light scattering alone cannot be responsible for the decrease in the asymmetry of the observed brightness indicatrix $\mu(\varphi)$ with a decrease in λ. This agrees with the conclusions of [32].

As an illustration, the results of an approximation of the scattering indicatrix in three spectral regions by the formula

$$f_1(\varphi) = 1 + B_1(e^{-3\varphi} - 0.009) + Q_1 \cos^2 \varphi + S_1 e^{-36\varphi}, \tag{2.11}$$

are shown in Fig. 20 for two days of observations after a rain and in the presence of haze. The empirical formula, derived for the atmospheric brightness indicatrix with appropriate values of the parameters B_1, Q_1 and S_1, remains valid for the scattering indicatrix $\mu_1(\varphi)$.

In this case the scattering optical thickness

$$\tau_1 = 2\pi \int_0^{\pi} \mu_1(\varphi) \sin \varphi d\varphi \tag{2.12}$$

will be equal to

$$\tau_1 = 4\pi \mu_1(90°) \cdot (1 + 0.041 B_1 + \tfrac{1}{3} Q_1 + 0.00039 S_1). \tag{2.13}$$

A detailed analysis of the errors in determining the quantity $\mu_D(\varphi)$ (Table 5) shows that the aerosol scattering indicatrix can be isolated only for scattering angles of $\varphi \leqslant 90°$. The errors in determining the rear portion of the scattering indicatrix exceed the $\mu_D(\varphi)$ values. Therefore all the results of determining $\mu_D(\varphi)$ in the visible portion of the spectrum, entering into every textbook and monograph [32, 58, 35], and also in the first part of this paper [33], do not reflect the true optical properties of the aerosol. As seen from Table 5, the aerosol scattering indicatrix can be determined with an accuracy of <10% only at scattering angle of $\varphi \leqslant 10°$—15°.

Let us discuss some properties of the aerosol scattering indicatrix. First of all, let us consider the results of autumn-summer spectral measurements of indicatrices at angles of $\varphi = 2—8°$.

/35

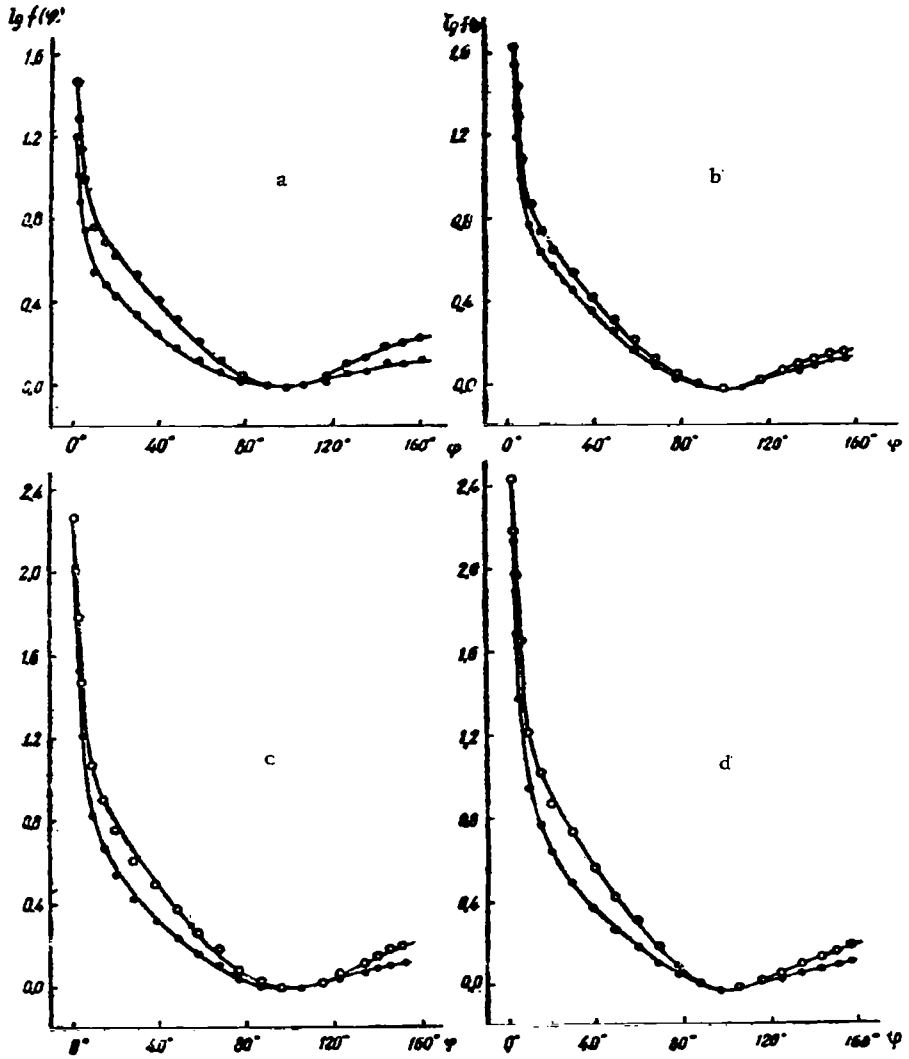

Figure 20. Brightness (circles) and Scattering (points) Indicatrices, Represented by Eqs. (2.8) and (2.11): a) June 29, 1962, a.m. $\lambda = 0.450\,\mu$m; b) June 29, 1962, a.m., $\lambda = 0.634\,\mu$m; c) Sept. 17, 1962, a.m., $\lambda = 0.542\,\mu$m; d) Sept. 17, 1962, a.m., $\lambda = 0.634\,\mu$m. Approximating Function is Represented by Solid Line.

The value of μ_D (2°) in the $\lambda = 0.553\,\mu$m spectral region can vary from 0.168 (Oct. 4, a.m.) to 4.0 (Aug. 18, a.m.), i.e., by about a factor of 24 (Table 6).

These variations decrease with an increase in the scattering angle. Thus, μ_D (8°) is changed by a factor of 14 in this same spectral region. If the asymmetry of the aerosol scattering indicatrix at small φ angles is characterized by the ratio $\gamma_D = \frac{\mu_D(2^\circ)}{\mu_D(8^\circ)}$, then the quantity γ_D can: remain constant (13 out of 27 series of measurements), increase in the short wavelength (9 series) or in the long wavelength portion of the spectrum (3 series). For all days on which observations were made, μ_D (2°) characteristically increased with a decrease in wavelength, with a more or less well-pronounced maximum frequently (15 cases out of 50) appearing, primarily in the λ=0,42—0.47 μm portion of the spectrum. Such a spectral dependence for the quantity μ_D indicates the presence, in the atmosphere, of aerosol particles with some preferential radius $r_{eff} \simeq 0.4 - 0.5$ μm [153]. /36

TABLE V. $\mu_D(\varphi)$ Values and Errors in Their Determination

λ=0,450 μm			λ=0,542 μm			λ=0.634 μm		
φ°	μ_D	$\delta\mu_D$, %	φ°	μ_D	$\delta\mu_D$, %	φ°	μ_D	$\delta\mu_D$, %
1,9	0,344	6	1,9	0,217	5	1,9	0,272	5
4,2	0,131	6	4,2	0,080	6	4,2	0,106	5
5,8	0,097	7	5,8	0,0537	6	5,8	0,071	6
9,8	0,0487	9	9,8	0,0317	8	9,8	0,0369	6
14,8	0,0378	10	14,7	0.0216	10	14,7	0,0237	7
19,7	0,0299	11	19,5	0,0168	11	19,5	0,0174	9
29,7	0,0212	13	29,3	0,0122	15	29,3	0,0117	11
39,6	0,0133	17	39,0	0,0083	18	39,0	0,0081	14
59,0	0,0054	35	48,7	0,0057	25	48,7	0,0057	18
78,5	0,0018	89	58,1	0,0034	38	58,4	0,0046	22
88,3	0,0008	200	67,7	0,0027	48	77,8	0,0022	43
107,5	0,0005	320	77,3	0,0019	63	87,3	0,0017	55
126,4	0,0001	1700	86,7	0,001	109	124,3	0,0012	88
144,2	0,0001	1800	105,4	0,0006	200	148,2	0,0009	100
151,8	0,0001	1800	123,0	0,0003	400	—	—	—
—	—	—	139,5	0,0002	600	—	—	—
—	—	—	152,0	0,0004	320	—	—	—

Note: Commas represent decimal points.

It is characteristic for the absolute values of $\mu_D(\varphi)$ to decrease for winter conditions, compared with summer (Table 7). Thus, for λ=0.553 μm for function μ_D (2°) assumed a value from 0.091 (Jan. 13, a.m.) to 0.81 (Feb. 11, a.m.). The quantity γ_D, characterizing the indicatrix asymmetry, was independent of φ at small λ values in 10 cases, and in 12 cases it increased monotonically with an increase in wavelength. Curves of $\mu_D(2^\circ)=\mu_D(\lambda)$ often have a maximum in one region of the spectrum or another (13 cases out of 31).

Let us consider the results of studies of certain optical characteristics of aerosol mists, causing transient variations in atmospheric conditions.

The observations were made at the observatory of the Astrophysics Institute AN KazSSR in 1965-1966 with the aid of the spectro-electrophotometer described

in Part 1 of this paper [33]. The direct and scattered solar radiation in the solar almucantar were measured at an angular distance of $\varphi = 2—10°$ and $\varphi = 57°$ from the sun. A period of 10-12 minutes elapsed during such a series of measurements. In the presence of dense hazes (usually after noon) the direct and scattered radiation were only measured at $\varphi = 2°$ (this took ~ 3 minutes).

As indicated previously, in an optically stable atmosphere the observed indicatrix (visual portion of the spectrum) remains constant as the solar zenith distance changes. Variations in the directional light scattering coefficient $\mu(\varphi)$ indicate fluctuations in the aerosol component of the atmosphere. Knowing the quantity μ' and the total optical thickness τ' of the atmosphere in a stable period and after a change in its properties—μ'' and τ'', one can determine the optical parameters of the atmospheric haze $\mu_h = | \mu' - \mu'' |$ and $\tau_h = | \tau' - \tau'' |$. It must be stated that if this is more or less valid for small scattering angles where one can neglect the variation of contributions caused by multiple scattering, then at large φ this method of determining the haze scattering function μ_h requires a more rigorous consideration of multiple scattering. /37

Brightness changes at small φ are caused primarily by variations in the coarse fraction of the aerosol. Studies of the fine fraction of haze on the basis of sky brightness measurements at $\varphi > 20°$ are difficult in view of the large errors in determining μ_h (50% and more).

For the reasons cited above, major attention was directed to the study of the scattering functions of atmospheric haze μ_h at small angles φ and of its optical thickness τ_h. Let us consider the aerosol haze characteristics determined by us. In Tables 8 and 9 data are presented on the optical thicknesses and scattering functions of autumn-summer and winter hazes. The values of τ_h and $\mu_h(2°)$ for $\lambda = 0.553$ μm vary within the limits $0.01 \leqslant \tau_h \leqslant 0.06$ and $0.006 \leqslant \mu_h(2°) \leqslant 0.29$; $0.02 \leqslant \tau_h \leqslant 0.015$ and $0.024 \leqslant \mu_h(2°) \leqslant 0.80$ respectively, for winter and autumn-summer observations. In view of the fact that the errors in determining the values of τ_h and μ_h vary from day to day, in each specific case it is necessary to determine the absolute error of the desired quantity (Tables 8 and 9).

Curves of the spectral dependence of the μ_h function at $\varphi = 2°$ and of the optical thickness $\tau_h(\lambda)$. of the haze are presented in Figs. 21 and 22. Changes in atmospheric conditions produce quite drastic changes in the optical properties of hazes even over a short interval of time. The scattering functions μ_h at $\varphi = 57°$ also reflect variations in the haze particle composition.

However, in spite of the large variety of curve shapes, the functions $\mu_h(2°) = \mu_h(\lambda)$ and $\tau_h = \tau_h(\lambda)$ can be grouped into definite classes. Four types of curves can be identified in terms of the nature of the wavelength dependence of the function $\mu_h(2°)$

1) $\mu_h(2°)$ is independent of λ (constitutes 25% of the 55 autumn-summer and 7% of the 59 winter curves);

2) $\mu_h(2°)$ increases more or less monotonically with a decrease in λ (32% of the autumn-summer and 41% of the winter measurements);

3) $\mu_h(2°) = \mu_h(\lambda)$ with maxima and minima in different portions of the visible spectrum (36% of the autumn-summer and 42% of the winter hazes);

4) the value of the function $\mu_h(2°)$ decreases in the short wavelength region (7% of the autumn-summer and 10% of the winter measurements).

Curves of the spectral dependence of the optical thickness of a haze can be divided into 3 groups: 1) the nonselective type of $\tau_h(\lambda)$ dependence is characteristic of one-tenth of the autumn-summer series and two out of thirteen winter series; 2) four summer and seven winter hazes are distinguished by an increase in optical thickness τ_h at small λ; 3) the curves of $\tau_h = \tau_h(\lambda)$ exhibit maxima and minima in various regions of the spectrum for five autumn-summer and four winter hazes.

An attempt was made to represent the optical thickness of haze in the form $\tau_h = k/\lambda^n$ (k and n are certain constants). However, this was not always possible. In those cases when such a relationships does exist, the values of n often varied, depending on the spectral region. Results of a determination of the exponent n are presented in Table 6 (the lines indicate that n could not be determined).

As seen from the table, the n values lie within a broad interval (from n = -5.33 to n = 4.57). We note that such large values (both positive and negative) are characteristic of the $\tau_h(\lambda)$ relationship when maxima and minima are present /38
on the curve. In some cases the entire visible region of the spectrum is characterized by one value of n. Hazes, having an optical thickness which could be characterized by an exponent n = 0.00, if the 0.553-0.693 μm region (where the value of τ_h is observed to rise) is excluded, were observed on two days (Jan. 7 and May 15, 1965, a.m.).

As seen from the character of the spectral dependence curves of the scattering function $\mu_h(2°)$ and of the optical thickness $\tau_h(\lambda)$ (see Figs. 21 and 22), one /39
can, in many cases, speak of the existence of a preferential particle size appearing in the aerosol haze. For autumn-summer hazes the value of $\mu_h(2°)$ reaches a maximum in the regions: 0.420-0.430 μm (3 cases), 0.450-0.460 μm (3 cases), 0.520 μm (1 case). An analysis of the $\tau_h(\lambda)$ and $\mu_h(\lambda)$ curves for the same haze (Fig. 24) leads to these results: on Sept. 20 the τ_h and $\mu_h(2°)$ values reach a maximum at $\lambda \approx 0.425$ μm; on Oct. 8 and Oct. 9 a rise at $\lambda = 0.470$ μm was observed in the haze optical thickness curve $\tau_h(\lambda)$; however, it is not detected from measurements of $\mu_h(2°) = \mu_h(\lambda)$. A fairly broad maximum, centered at $\lambda \approx$ 0.450 μm, was observed in the $\tau_h(\lambda)$ curve on June 7. Knowing the wavelength /40
of the radiation that is scattered most, one can estimate the effective particle

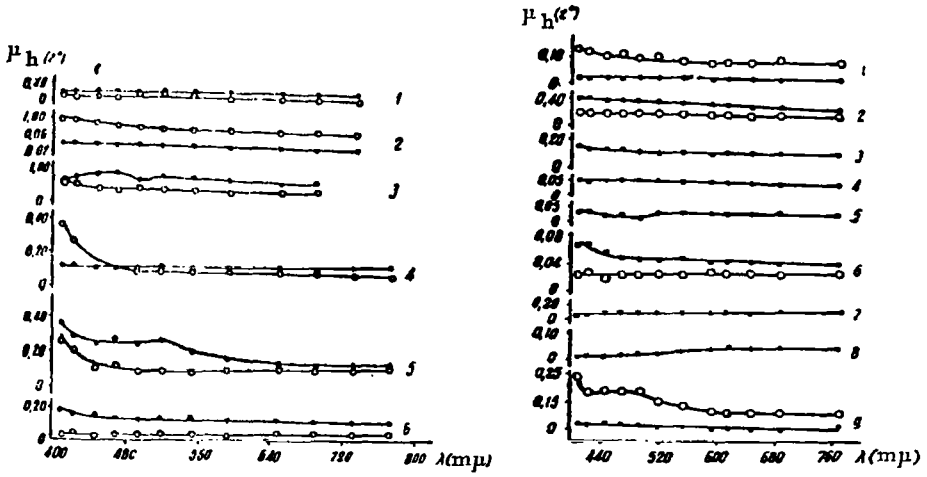

Figure 21. Spectral Dependence of Scattering Function μ_h of Atmosphere Haze at $\varphi=2°$: a) Autumn-Summer Observations: 1—May 6, 2—June 5, 3—May 12, 4—Oct. 9, 5—Oct. 16, 6—Oct. 14, (1965, a.m.); b) Winter Observations: 1—Dec. 13, a.m., 2—Dec. 13, p.m., 3—Dec. 10, p.m. (1965), 4—Jan. 10, a.m., 5—Jan. 12, a.m., 6—Jan. 13, a.m., 7—Feb. 10, p.m., 9—Feb. 14, p.m. (1966).

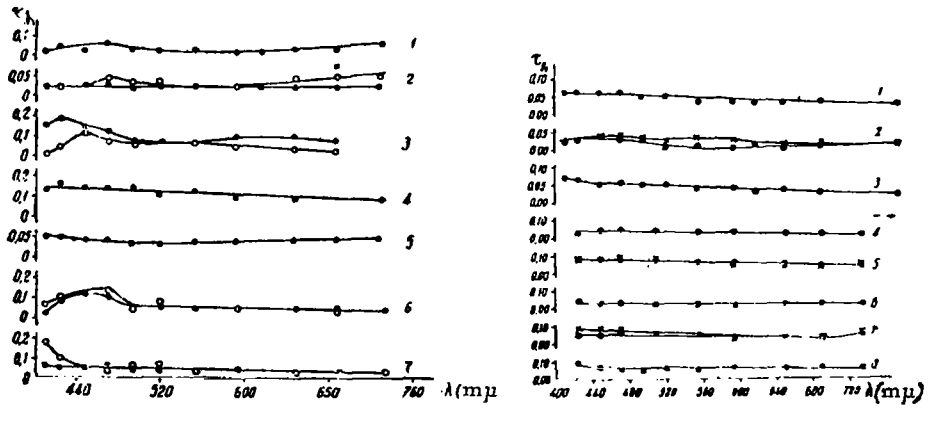

Figure 22. Spectral Dependence of Optical Thickness τ_h of Atmosphere Haze: a) Autumn-Summer Observations: 1—Oct. 9, 2—Oct. 8, 3—Sept. 20, 4—Sept. 18, 5—Aug. 18, 6—June 7, 7—May 15 (1965), a.m.); b) Winter Observations: 1—Jan. 13, a.m. (1966), 2—Dec. 17, a.m., 3—Dec. 13, a.m., 4—Jan. 7, p.m., 5—Jan. 4, a.m., 6—Jan. 4, p.m., 7—Jan. 4, a.m. (1965), 8—Dec. 28, a.m. (1964).

radius $r_{eff} \approx \lambda$ [153]. For different hazes the value of r_{eff} varies within the limits $0.42 \leqslant r_{eff} \leqslant 0.52\ \mu m$.

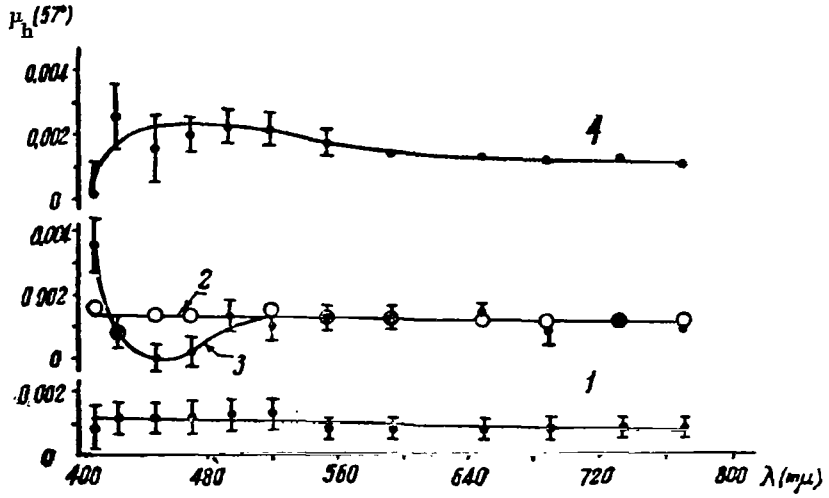

Figure 23. Spectral Dependence of Atmosphere Haze Scattering Function μ_h at $\varphi = 57°$: 1—16.X, 2, 3—9.X, 4—14.X (1965, a.m.).

In winter, analogous maxima in the spectral dependence curve $\mu_h(2°) = \mu_h(\lambda)$ are shifted toward the long wavelength region. Thus, a "peak" is observed at $\lambda = 0.650\ \mu m$ (Feb. 14, p.m.), $0.620\ \mu m$ (Feb. 10, p.m.); maxima are also encountered at $\lambda = 0.520\ \mu m$ (3 cases), in the $\lambda = 0.490$–$0.500\ \mu m$ region (2 cases), $\lambda = 0.470\ \mu m$ (1 case), $\lambda = 0.425\ \mu m$ (2 cases). Thus, particles with a preferential size ($r_{eff} \approx 0.42$—$0.65\ \mu m$) are also often observed in the aerosol distribution of winter hazes.

As already mentioned, in a number of cases the curves of $\mu_h(2°) = \mu_h(\lambda)$ have minima which are possible explained by a deficiency of one particle size or another in the atmospheric haze.

It is interesting to compare our data with theoretical calculations of the scattering functions of a polydisperse aerosol for a Junge type of particle size distribution [14, 74]. Previously, we attempted to represent the indicatrices obtained for some hazes by the Van de Hulst formula at small angles φ (Fig. 25, Table VII)

$$\mu_h(\varphi) = C\varphi^{-q}.$$

The value of q lies in the interval $1.2 \leqslant q \leqslant 2.8$ (ignoring two cases when $q = 0.5$ and $q = 0.2$). For the same haze, the character of the angular dependence

TABLE VI. n Values from Data for Winter and Autumn-Summer Measurements

Winter measurements				Autumn-summer measurements			
Date	Haze No.	n	λ, μm	Date	Haze No.	n	λ, μm
28. XII 1964, a. m.	1	—0,57	0,735—0,495	15. V 1965, a. m.	1	0,00	0,735—0,553
»	1	4,57	0,495—0,423	»	1	—	0,520—0,410
4. I 1965, a. m.	1	0,70	0,735—0,423	»	2	1,00	0,735—0,410
»	2	2,40	0,735—0,423	»	3	0,00	0,735—0,593
				»	3	0,00	0,553—0,447
4. I 1965, a. m.	1	0,70	0,735—0,423				
»	2	2,40	0,735—0,423				
4. I 1965, p. m.	1	0,00	0,735—0,423	7. VI 1965, a. m.	1	—5,33	0,470—0,410
7. I 1965, a. m.	1	0,00	0,735—0,650	»	1	1,60	0,735—0,495
»	1	0,00	0,593—0,447	18. VIII 1965, a. m.	1	2,00	0,470—0,410
»	1	0,00	0,735—0,553	»	1	—0,90	0,470—0,735
»	2	0,00	0,508—0,447	18. IX 1965, a. m.	1	0,00	0,735—0,593
»	2	0,00	0,691—0,553	»	1	0,89	0,593—0,410
»	3	0,00	0,508—0,447	20. IX 1965, a. m.	1	3,13	0,691—0,470
13. XII 1965, a. m.	3	1,75	0,772—0,410	»	1	—2,65	0,447—0,410
17. XII 1965, p. m.	1	0,00	0,470—0,410				
13. I 1966, a. m.	1	0,82	0,772—0,495	3. X 1965, a. m.	1	0,00	0,735—0,410
14. II 1966, a. m.	1	0,00	0,735—0,617				
»	1	2,66	0,593—0,410				

Note: Commas represent decimal points.

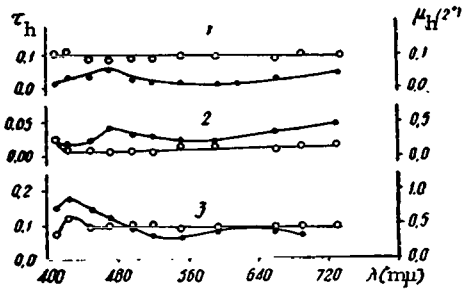

Figure 24. Spectral Dependence of Scattering Function $\mu_h^{(2^\circ)}$ (circles) and of Optical Thickness τ_h (points) of Atmosphere Haze: 1—Oct. 9, a. m., 2—Oct. 8, p. m., 3—Sept. 20, a. m. (1965).

of the scattering functions varies with wavelength. Thus, the Sept. 17 indicatrices for the short wavelength region were more asymmetrical than for large λ (q increases toward smaller λ). In two cases a significant difference was observed in the shape of the $\mu_h(\varphi)$ curve for $\lambda = 410$ and $\lambda = 450$ millimicrons (see data for May 15 and Sept. 17). The q values for the theoretically calculated indicatrices [14] of a polydisperse aerosol with a Junge type of particle size distribution were found to be: q = 0.7 for $\nu^* = 3$, q = 1.2 for $\nu^* = 2.5$, and q = 1.7 for $\nu^* = 2$. Thus, in many cases the $\mu_h = \mu_h(\varphi)$ curves are steeper than the indicatrices calculated for a value of $\nu^* = 2$. Some $\mu_h(\varphi)$ functions are characterized by a Junge exponent lying within the interval $2 \leqslant \nu^* \leqslant 2.5$. In two cases the haze indicatrices were less elongated forward than the corresponding theoretical curves for $\nu^* = 3$.

/41

It is of interest to consider some average characteristics of atmospheric haze. The results of averaging the scattering function at $\varphi = 2^\circ$ (for 42 autumn-summer and 8 winter days) are shown in Figs. 26 and 27. We note that the values

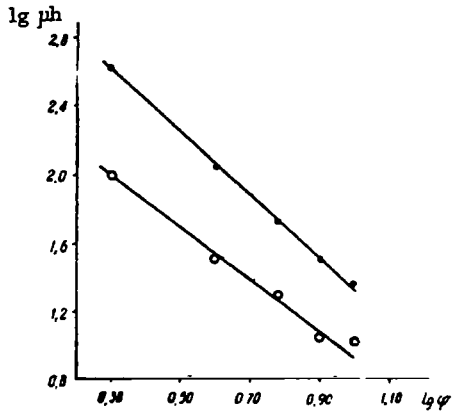

Figure 25. Haze Indicatrix at Small φ According to Van de Hulst.

of $\bar{\tau}_h$, and especially $\bar{\mu}_h$, from the autumn-summer observations, exceed the values of the corresponding parameters of winter haze, which indicates that the haze is generally denser in the summertime than in the winter. The average values of the function μ_h (2°) and of the optical thickness $\bar{\tau}_h$, for both summer and winter hazes, increase in the short wavelength spectral region, with the $\bar{\tau}_h(\lambda)$ curve from the winter observations being steeper than the analogous curve for the autumn-summer period. However, the value of $\bar{\mu}_h$ (2°) for a winter haze increases toward short wavelengths somewhat more slowly than the average values of the light scattering function of an autumn-summer haze.

TABLE VII. Values of Parameter q

Winter haze

λ, μm	13. XII 1965, a. m.	12. I 1966, a. m.	13. I 1966, a. m.	11. II 1966, a. m.
0,772	1,9	1,9	1,5	2,6
0,650	1,9	2,1	1,8	2,6
0,350	—	—	1,5	2,6
0,450	1,5	—	1,3	—
0,410	—	—	—	—

Summer haze

λ, μm	15. V 1965, a. m.	5. VI 1965, a. m.	7. VI 1965, a. m.	17. IX 1965, a. m.	18. IX 1965, p. m.
0,730	2,8	1,4	2,2	1,9	1,9
0,650	1,8	1,6	2,1	1,9	1,9
0,550	2,2	1,9	2,3	1,5	1,9
0,450	—	2,2	2,0	0,5	1,9
0,410	0,2	—	1,9	—	1,9

Note: Commas represent decimal points.

We note that our average values of τ_h characterize a fairly dense haze, approaching the observatory from the city during the midday low-pressure area. The μ_h functions, however, primarily relate to hazes which produce a change in the atmosphere optical properties in the morning hours.

It is of considerable interest to find out not only the particle distribution of the atmospheric haze but also what their physical structure is. We attempted

to draw a conclusion concerning the haze composition (dry or wet) by comparing the daytime behavior of the absolute humidity in the vicinity of the observations /42
(it was measured about 100 meters below the observatory) and the total scattering function at an angle of $\varphi = 2°$. The fact that T. P. Toropova [94] observed, for our locale, a close correlation (the correlation coefficient was equal to 0.87 ± 0.03) between the absolute humidity at the earth's surface and the amount of water vapor in the atmosphere attests to the competence of such an analysis.

Synchronized fluctuations of the absolute humidity and the value of $\mu(2°)$ were observed on only one of ten autumn-summer days (June 15, 1965, a.m.). For all the other days, however, the character of the variations of $\mu(2°)$ and of the humidity with time were often quite different from each other (Fig. 28). In the autumn-summer period the absolute humidity frequently remained constant during the midday low-pressure when a dense haze appeared from the direction of the city. From this one can conclude that it consists primarily of dry particles. /43

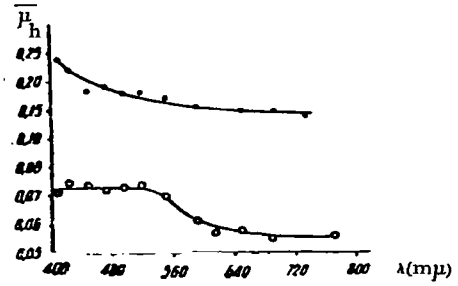

Figure 26. Spectral Dependence of Average Scattering Function μ_h of Atmosphere Haze at $\varphi = 2°$. Points—Autumn-Summer, Circles—Winter Observations.

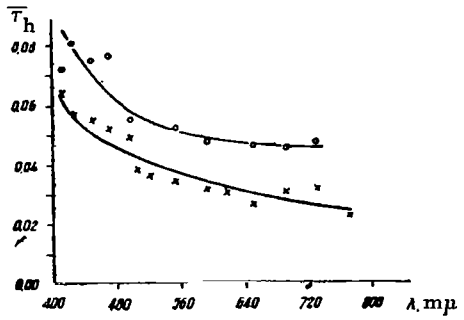

Figure 27. Spectral Dependence of Average Haze Optical Thickness. Circles—Autumn-Summer, Crosses—Winter Observations.

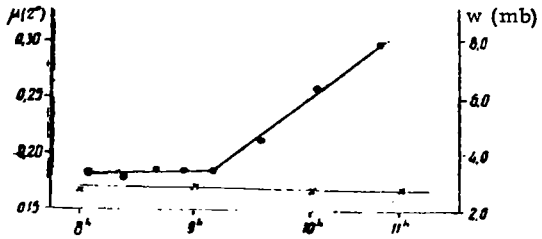

Figure 28. Example of Daytime Variation of Absolute Humidity w (crosses) and of the Directed Scattering Coefficient $\mu(2°)$ (points); $\lambda = 0.553\,\mu m$ (summer observations).

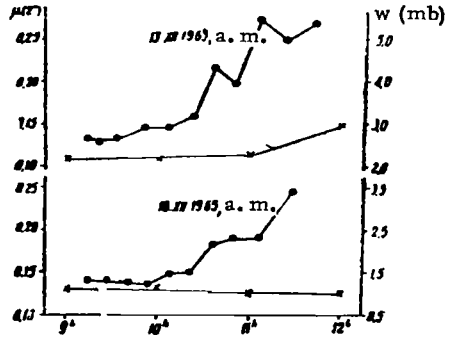

Figure 29. The Same as in Fig. 28 (winter observations.).

The interpretation of the winter time observations, however, is less definite. A distinct correlation between the temporal behavior of the directional scattering coefficient $\mu(2°)$ and the absolute humidity is noted on 6 of 16 days (Fig. 29). On two days the connection between humidity variation and variations in the value of $\mu(2°)$ was observed only at midday when the dense haze appears. On the remaining days the fluctuations of μ (2°) were practically unrelated to the absolute humidity variations. An increase in the μ (2°) function was accompained both by a decrease and increase in humidity.

Thus, it is impossible to draw a definite conclusion concerning the predominance of dry or wet atmospheric haze particles under winter conditions. This conclusion agrees with the results of [58, 95].

2. Optical Thickness. Atmosphere Stability

Spectral measurements of atmosphere transmission have recently been made at the Astrophysics Institute AN KazSSR in conjunction with the sky brightness observations, at small angular distances from the sun, described above. The measurements were made on the spectrophotometer with automatic spectrum recording described in Part 1 of this paper [33]. Atmosphere transmission coefficients have been measured by various observers on the V. G. Fesenkov photometer, fitted with three Schott filters—blue (λ_{eff} = 0.455 μm), green (λ_{eff} = 0.546 μm) and red (λ_{eff} = 0.636 μm), for a long period of time, starting in 1946, under the direction of Ye. V. Pyaskovskaya-Fresenkova.

Analyzing the data from the aureole photometer observations, we separated out the data relating to quasi-stable periods and to periods of serious deviations from stability. We will present some results of analyzing the observations during the 1949-1963 period.

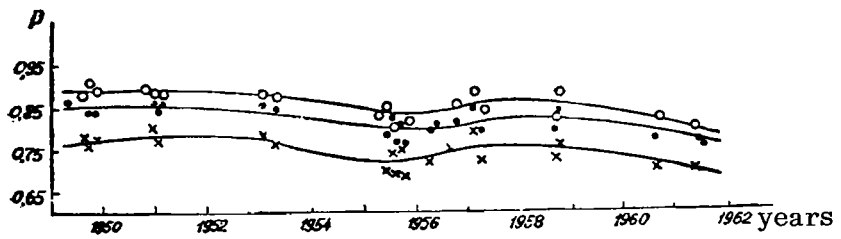

Figure 30. Circles Correspond to λ= 0.636 μm, Points—to λ= 0.546 lm, Crosses—to λ= 0.445 μm.

The behavior of the transmission is shown in Fig. 30 for all the years of observations with the aureole photometer at λ_{eff} = 0.445, 0.546 and 0.636 μm. Each point represents the value of p, averaged over a month (unfortunately, data do not exist for all the years and the months of each year).

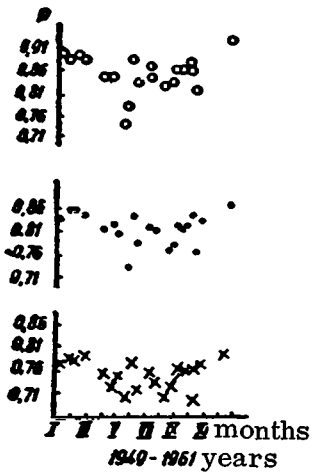

Figure 31. Average Annual Transmission Variation. Circles Correspond to $\lambda = 0.636\,\mu m$, Points—to $\lambda = 0.546\,\mu m$, Crosses—to $\lambda = 0.445\,\mu m$.

The average annual behavior of the transmission (from data for all the years) is shown in Fig. 31. The points reflect the p values over a ten-day period of the designated month.

The results of determining the average transmission and the limits of its variation during the entire period and during the individual seasons are listed in Table 10 (the corresponding optical thickness values are enclosed within the parentheses). From the table it is seen that the highest transmission is observed in winter, a somewhat lower value—in the autumn, and a still lower value—in spring and in summer; the extent to which this is true varies for different spectral regions. It should be realized that the number of measurements is quite different for each season (most observations were made in the autumn). The transmission is clearly lower in the afternoon than in the morning.

After representing the λ dependence of the aerosol optical thickness τ_D in the form $\tau_D = \frac{k}{\lambda^n}$ or $\lg \tau_D = c - n \lg \lambda$, one can attempt to determine the exponent n for those series of measurements where a linear dependence of $\lg \tau_D$ on $\lg \lambda$ is observed. Of the 26 series of measurements represented here, 18 were characterized either by a nonselective dependence of τ_D on λ or by a decrease of τ_D with an increase in wavelength. In five cases a maximum and in two cases a minimum was observed at $\lambda = 546\,\mu m$. One series showed an increase of τ_D with λ. The exponent n could be determined for 11 of the 18 series because the dependence of $\lg \tau_D$ on $\lg \lambda$ was linear. The results are shown in Table 8. The average value of n is equal to 0.81, and the range of variation of n is quite large—from 0.30 to 2.15.

Thus, from quite a large series of observations it is seen that the use of a certain exponent n cannot always be justified to characterize the spectral dependence of the aerosol optical thickness. An increase of τ_D with a decrease in λ or a nonselective dependence on λ is observed in only 70% of the cases, but of these the number of series, for which a linear dependence of $\lg \tau_D$ on $\lg \lambda$, exists, amounts to less than half (about 40%) of the total number of series. The exponent n of the individual series can differ drastically from the average value.

Values of the total optical thickness τ_h and of the aerosol optical thickness τ_D, determined under typically quasi-stable conditions, are shown in Figs. 32 and 33, respectively. The optical thickness values are rounded off to hundredths and are grouped.

From the figures it is seen that the range of variation of the optical thickness values increases with an increase in wavelength. For $\lambda = 0.445\,\mu m$ the optical thickness can vary by about a factor of two from series to series, by a factor of

TABLE VIII.

Date	n
12. III 1953, p.m.	0.52
4. VI 1953, a.m.	0.59
15. IX 1954, a.m.	1.12
6. X 1954, p.m.	0.80
7. X 1954, a.m.	1.35
8. X 1954, a.m.	0.75
9. X 1954, a.m.	1.10
9. X 1954, p.m.	0.62
24. X 1954, p.m.	0.83
11. VII 1955, p.m.	0.96
15. VIII 1955, p.m.	0.30
n_{avg}	0.81

≈ 2.5 for $\lambda=0.546\ \mu$m, and by almost a factor of four for $\lambda=0.636\ \mu$m. This is associated with an increase in the importance of the Rayleigh optical thickness in the short wavelength region of the spectrum and with the fact that the aerosol optical thickness τ_D depends weakly on λ (Fig. 34). Of special interest is the fact that the frequency with which certain values of both τ_h and τ_D are observed is characterized by a bell-shaped curve with a fairly sharp maximum; certain average optical thickness values are observed very frequently whereas examples of appreciable deviations from these average values are rare. /47

There is no doubt that τ_h and τ_D values, lying within wider limits, would be observed if a larger mass of data were used. But the relationships for quasi-stable periods remain basically the same.

The method, described in the first part [33], for monitoring atmospheric transmission from the slope of the line $\lg\frac{B}{m_\odot}=f(m_\odot)$ is very useful in interpreting the spectral measurements presented below.

The results of spectral observations of the transmission, determined by two methods—according to Bouguer (p_b) and from the slope of the line $\lg\frac{B}{m_\odot}=f(m_\odot, p_o)$—are given in Table 11. Values of the instability factor $\varkappa$ (%), which sometimes vary markedly over the spectrum, were determined on a number of days. On Jan. 6, 1965 and June 5, 1965 the $\varkappa$ factor was practically equal to zero. This means that in this case the instrument errors are greater than the errors produced by the change in the atmosphere optical properties. It makes sense in only this case to determine the rms error in the value of p_b by the least squares methods. Cases of such stability are extremely rare. It usually amounts to about 2-3%. An example of the daytime behavior of $\lg\frac{B}{m_\odot}$, $\lg E$ and $\mu(2°)$ as a function of the atmosphere mass $m_\odot$ is presented in Fig. 35, a, ($\varkappa=2,5\%$).

The parallelism of the line, representing the daytime variation of $\mu(2°)$, and the abscissa axis, which indicates the degree of transmission variation [32], is disturbed when the instability is large. If $\lg\frac{B}{m_\odot}$ is a linear function of the atmosphere mass $m_\odot$, then one can determine the factor $\varkappa$. Figure 35, b, in which the results of observations on Sept. 18, 1965, a.m., are presented, exemplifies such a quasi-stable day. The function μ (2°) has a marked slope with respect to the abscissa axis (curves 3). The transmission increased until noon. The slopes of the lines—Bouguer and $\lg\frac{B}{m_\odot}=f(m_\odot)$—are different; $\varkappa=8\%$. /48

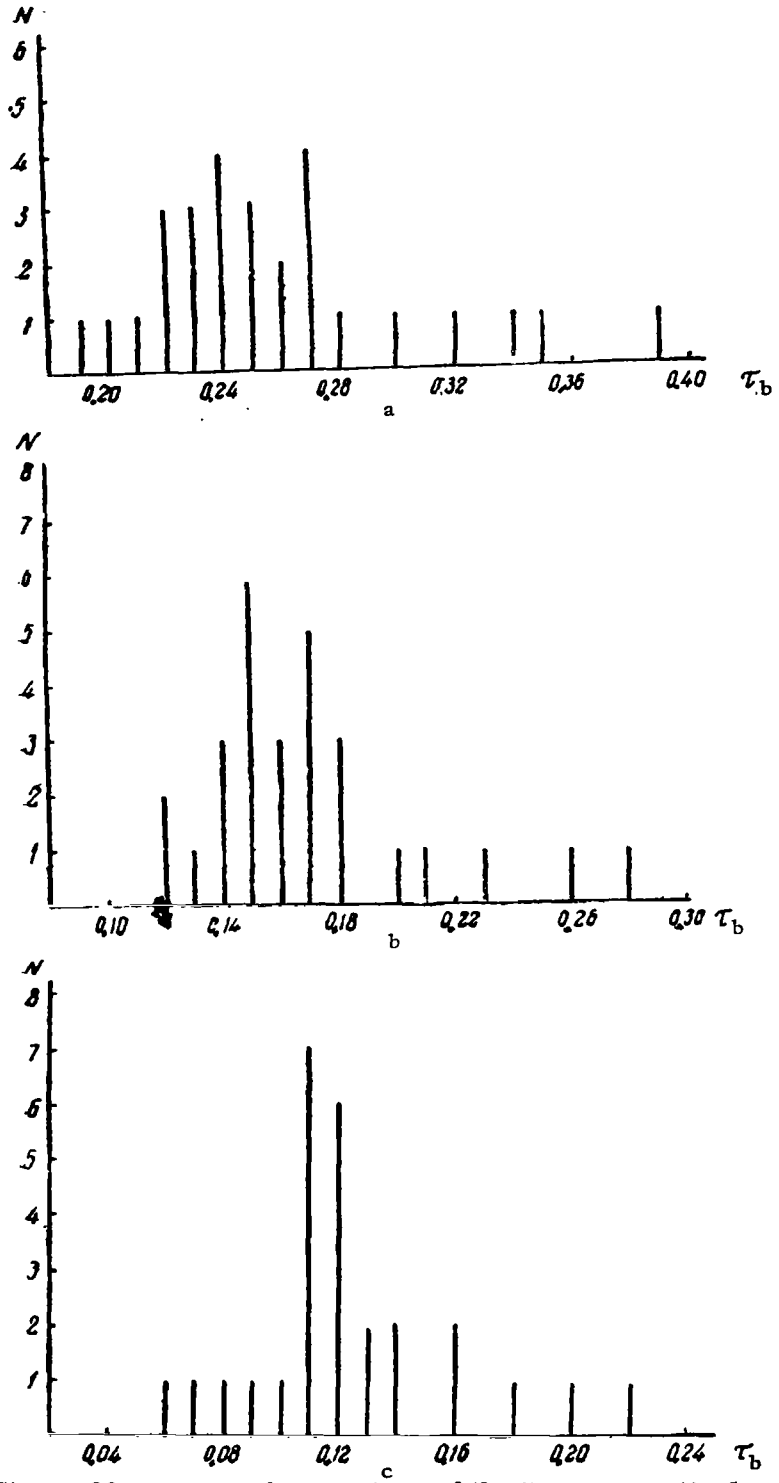

Figure 32. Range of Variations of the Bouguer Optical Thicknesses τ_b, N is the Number of Measurement Series. a) $\lambda = 0.445$ μm, b) $\lambda = 0.546$ μm, c) $\lambda = 0.635$ μm.

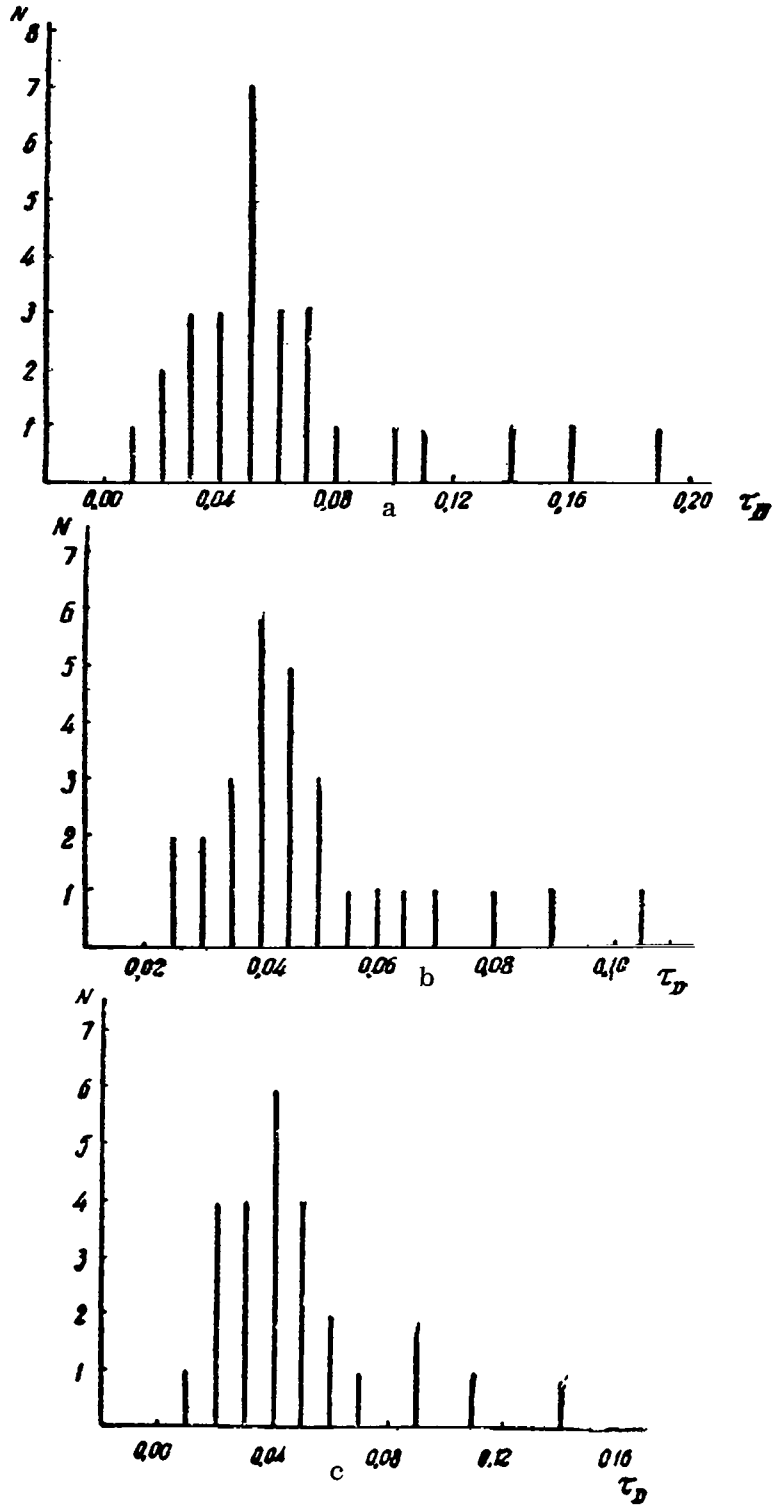

Figure 33. Range of Variations of Aerosol Optical Thicknesses τ_D. a) $\lambda = 0.445$ μm, b) $\lambda = 0.546$ μm, c) $\lambda = 0.635$ μm.

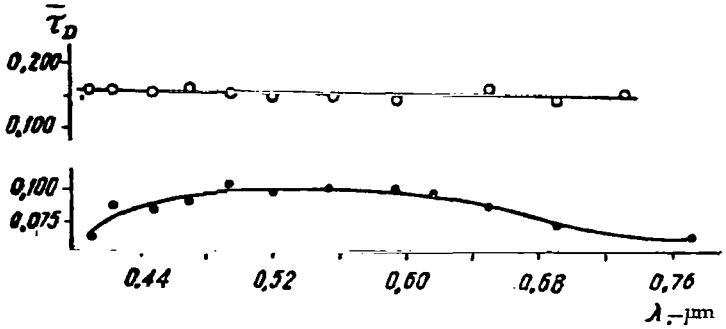

Figure 34. Dependence of τ_D on λ (circles—summer, points—winter data).

Numerical values of the optical density D of the atmospheric aerosol are listed in Table 12 for different λ, the errors, which depend on the degree of atmospheric stability and can be estimated from the $\varkappa$ factor, are indicated. The use of the instability factor for estimating errors enables one to judge, with reliability, the authenticity of the observed effects and of the values of the individual atmospheric parameters. Thus, after representing the atmospheric optical density as a function of λ^{-4}, one can obtain lines whose linearity is disturbed only by the presence of ozone. This enables one to determine on each day the ozone optical density and the amount of ozone. Results of such measurements are listed in Table 9. /49

The ozone content varied from 1.6 ($\pm$0.4) to 4.9 ($\pm$7) mm. The average content is equal to 3.0 mm.

Let us note that the error in determining the ozone thickness from the Chappuis band depends on the accuracy with which the transmission is determined throughout the entire visible portion of the spectrum. The error in determining the equivalent ozone thickness χ depends on the accuracy with which $D = -\lg p$ is determined, i.e., the accuracy of determining the transmission factor p. In view of this, the accuracy of the χ determination does not exceed 10%, even on a stable day ($\varkappa \sim 1\%$). For less stable days, the accuracy is correspondingly reduced.

3. Properties of the Aerosol Scattering Function, Interrelationship of Certain Parameters, and Pure Absorption in Aerosols

Since the individual factors do not function independently of each other, the establishment of a relationship for as large a number of parameters as possible, taking their spectral dependence into account, is desirable. This is a very complex problem. We have attempted to establish a relationship only among the parameters τ_b, τ_o, τ_R, τ_a and Γ, which become possible after a consideration of the data from direct observations of the $\mu(\varphi)$ functions and the determination of some of the characteristic properties for the function $\mu_1(\varphi)$ and the aerosol indicatrix $\mu_D(\varphi)$. From these data one can trace the wavelength dependence of $\mu(\varphi)$. With an increase in λ the effect of aerosols increases and Rayleigh and multiple scattering

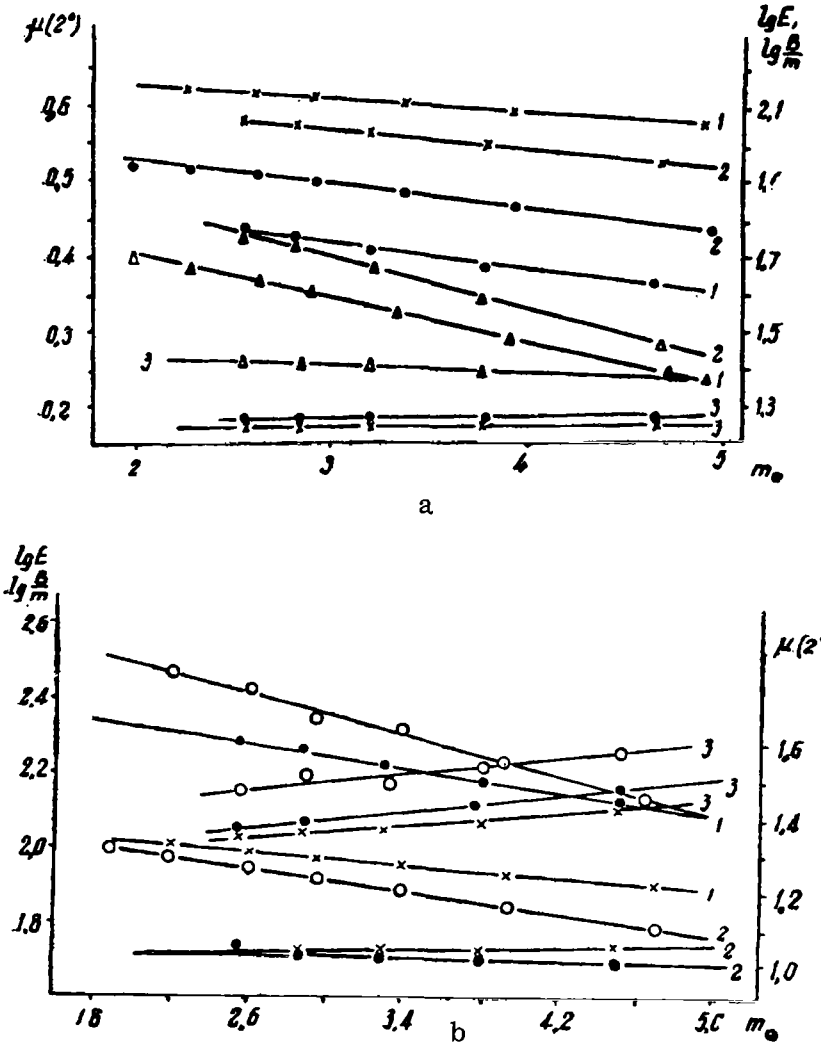

Figure 35. Behavior of Bouguer Lines (1), $\lg\frac{B}{m_\odot}=f(m_\odot)$ (2) and $\mu(2^\circ)$ (3) in Different Spectral Regions on a Stable (a) and Quasi-Stable (b) Day.

decrease. These factors play a major role and affect the overall shape of the spectral dependence of the function $\mu(\varphi)$.

The function $\mu(\varphi)$ in the ultraviolet region of the spectrum is characterized by a very small degree of asymmetry. This means that the component of the scattered light intensity caused by multiple scattering and reflection from the underlying surface is approximately symmetrical with respect to the scattering angle Φ, equal to 90°. The small diffraction "point" of the function $\mu(\varphi)$ in the ultraviolet region is caused by the aerosol and not by secondary effects (see Fig. 19). Theoretical calculations confirm the small degree of asymmetry of the

/50

TABLE IX. Equivalent Ozone Thickness χ

Date	28. XII 1964, a.m.	4. I 1965, a.m.	6. I 1965, a.m.	6. I 1965, p.m.
χ, mm	4.9±0.7	1.6±0.4	4.1±0.4	4.1±0.4

Date	6. V 1965, a.m.	12. V 1965, a.m.	15. V 1965, a.m.	5. VI 1965, a.m.
χ, mm	1.6±0.4	1.6±0.4	1.8∓0.4	4.9±0.7

Date	7. VI 1965, a.m.	4. X 1965, a.m.	14. X 1965, a.m.
χ, mm	2.3±0.3	2.3±0.3	1.6±0.3

$B_2 + B_q$ component of the brightness. These properties of the $B_2 + B_q$ component, and consequently of $\mu_2+\mu_q$, permit considerable simplification of the problem if, in addition, some properties of the aerosol scattering function are taken into account. The latter, as is known, is severely elongated forward because of the Mie effect. Studies in the atmosphere near the earth's surface have repeatedly confirmed this situation. Thus far, however, no aerosol scattering indicatrix, relating to the entire atmosphere height, has been evolved. The method sometimes used for isolating the aerosol indicatrix by subtracting the Rayleigh function from the observed $\mu(\varphi)$ function, in fact gives nothing at all. The "aerosol" indicatrix obtained in this manner, as stated above, cannot even be considered as an approximation.

This difficulty cannot be overcome by increasing the accuracy of the measurements. Fluctuations of the atmosphere components (its transmission, aerosol composition, etc.) impose limitations and prevent a highly accurate determination of the function.

A quite definite conclusion follows from this: the energy, scattered backward by the aerosol, can be neglected in many problems. Without particular difficulty it can be determined in what problems this can be done because it is known that the total energy scattered "backward" by the aerosol amounts to only a few percent of the optical thickness τ_0.

On the other hand, when the scattering indicatrices are not too elongated, the sky brightness component B_2, produced by multiple light scattering, has an extremely weak angular dependence [79]. The same can be said about the component B_q.

If it is assumed that the aerosol scatters light only in the forward hemisphere and that the brightness components B_2 and B_q are symmetrical with respect to the

scattering angle $\varphi = 90°$, then a quantitative interrelationship can be established between a number of optical parameters.

From the first assumption it follows that the aerosol scattering optical thickness τ_D can be expressed by the formula:

$$\tau_D = 2\pi \int_0^{\pi} \mu_D(\varphi) \sin \varphi d\varphi = 2\pi \int_0^{\pi/2} \mu_D(\varphi) \sin \varphi d\varphi. \tag{2.14}$$

On the basis of the second assumption, one can write the relation:

$$2\pi \int_0^{\pi/2} (\mu_R + \mu_2 + \mu_q) \sin \varphi d\varphi = 2\pi \int_{\pi/2}^{\pi} (\mu_R + \mu_2 + \mu_q) \sin \varphi d\varphi, \tag{2.15}$$

where μ_R is the absolute Rayleigh scattering indicatrix, μ_2 is an addition to the absolute brightness indicatrix that depends on multiple scattering, and μ_q is an addition caused by light reflection from the underlying surface.

If the aerosol only scatters light in the forward hemisphere, then /51

$$2\pi \int_{\pi/2}^{\pi} (\mu_R + \mu_2 + \mu_q) \sin \varphi d\varphi = 2\pi \int_{\pi/2}^{\pi} \mu(\varphi) \sin \varphi d\varphi. \tag{2.16}$$

The optical thickness τ_o, determined from the observed brightness indicatrix, can be expressed by the following formula:

$$\tau_o = 2\pi \int_0^{\pi} \mu(\varphi) \sin \varphi d\varphi = 2\pi \int_0^{\pi/2} \mu_D(\varphi) \sin \varphi d\varphi + 2\pi \int_0^{\pi/2} (\mu_R + \mu_2 + \mu_q) \sin \varphi d\varphi + 2\pi \int_{\pi/2}^{\pi} \mu(\varphi) \sin \varphi d\varphi. \tag{2.17}$$

Using Eqs. (2.14) and (2.17), one can arrive at the relation

$$\tau_D = \tau_0 - 2 \cdot 2\pi \int_{\pi/2}^{\pi} \mu(\varphi) \sin \varphi d\varphi. \tag{2.18}$$

Introducing the observed asymmetry coefficient of the scattered light energy

$$\Gamma = \frac{\int_0^{\pi/2} \mu(\varphi) \sin \varphi d\varphi}{\int_{\pi/2}^{\pi} \mu(\varphi) \sin \varphi d\varphi},$$

we obtain

$$\tau_D = \tau_0 \left| \frac{\Gamma - 1}{\Gamma + 1} \right|. \tag{2.19}$$

Since the Bouguer optical thickness τ_b is the sum of three components: Rayleigh τ_R, aerosol τ_d and true absorption τ_a, then the desired interrelationship among the optical parameters is written in the form

$$\tau_b = \tau_R + \tau_0 \left(\frac{\Gamma - 1}{\Gamma + 1} \right) + \tau_a. \tag{2.20}$$

The approximateness of this formula is caused by the simplifying assumptions that have been made. Assuming that the term $B_2 + B_q$ is symmetrical with respect to $\varphi = 90°$ and subtracting twice the amount of energy scattered "backward," we thereby somewhat overestimate the value of τ_D because at small angles multiple scattering is somewhat greater because of the indicatrix effect. However, assuming that the aerosol scatters absolutely nothing "backwards," we reduce the value of τ_D determined by this fashion. To clarify to what extent these errors compensate each other in each specific case is an extremely complex problem. Therefore an evaluation of the reliability of the derived expression, relating a number of important parameters, must be based on direct observations.

Observational data of the sky brightness in the solar almucantar, obtained by various observers and under different conditions, were used for this purpose. For the observations the transmission coefficient p_b was determined by the Bouguer method and, thus, one could find both the left $\tau_b = -\ln p_b$, as well as

/52

the right side of Eq. (2.20) (here it is necessary to specify the optical thickness τ_a in the absorption band region). The results of these investigations are listed in Table 13. The results of calculations of the transmission coefficient from Eq. (2.20) are compared in Fig. 36 with the Bouguer values, determined from direct observations.

From these data it is seen that Eq. (2.20) can serve as the basis for a shortcut method for determining p_b, which has big advantages. It is applicable over a wide range of optical thickness, wavelengths and observation conditions (both summer, and winter with a snow cover).

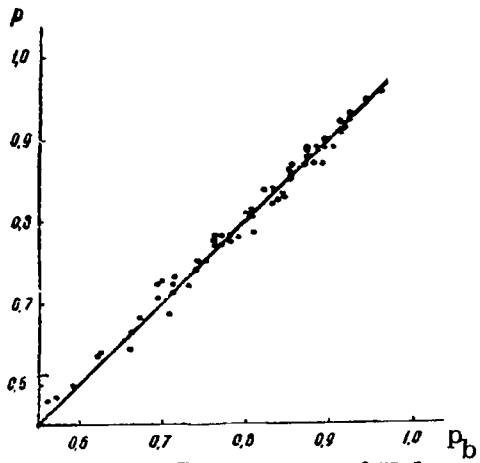

Figure 36. Comparison of Values of the Atmospheric Transmission Coefficient, Determined by the Bouguer Method (p_b) and from Sky Brightness (p) Under Summer and Winter Conditions.

It should be mentioned that Eq. (2.20) can be used for the ultraviolet region only under the condition that the observations are within fairly narrow spectral intervals to avoid significant errors due to the Forbes effect.

The interrelationship of the different parameters, described by Eq. (2.20), opens up the possibility of solving other interesting problems. Thus, one of the problems of ozonometry is the measurement of the amount of ozone in the atmosphere with the effect of aerosol attenuation of light taken into account. If the aerosol attenuation in the Hartley band is sufficiently large and, moreover, it varies appreciably over the spectrum, then the determination of the ozone content encounters serious difficulties, in connection with the necessity of isolating the components of the optical thicknesses. Thus far there are insufficient reliable data, for this spectral region, concerning the individual components of the atmosphere extinction. Using Eq. (2.20), which should be satisfied most accurately in the ultraviolet region itself, one can isolate the desired optical thickness, for light absorption by ozone, from the difference of the observed and calculated values of τ_b. The aerosol optical thickness can be calculated on the basis of the formula given above: $\tau_D = \tau_0\left(\frac{\Gamma-1}{\Gamma+1}\right)$, which also is most applicable in the ultraviolet region for the same reasons.

At the same time, it should be mentioned that in establishing the interrelationship of the parameters cited above, we bypassed the problem of the components of τ_a. Light absorption can be caused both by the presence of molecular bands (for example, the Chappuis band) and by the presence of an aerosol.

The question of pure light absorption by an atmospheric aerosol has not been studied sufficiently. In spite of an abundance of theoretical papers on light scattering by various types of aerosol praticles, few calculations of the pure absorption have been made, and the experimental data, especially for dry particles, are inconsistent [96-100]. /53

A portion of the total aerosol optical thickness, depending on pure absorption, can characterize the absorbing properties of the aerosol layer.

The direct method of experimentally isolating aerosol optical thicknesses reduced to a simultaneous determination of the transmission coefficient p_D and the scattering indicatrix $\mu_D(\varphi)$ of the aerosols.

Starting with data from such observations and using the known relationships $\tau_D = -\ln p_D$, $\tau_1 = 2\pi \int_0^\pi \mu_D \sin\varphi d\varphi$; and $\tau_D = \tau_1 + \tau_a$, one can fine the values of τ_1 and τ_a.

However, it is quite difficult to accomplish this direct method. To calculate the integral $\int_0^\pi \mu_D \sin\varphi d\varphi$ it is necessary to know the $\mu_D(\varphi)$ functions for all scattering angles φ, in particular at small angles φ (with respect to the direct ray). The difficulties involved in these measurements are well known. Meanwhile, the coarse aerosol particles scatter light primarily forward, but the shape of the indicatrix at small angles for polydisperse aerosols can be very complicated, and and extrapolation toward small angles can lead to large errors [12]. In view of this we have developed a laboratory method of isolating the optical thickness τ_1 and τ_a with which indicatrix measurements can be bypassed.

The concept of the method is as follows. The total optical thickness τ_D of the aerosol layer is determined by measuring the incident energy I_0 and the energy I transmitted by the layer, if multiple scattering does not exert a significant effect. The transmission coefficient $p_D = I/I_0$ characterizes the light attenuation due to scattering and absorption.

If, by some method, all the scattered light is collected and directed onto a receiver that measures the transmitted energy, then the reading for I is increased by some amount ΔI.

It is obvious that the value p_a, defined by the formula

$$p_a = \frac{I + \Delta I}{I_0},$$

is the transmission coefficient of the layer, characterizing only the light attenuation due to absorption.

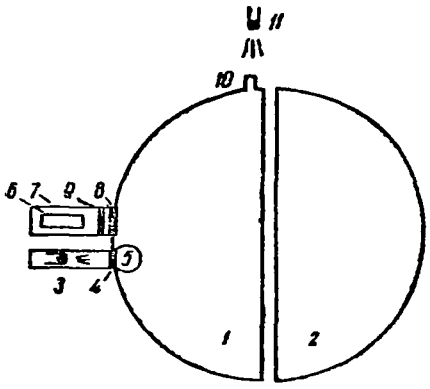

Figure 37. Sketch of Laboratory Apparatus.

The apparatus, built by us and enabling us to utilize this method of isolating the optical thicknesses, is arranged in the following manner (Fig. 37). An Ulbricht sphere, whose surface is coated with magnesium oxide, is used as the system for "collecting" the light energy ΔI. The sphere comprises two hemispheres (1 and 2), which can be separated, sliding along tracks. The sphere is 20 cm in diameter. Light from a small lamp enters through the tube (3), on the end of which is mounted a frosted glass (4), also coated with magnesium oxide ($\varnothing$ = 20 mm). A hemispherical glass cover (5), on the surface of which is deposited a layer of the aerosol to be studied, is put on the tube. Light, multiply scattered within the sphere, is measured by the photomultiplier (6), in the tube (7) whose end (8) is located flush with the surface of the sphere and is also covered by frosted glass ($\varnothing$ = 20 mm) and magnesium oxide. Interchangeable interference filters, with a half bandwidth of 0.010-0.012 μm and maximum transmission wavelengths λ. equal to 0.405, 0.496, 0.556 and 0.696 μm, were mounted in front of the FEU-51 photomultiplier. An IKS-2 filter and an FEU-62 photomultiplier (λ_{eff} = 0.977 μm) were used for measurements in the near-IR region.

A 10-mm diameter tube (10) is located in the upper portion of the sphere. Its end (without optics) is also flush with the surface of the sphere. Light from the upper illuminator (11) can enter the sphere through the tube opening. The photocurrent, amplified by a differential cathode follower, was recorded on an EPP-09 automatic recorder.

The method of observations was as follows. A very thin glycerin film was deposited onto the transparent walls of a hemispherical glass bulb. By sequentially placing the bulb, dust-free and coated over its entire surface with the dust to be studied, over the tube (10), one could determine the total optical thickness by the usual method.

Then the sphere was pulled apart and the bulb was put on the tube (3). By making similar readings with dust (I') and without dust (I'_0) with the hemispheres closed, one could determine τ_a. In the given case the redistribution of the light energy, through scattering by the aerosol particles, does not alter the brightness of the sphere walls. A change in brightness can occur only through absorption. Thus, the readings I' and I'_0 at low absorptions should be exactly identical if the aerosol particles do not absorb light energy. This was confirmed experimentally with nonabsorbing particles (ATS-4 white plastic powder).

In calculating τ_a from measurements of I' and I'_0 it is most essential to take account of light absorption in aerosols due to its repeated reflection from the sphere walls. The coefficient $p_a = -\ln \tau_a$ can be calculated, if the ratio I'_0/I' is

known, starting from the following considerations. Since the end surfaces of the tubes through which light passes are small compared with the sphere surface, in the calculations only the absorption at the sphere walls need be taken into account. If η is the diffuse reflection coefficient, then for light entering the sphere with no aerosol present (no dust on bulb) the wall brightness is expressed by the series $B\eta + B\eta^2 + \ldots + B\eta^n + \ldots$, a geometric progression, which equals

$$I_0' = \frac{B\eta}{1-\eta}. \tag{2.21}$$

as $n \to \infty$. We have expressed the wall brightness by $B\eta$ for a single reflection (for a second reflection it is equal to $B\eta^2$, for the third—$B\eta^3$, etc.).

The calculation is similar for the case when the bulb with aerosol is placed on the illuminator. Here, $B\eta p_a$ should replace $B\eta$ because the light is attenuated during the initial event (incidence and reflection) by an amount determined by the absorption coefficient. In the second reflection act for calculating the "second order" brightness, one should take into consideration that part of the flux from /55
the entire sphere, incident on some element of sphere surface ΔS, passes through the bulb with the aerosol. If the bulb is placed in the center and it subtends a solid angle $\Delta\omega$, from any point on the sphere, then the fraction of the total light flux, incident on ΔS, after absorption through multiple scattering amounts to $\frac{\Delta\omega}{\pi}$, because the illumination of the element ΔS by all the flux is equal to $\pi B\eta p_a$, and the flux, passing through the bulb, is $\Delta\omega B\eta p_a$. Hence the "secondary" brightness will be

$$B\eta^2 p_a\left[\left(1-\frac{\Delta\omega}{\pi}\right) + \frac{\Delta\omega}{\pi} p_a^2\right], \tag{2.22}$$

since the light passes through the bulb walls twice. The common multiplier p_a remains unchanged because it represents the initial act of the passage of all (not just part) of the initial light through the bulb walls. We note that this initial act plays a very significant role at large values of p_a. In the case given, because $\frac{\Delta\omega}{\pi} \approx 0.01$ (a small quantity) taking account of the absorption due to multiple scattering adds relatively little. In the third act, for the "third order" brightness we have

$$B\eta^3 p_a\left[\left(1-\frac{\Delta\omega}{\pi}\right) + \frac{\Delta\omega}{\pi} p_a^2\right]^2 \tag{2.23}$$

and so forth. Finding the series limit, we obtain

$$I' = \frac{B\eta p_a}{1-\eta\left[\left(1-\frac{\Delta\omega}{\pi}\right)+\frac{\Delta\omega}{\pi}p_a^2\right]}. \qquad (2.24)$$

From Eqs. (2.21) and (2.24) we have

$$\frac{I'}{I_0'} = \frac{(1-\eta)p_a}{1-\eta\left[\left(1-\frac{\Delta\omega}{\pi}\right)+\frac{\Delta\omega}{\pi}p_a^2\right]}. \qquad (2.25)$$

The following comments must be made. The bulb used in the experiments is hemispherical with a diffuse bottom through which the primary light flux enters. Upon multiple reflection from the sphere walls, a portion of the rays pass through the bulb wall. This should not introduce much difference from the calculations made under the assumption that the bulb is spherical and is traversed twice by the rays reflected from the sphere walls without additional scattering from the diffuse bottom of the bulb. The bulb itself may not be located at the center of the sphere. Calculations, made for the case when the bulb is located at the center, remain valid for any case because the total light field of the multiply reflected and scattered light within the sphere is uniform; the energies passing through some constant volume ΔV are identical for any point of the sphere.

For specific apparatus parameters of η and $\Delta\omega$, Eq. (2.25) permits one to find p_a from measurements of I'/I'_0.

A small portion of the flux in the initial act is scattered "backward" by the aerosol and then, being reflected from the diffuse bottom on which the bulb is mounted, is again scattered by the aerosol. A certain portion of the flux passes through the aerosol obliquely. Therefore the values of τ_a determined by the proposed method will be somewhat too large and, consequently, will give some upper limit for the pure absorption effect. Since the light fluxes pass through the aerosol layer in very different directions, one can assume that the optical thickness τ_a determined from Eq. (2.25) characterizes some average oblique orientation, rather than perpendicular, of the absorbing layer. Therefore the values of t_a should be divided by some certain coefficient and, thereby, yield the values for perpendicular orientation. Starting from the bulb dimensions and the aerosol layer thickness, one can find the average weighted value of the optical path $\bar{l}$ of a ray passing through the hemispherical aerosol layer. The ratio of $\bar{l}$ to the layer thickness was found equal to 1.57, which also yields the appropriate correction coefficient. /56

Studies were made with different aerosol particles: soot; coal slag dust; sand dust; clay dust; cement dust; room dust; meteoritic particles, obtained by mechanical crushing of stony meteorites ("Elenovka" and "Saratov"); volcanic lava particles, obtained by crushing gray and red lava; graphite.

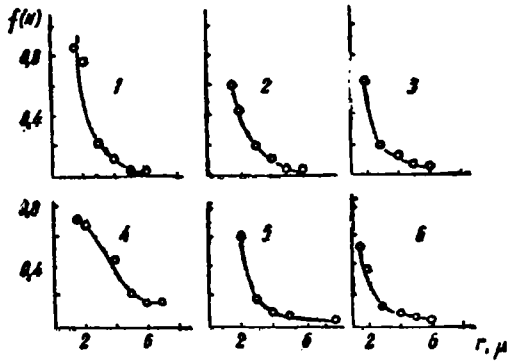

Figure 38. Aerosol Size Distribution Functions: 1—Sand Dust, 2—Cement Dust, 3—Room Dust, 4—Soot Particles, 5—Slag Particles, 6—Clay Dust.

The particle size distribution functions for the coarse fraction of the aerosols studied by us are approximately identical. The particle size distributions of some of the aerosols, determined with the aid of a microscope by direct measurements of the coarsest fraction (starting with 3.3 μm and larger), are shown in Fig. 38.

The ratios of the absorption optical thicknesses t_a to the total optical thicknesses are shown in Fig. 39 for some aerosols.

The plotted values of τ_a/τ_D are average data obtained from several series at different τ_D. The bulb was recoated with dust for each series so that the particle distribution may differ from series to series. The aerosol layer on the bulb was not completely uniform. The value of τ_a also depends on external conditions (temperature, humidity). All these factors lead to deviations of 20-30% from the plotted average values of τ_a/τ_D. However, the relative spectral behavior of the curves is quite stable in that we verified them by repeating several series of measurements. The experimental results are listed in Table 10.

/57

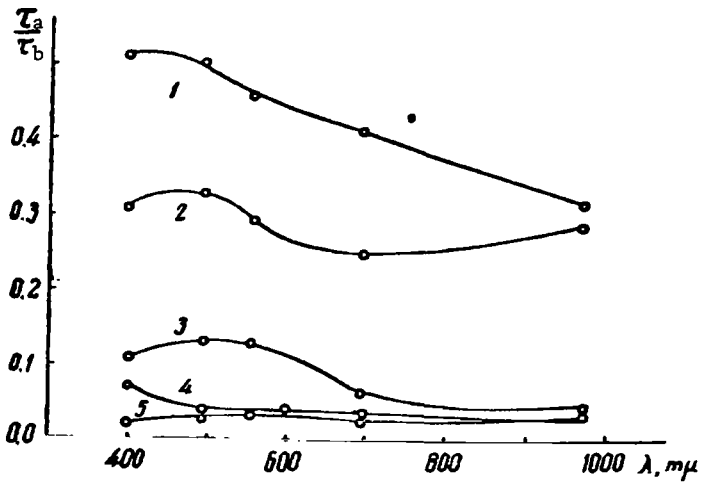

Figure 39. Ratio of the Absorption Optical Thicknesses to the Total Thickneses for Aerosols as a Function of the Wavelength: 1—Soot Particles, 2—Coal Slag Particles, 3—Sand Dust, 4—Clay Dust, 5—Particles of "Elenovka" Meteorite.

TABLE 10. Values of the Ratio of the Light Absorption Optical Thicknesses to the Total Optical Thicknesses of Some Aerosols

Material	λ, μm					
	0,398	0,405	0,496	0,556	0,696	0,977
"Elenovka" meteorite	0,021	—	0,027	0,033	0,024	0,030
"Saratov" meteorite	0,053	—	0,080	0,048	0,046	0,055
Lava (red)	0,039	—	0,075	0,19	0,030	0,018
Lava (grey)	0,039	—	0,088	0,078	0,096	0,074
Graphite	0,41	—	0,32	0,38	0,38	0,54
Soot	—	0,52	0,50	0,46	0,42	0,31
Coal slag	—	0,31	0,33	0,29	0,25	0,29
Room dust	—	0,13	0,10	0,056	0,080	0,026
Clay dust	—	0,095	0,14	0,055	0,055	0,041
Sand dust	—	0,10	0,13	0,13	0,061	0,044

Note: Commas represent decimal points.

On the basis of the data presented one can draw the following conclusion. Coal slag dust and especially soot are distinguished by large values of τ_a/τ_D.

The presence in the atmosphere of such aerosols as clay and sand dust does not lead to appreciable light attentuation due to pure absorption. For example, if the atmosphere optical thickness τ_b in the $\lambda=0.55$ μm region, determined from the Bouguer method, amounts to 0.2, then the aerosol optical thickness τ_D after subtracting the Rayleigh τ_R from τ_b (for our observatory $\tau_R=0.085$ at $\lambda=0.55$ μm) will be equal to 0.115 if light absorption in the Chappuis band is neglected. In this case the optical thickness of light absorption by the aerosol, calculated from the data of Table 10 under the assumption that the aerosol is clay-sand dust, will be equal to 0.01 or amounts to approximately 5% of τ_b. The accuracy of the optical thickness determination by the Bouguer method in this spectral region usually amounts to ~ 7—8% when the stability of the atmospheric optical properties is controlled. Thus, we see that in mountainous and valley locales far from industrial centers the actual light absorption by the atmospheric aerosol is small. Moreover, it should be realized that a significant portion of atmosphere aerosols is small water droplets whose absorption in the visible spectrum is small. Finally, "dry" particles in the atmosphere can serve as condensation nuclei and be sheathed by a layer of water. The outer sheath plays a significant role in the attenuation of light by two-layer particles [12]. Therefore it is not mere chance that the search for atmospheric aerosol light absorption effects in daytime sky brightness measurements in mountainous locations did not lead to significant results [100].

/58

***

The data presented can be widely used in solving any problems associated with light propagation in a real atmosphere, in particular to solve the direct problem of determining the radiation field whose character depends primarily on the fundamental parameters discussed here.

Knowledge of the characteristic features and behavior of these parameters is also necessary to solve the most pressing inverse problem; the following, third, chapter of this paper is devoted to an analysis of this problem.

Chapter 3

THE POSSIBILITIES OF SOLVING THE REVERSE PROBLEM FROM OBSERVATIONS OF THE BRIGHTNESS AND POLARIZATION OF THE CLEAR, SKY DAYTIME /59

In atmospheric optics the term "inverse problem" refers to the study of atmospheric physical characteristics wholly or partly on the basis of observations of radiation that has been transformed by a medium.

Attempts to solve the inverse problem were begun immediately after the appearance of data on light scattering by aerosol particles; however, the early research primarily amounted to crude estimates only (the presence or absence of Mie particles, a large or small coarse particle fraction in the aerosol).

Among the earliest papers, the research of Siedentopf [101], which approached the problem of solving the inverse problem using models of a polydisperse aerosol, should be mentioned.

We do not intend to survey the work on solving the inverse problem in the atmosphere near the earth's surface. Let us only indicate that this type of research has been continued practically uninterruptedly and is being carried on at the present time. The results of this research have been published in a large number of papers. An attempt at some generalization of the data that have been gathered is made in the recently published review of K. Bullrich [50]. Information of a review nature, concerning measurements of scattering functions, can be found in the books by K. Ya. Kondrat'yev [34], G. V. Rozenberg [35], K. S. Shifrin [12], as well as in other monographs (for example, [58]). An objective evaluation of both foreign and domestic research is given in these documents. A large amount of original work, devoted to the inverse problem, has been done by K. S. Shifrin and co-workers [102-108].

The question of solving the inverse problem is considered in the present paper, not for the layer near the earth's surface but for the entire atmosphere thickness.

1. General Properties of the Atmosphere Aerosol

Let us briefly discuss those aerosol properties which are of greatest interest from the standpoint of the problem being considered (a detailed review of aerosol studies has been made by C. Junge [95]).

Particles of very different dimensions, from microscopic, representing groups of molecules, to so-called gigantic, with average radii of about 10-20 /60
μm are detected in the atmosphere.

The particles can be classified both in terms of size as well as in terms of their role in different atmospheric processes. The table, presented in C. Junge's monograph [95], which we have reproduced in Fig. 40, graphically illustrates this.

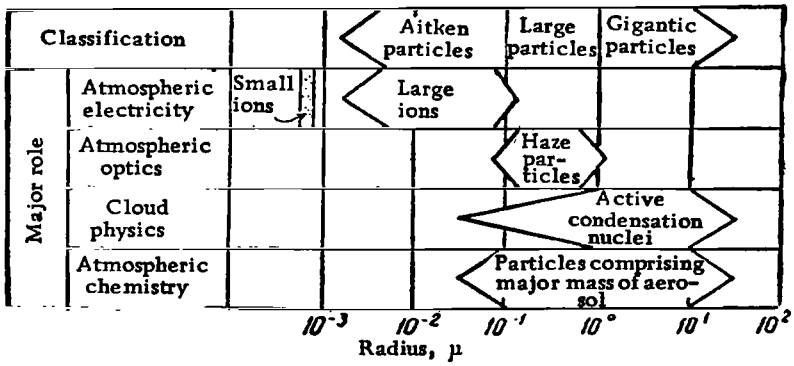

Figure 40. Classification of Atmospheric Aerosol Particles.

Direct methods of measuring particle numbers and distribution are extremely varied not only because of different sizes but also because of the different aerosol natures. In addition to the widely known counters of Aitken and Owens, centrifuges [112], various types of impacters [113], etc., as well as methods based on a determination of the particle diffusion coefficient [109], the mobility of charged particles in an electric field [110], and precipitation methods [111] are also used.

The total particle distribution can be determined by direct methods only through simultaneous measurement on different instruments because each instrument can cover only a limited portion of the distribution and can isolate only particles with certain physical properties. The fact that information on the total particle distribution has been inadequate up to now is explained by this. Only relatively recently, in spite of the prevailing opinion concerning the existence of discrete sharply defined aerosol groups, has it been concluded that a continuous distribution is more characteristic of the particle distribution [114, 115]. Until now there have been no reliable data on aerosol density; it is only known that in most cases its value varies from 1 to 2 g/cm^3.

The upper and lower limits of the particle distribution are subject to variations. The composition and nature of the particle size distribution can change from day to day. Examination of averaged data [114, 116, 117] shows that the particle distribution can be approximated by a smooth curve with a regular increase in the number of particles as their size decreases down to particle radii of about 0.1 μm. The maximum concentration lies in the 0.01-0.1 μm interval and most frequently corresponds to a radius of 0.03 μm.

In conjunction with established interrelationships, attempts have been made to explain the observed distribution theoretically, taking into consideration the simultaneous effect of coagulation and sedimentation processes [118], as well as condensation and evaporation. For the present, however, no satisfactory theory has been developed.

The mean data that have been obtained refer primarily to continental regions. /61
There are very few measurements for sea air. It is quite probable that the characteristics of maritime and continental aerosol are different. Starting from existing data [119], the maximum of the distribution for sea salt particles is located near a radius value of 0.25 μm.

The aerosol concentration undergoes drastic spatial and temporal changes. Depending on the conditions, the number of large particles in 1 cm^3 can vary from 10 to 10^5, with this not always being caused by the effect of industrial centers. The variation limits for very large particles are considerably tighter—from 0.1 to 1 cm^{-3}.

If aerosol particles can be crudely divided into maritime and contiental, on the basis of their origin, then , in terms of their physical structure, they can be classified as dry insoluble particles and slat solution droplets.

Most frequently encountered are particles, characterized by a change in size as a function of the relative humidity, with the rate or change being determined, in particular, by the ratio of insoluble to soluble fractions. In view of this, the question of aerosol properties under various relative humidity conditions is of interest. Some experiments have shown, for example, that at a relative humidity below 70% the dry fraction is an appreciable portion, whereas as the humidity increases beyond 70%, the particles assumed a droplet structure [120]. A further increase in humidity and a decrease in temperature lead to the formation of cloud droplets and crystals. In clouds and fogs, in contrast to clear weather conditions, a bimodal structure is often observed.

Studies of the chemical composition of an aerosol are highly complex. Thus, for example, at the present time it is impossible to say anything definite with regard to the most probable chemical composition of the Aitken particles. It is known that these particles, playing a most important role in the atmosphere, can lead to the formation of mists, after reactions between different gaseous impurities, through the dispersion of the surface material of the continents and oceans.

The combination of maritime aerosols with continental can lead to a wide variety of chemical reactions. By means of various new methods, including electron microscopy [123], various compositions of sea salt, combustion products and soil materials have been detected in aerosols. Chemical analysis results indicate the presence of iron, lead, manganese, copper and many other elements, as well as SO_4^2, NO_3, SO_4, NH_4, Cl ions, etc. Different organic compounds and mineral dust play a large role. In spite of numerous observations, the mechanism of particle formation has not been finally clarified.

The amount and distribution of aerosols change withthe height above the earth's surface [124]. The vertical profiles of aerosols can vary considerably with time [124]. A general tendency for the amount of aerosols to decrease with height is observed up to about 5 km, and in the upper layers of the troposphere their concentration is often found to be constant. Dust is often found at a level below temperature inversions. As a result of the effect of various contaminants, present over continents, the lowest five-kilometer thick layer

of the atmosphere can have an extremely complex aerosol structure. Above this layer, a more uniform aerosol distribution is found with average concentrations of 200-300 particles in 1 cm^3, determining an aerosol background which is caused by old aerosols [95]. Such a distribution and the presence of a background are associated with complex meteorological processes, turbulent diffusion, the rate of aerosol particle removal by elution, coagulation and gravitational precipitation. /62

Taking all these factors into account the making certain simplifications, one can formulate relatively simple differential equations enabling one to determine the steady-state conditions of an aerosol atmosphere [125-118].

As a result of studies of stratospheric aerosols, performed with rockets and balloons [125-128], it has been established that the concentration of Aitken particles decreases above the tropopause. For large particles, a maximum is found between 16 and 23 km. An analysis of stratospheric aerosol tests, performed with an electron microscope and x-rays, showed that the predominant element is sulfur in different compounds. Other elements, in particular Al, Cl, Ca and Fe, are present in small amounts. The sulfur undoubtedly originates in the troposphere.

Only small globules of manganese, Fe_2O_3 and a small amount of FeO were collected from aerosols originating in outer space, whose most important source is the zodiacal cloud [129-131]. The existence of a dust layer at a height of 15-25 km has been noted by several investigators. The band of nacreous and noctilucent clouds should also be mentioned. The latter are observed at a height of about 80 km. Cosmic, especially meteoritic, dust, entering the atmosphere at the rate of about 100 tons every day, undoubtedly plays an appreciable role in the formation of aerosol layers in the upper atmosphere. The study of the dust layer in the high layers of the atmosphere is currently being done by means of laser and radio observations [131, 132, 133] with the use of satellites [46] and rockets [45]. The data that have been obtained confirm, in particular, the existence of an extremely stable aerosol layer at a height of about 20 km [134, 46].

Even with a cursory summary of the most characteristic properties of an atmosphere aerosol, one can appreciate its extremely complex composition and variability. The character of the distribution and amount of aerosol depend on meteorological conditions, locale, season, height above sea level, activity of the various sources themselves and other causes. Many important questions, relating to aerosols, are still unexplained. Solving specific inverse problems requires as much reliable preliminary data as possible.

In view of this, we will attempt to consider in greater detail that information which, in our opinion, can facilitate solving the problem and, by using optical methods of studying the incoming radiation field, can determine the conditions under which one can expect favorable results.

2. Light Scattering and the Atmospheric Aerosol

The earth's atmosphere possesses one remarkable property: in spite of the continuously occurring circulation of air masses in it, gigantic processes of a turbulent nature and severe disturbances, clear cloudless weather is often established over vast regions of the earth's sphere and for a relatively long period of time. Cloudless days are frequently characterized by remarkable stability. The very existence of such conditions is, of necessity, explained by the formation, /63
in the atmosphere, of a stable equilibrium between different physical processes about which only small fluctuations are possible. When this condition is not fulfilled, the process must develop in one direction or another, which occurs, for example, during the formation and growth of clouds.

Thus, on clear cloudless days, characteristic of very large areas of the earth's surface, the aerosol composition can be quite stable for a long time which, undoubtedly, can serve as a starting point of the relationships being sought.

It has already been mentioned above that, within certain limits, the number of particles increases with a decrease in their size, with the change being so sharp that the size distribution curves are often plotted on a logarithmic scale.

After having selected an infinitely small radius increment dr, one can write the explicit equation

$$dn = f_0(r)\,dr, \tag{3.1}$$

where dn is the number of particles with radii from r to r + dr, and the function $f_0(r)$ characterizes the distribution density and represents the number of particles per unit interval of radius. The total number of particles, with sizes limited by the radii r_1 and r_2, is determined by the integral

$$n = \int_{r_1}^{r_2} f_0(r)\,dr. \tag{3.2}$$

In logarithmic form the distribution law can be given by the formula

$$dn = f(r)\,d\lg r. \tag{3.3}$$

The function f(r) represents the number of particles per unit interval of the logarithm of the radius. The relationship between $f_0(r)$ and f(r) has the simple form

$$f(r)=\frac{dn}{dr}r=f_0(r)r. \tag{3.4}$$

If one is dealing with average and most probable values, then in accordance with the studies of C. Junge [95] and other authors [124, 136-140] the particle size distribution law can be represented by the formula

$$\frac{dn}{dr}=\frac{c_0}{r^{\nu}} \tag{3.5}$$

or

$$\frac{dn}{d(\lg r)}=\frac{c}{r^{\nu^*}}, \tag{3.6}$$

where c_0 and c characterize the total number of particles in 1 cm^3, and the exponents ν and ν^* characterize the shape of the distribution. It is obvious that $\nu=\nu^*+1$. Below, we will make use of Eq. (3.6). C. Junge [95] found that the most probable value of ν^* is equal to 3. The limits of the particle distribution for a so-called normal size distribution are determined by the radii $r_1=0.04$ μm and $r_2=10$ μm. Deviations from these average values can be appreciable both with respect to the exponent ν^* and the limits r_1 and r_2 and, of course, the total number of particles [141]. Moreover, as already mentioned, Junge's law can in some cases be violated, in particular because of the presence of particles with a preferential size [141, 142]. If, however, consideration is restricted to the Junge model, specified by different values of ν^*, r_1 and r_2, then calculations of the primary optical parameters of such a polydisperse aerosol can be made if the refractive index and shape of the particles are known. /64

Available data do not yet permit a final conclusion concerning the value of the refractive index of natural aerosols. Realizing that aerosol haze has a two-layer structure and consists of a nucleus and a liquid sheath, playing a major role in light scattering processes [12], one can surmise that the parameter m should assume a value of 1.33. Several authors hold this opinion [143-145]. C. Junge [128] adopts an average refractive index value of 1.44. Some studies, for example [146], have shown that on the average it is better to assume m = 1.5. Aerosols, containing salt solutions, have a refractive index whose value is little different from that cited above (Junge [147], Volz [146], Volz and Goody [148], Giese, Bary, Bullrich and Vinnermann [149]). K. S. Shifrin and E. A. Chayanova [74] calculated polydisperse indicatrices for a whole set of refractive indices (m = 1.33, 1.44, 150 and 2.105) for Junge and Junge-type distributions. The results obtained illustrate the significant effect of the refractive index. The elongation of the scattering indicatrix decreases drastically with an increase in m [12, 17].

In the calculations, the particles are usually assumed to be spherical in shape. For nonspherical particles the theory is very complex and it is impossible to completely reduce the problem to the spherical case, even if a possible

averaging of the scattering due to random orientation of the irregularly shaped particles is taken into consideration [12]. Let us mention one important fact: light scattering at small angles is essentially independent of the refractive index and is determined only by the particle shape and size [12, 17]. This, in principle, enables one to draw certain conclusions about the distribution of the coarse fraction of particles from optical observations, without knowing the value of m.

The particle distribution, especially in the 0.08-0.5 μm radius interval, is very difficult to determine by the usual direct methods. Here, apparently, the most successful are optical methods. Some optical effects are explained quite well by a continuous particle size distribution of the Junge type [50, 95]. The Angstrom formula, according to which the aerosol optical thickness τ_D is proportional to $\lambda^{-\alpha}$, where λ is the wavelength and α is a constant coefficient, can be derived on the basis of a Junge particle distribution. In this case it turns out that $\alpha = \nu^* - 2$. The most probable distribution is characterized by a value of $\nu^* = 3$ and, consequently, by a value of $\alpha = 1$, which is close to the value found by Angstrom from a large number of observations ($\alpha = 1.3$). The value of the Angstrom exponent is especially sensitive to changes in ν^* when $\nu^* = 2$, which follows from the formula cited above: $\alpha = \nu^* - 2$. It is necessary, however, to take account of the fact that from these data it is impossible to make any judgement concerning the entire particle distribution. The particle size region from about 0.08 to 0.6 μm is the most active, optically speaking. According to the data of F. Volz [150], α varies within the limits 1.5 to 0.5. Similar results have been obtained by W. Middleton [151], F. Shmolinskiy [138], and others. C. Junge [95] assumes that the distribution with ν^* varying within very narrow limits (from 2.5 to 3.5 or somewhat larger), represents a universal scale effect for very different aerosol concentrations. This, however, refers to the layer near the earth's surface. According to the words of Junge [15], one gets the impression that the distribution with $\nu^* = 3$ is characteristic of a high aerosol concentration. Sky brightness observations in mountainous regions with clean air and high transmittance for the purpose of determining the aerosol distribution are very few. Lower values of ν^* are possible in maritime areas. /65

Let us give some formulas for the optical parameters of a polydisperse aerosol (we will adhere to the symbolism adopted in [50] and in the tables of K. Bullrich, E. Bary and B. Braun [14]). Let i_1 and i_2 be the mutually perpendicular polarization components of the light intensity, scattered by one particle, calculated from the formulas of Mie and expressed in units of the incident direct light intensity. They depend on the scattering angle φ and the parameter $\alpha = \frac{2\pi r}{\lambda}$. The total intensity in the φ direction is equal to $i(\varphi, \alpha) = \frac{i_1 + i_2}{2}$, and the total flux scattered by one particle is determined, in accordance with Mie theory, by the integral

$$\sigma_D(r, \lambda) = 2\pi \int_0^{\pi} \frac{r^2}{a^2} i(\alpha, \varphi) \sin \varphi d\varphi. \qquad (3.7)$$

If dn(r) particles are contained in a unit volume of air, then the scattering coefficient is equal to

$$\sigma_D'(r, \lambda) = \sigma_D(r, \lambda) dn(r). \tag{3.8}$$

Here, the differential dn(r) represents the number of particles whose radii lie within the interval from r to r + dr. The total scattering coefficient is determined from the relation

$$\tau_D'(\lambda) = \int_{r_1}^{r_2} \sigma_D(r, \lambda)\, dn(r). \tag{3.9}$$

The aerosol optical thickness of the entire atmosphere is related to $\tau_D'(\lambda)$ by the formula

$$\tau_D = \int_{r_1}^{r_2} \int_{0}^{\infty} \sigma_D(r, \lambda) N(r, h) dr\, dh = H_D \tau_D'(\lambda). \tag{3.10}$$

Here, N(r, h) is the density of particles of radius r at the height h, H_D is the height of the homogeneous aerosol atmosphere.

The total optical thickness is equal to the sum of Rayleigh τ_R, aerosol τ_D and absorption τ_a. Thus, a comparison of theoretical values of τ_D' with observational data of the aerosol optical thickness requires isolation of $\tau_D' = \tau_D / H_D$. With the determination of τ_D one can compare the relative spectral dependence of this quantity with τ_D', not by determining the actual height of the homogeneous aerosol atmosphere, i.e., by comparing the spectral behavior of τ_D' with the value of the aerosol optical thickness, weighted for the entire atmosphere.

Let us write analogous formulas for the aerosol scattering function $f_D(\lambda, \varphi)$. /66
If $\left(\frac{r_2}{a^2}\right) i(\varphi)$ is the scattering function for one particle, then for the entire particle distribution and for a unit volume the scattering function is equal to

$$f_D(\varphi, \lambda) = \int_{r_1}^{r_2} \frac{r^2}{a^2} i(\varphi)\, dr. \tag{3.11}$$

For the entire atmosphere as a whole we have

$$\mu_D(\varphi, \lambda) = f_D(\varphi, \lambda) H_D. \tag{3.12}$$

By observing the sky brightness, we obtain the function $\mu_0(\varphi, \lambda)$, weighted by Rayleigh and multiple scattering. After ridding $\mu_0(\varphi, \lambda)$ of the effect of these factors and isolating $\mu_D(\varphi, \lambda)$, we can compare both the relative spectral and the angular dependence of the observed values of $\mu_D(\varphi, \lambda)$ with the calculations of the function $f_D(\varphi, \lambda)$ without determining H_D.

Since the value of the aerosol scattering coefficient is equal to $\tau_D' = 2\pi \int_0^\pi f_D(\varphi, \lambda) \sin\varphi d\varphi$, then for a polydisperse aerosol we have

$$\tau_D' = 2\pi \int_0^\pi \int_{r_1}^{r_2} \frac{r^2}{a^2} i(\varphi) \sin\varphi d\varphi dr. \tag{3.13}$$

If the expressions

$$\eta(\varphi) = \int_{a_1}^{a_2} \frac{i_1 + i_2}{a^{\nu^*+1}} da, \quad k(a) = \frac{a_D}{\pi r^2} \tag{3.14}$$

are introduced and the Junge law is assumed for the particle size distribution, then it is easy to obtain the following formulas for the optical parameters of a polydisperse aerosol (see [50] for details):

$$\tau_D' = \frac{c}{\ln 10} \pi \left(\frac{2\pi}{\lambda}\right)^{\nu^*-2} \int_{a_1}^{a_2} \frac{k(a)}{a^{\nu^*-1}} da; \quad f_D(\varphi, \lambda) = \frac{c}{\ln 10} \left(\frac{2\pi}{\lambda}\right)^{\nu^*-2} \eta(\varphi). \tag{3.15}$$

The number of particles N per unit volume is equal to

$$N = \int_{r_1}^{r_2} dN(r).$$

The Junge law, if written in logarithmic form and containing an initial constant c, is expressed by the formula

$$dn(r) = \frac{c}{\ln 10} r^{-(\nu^*+1)} dr. \tag{3.16}$$

Whence /67

$$N = 0{,}434\, c \int_{r_1}^{r_2} \frac{dr}{r^{\nu^*+1}} = 0{,}434\, c \left(\frac{1}{\nu^* r_1^{\nu^*}} - \frac{1}{\nu^* r_2^{\nu^*}} \right). \tag{3.17}$$

Since $r_1^{\nu^*} \ll r_2^{\nu^*}$, the calculations should lead to the formula

$$N = \frac{0.434c}{\nu^* r_1^{\nu^*}}. \tag{3.18}$$

Thus (which is also obvious from qualitative considerations), to determine the number of particles per unit volume it is important to know the lower limit of the particle radii.

3. Deviations from the Theoretical Model

A theoretical model, based on a Junge particle distribution, represents, of course, some idealization of the actual properties of the atmosphere aerosol. A wide variety of deviations from this model are possible, and from the data of direct observations it is seen that some very significant departures from a continuous distribution exist which must be considered first of all. A recently published paper of K. Bullrich, E. de Bary, K. Danzer, R. Eiden and G. Hanel [16] is devoted to an analysis of the effect of deviations from the Junge distribution on the aerosol optical characteristics. In this paper, in particular, the question of the effect of variations in the number of Aitken particles on the spectral dependence of the aerosol optical thickness was discussed. Figures 41 and 42, which we have taken from the above-mentioned [16], illustrate the results of calculations for different aerosol models. Shown in Fig. 41 are the aerosol models used—pure Junge ($\nu^*=3$), designated number 1, and a series of others, labeled by numbers 2-6 and distinguished by a smaller number of Aitken particles. The spectral dependence of the aerosol optical thicknesses, corresponding to these models, are shown in Fig. 42 (the numbers designating the models are carried over into Fig. 42). From these data it is seen how strongly $\tau_D = \tau_D(\lambda)$ depends on the number of fine particles. With a deficiency of Aitken particles, the curve $\tau_D = \tau_D(\lambda)$ can be nearly parallel (within the limits of observational errors) to the abscissa axis, whereas with a normal distribution ($\nu^*=3$) the dependence of τ_D on λ should be expressed by the Angstrom formula $\tau_D = c\lambda^{\nu^*-3} = c\lambda^{-1}$. When the exponent ν^* is close to 2, the dependence of τ_D on λ for a pure Junge distribution will be analogous to the case with $\nu^*=3$, with a deficiency of Aitken particles. Thus, it is not always possible to make a judgment about the particle distribution only from observations of the spectral dependence of τ_D

The question of the effect of departures from the Junge distribution, detected by R. Fenn [152], for different air masses has received special attention in [16]. R. Fenn found a maximum in the particle distribution at $r \approx 0.4$ μm and a sharp minimum at $r = 0.2\text{-}0.25$ μm. A second group of deviations was localized in the large particle portion of the distribution where a maximum is observed, and a minimum in the 0.4-0.5 μm radius interval. Calculations of the angular scattering functions, made with these deviations taken into account [16], show that at large scattering angles the effect of particles, 0.2-0.3 μm in size, is quite appreciable. The size range from 0.4-0.5 μm produces a slight effect. At small Φ, the angular scattering functions are practically independent of these departures from the Junge law. Thus, the role of these groups of particles cannot be established from observations of the brightness gradient in the aureole region. However, their effect is significant at large Φ and, consequently, it affects the optical thickness τ_D (Fig. 43). /68

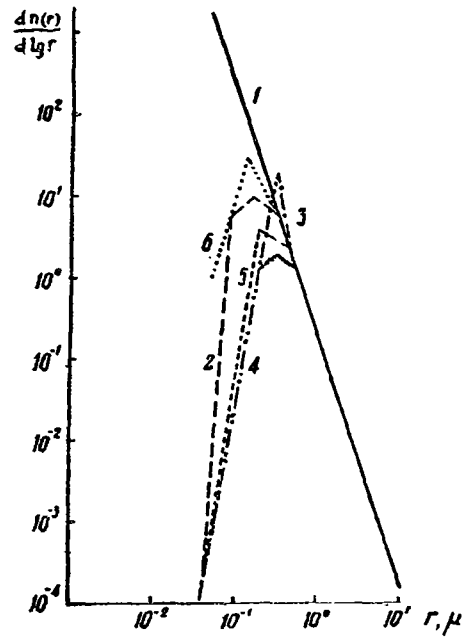

Figure 41. Different Aerosol Distribution Models, Differing in the Number of Aitken Particles, for which Calculations of the Spectral Dependence of the Scattering Coefficient were made (Fig. 42).

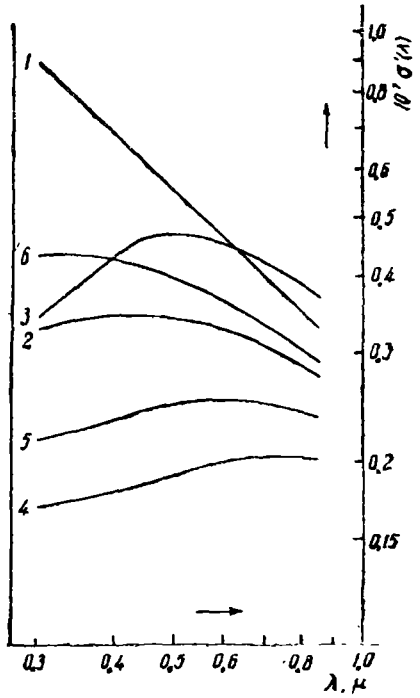

Figure 42. Spectral Dependence of the Scattering Coefficient for the Different Aerosol Models (Fig. 41).

The question of the effect of pure absorption in aerosols on the magnitude and shape of the scattering indicatrix, transmission and sky brightness was discussed by K. Danzer and K. Bullrich [18]. Calculations of the scattering functions have been made by them for a polydisperse aerosol whose distribution is given in the form

$$\frac{dn(r)}{d\log r} = \begin{cases} c(0.1\mu)^{-\nu^*} & \text{for } 0.04\ \mu\text{m} \leqslant r \leqslant 0.1\ \mu\text{m}, \\ cr^{-\nu^*} & \text{for } 0.1\ \mu\text{m} \leqslant r \leqslant 10\ \mu\text{m}. \end{cases}$$

The exponents m in the different models were assumed to have the following values: $m_1=1.5-0.1i$, $m_2=1.5-0.01i$, $m_3=1.5-0.001i$. The following results were obtained. The total extinction coefficient and its spectral behavior depend very weakly on the absorbing properties of the aerosol. The relationship between the scattering and absorption coefficients varies very drastically as a function of the complex coefficient $m=k+\varkappa i$. When $\varkappa=0.1$ the absorption coefficient amounts to 40% of the total extinction coefficient.

Calculations show [18], that the scattering functions of the absorbing particles are very much like those for nonabsorbing particles at small scattering angles. At large φ (especially when $\varkappa=0.1$) pure absorption exerts a very strong influence. A decrease in the absolute scattering function because of absorption is observed up to $\varphi=180^\circ$ where it is about five times less than the scattering function of nonabsorbing particles. The absorption exerts a somewhat weaker (because of the influence of Rayleigh scattering) effect on the daytime sky brightness. /69

Deviations from the calculations made for $m=1.5$ can be caused not only by absorption but also by a discrepancy in the refractive index of the real aerosol assumed in the calculations.

It was stated above that the influence of the refractive index should be very significant, especially at large scattering angles. There is no doubt that the scattering functions and other optical parameters change as a function of the real part of the refractive index. As a result of the cited work of K. S. Shifrin and E. A. Chayanova [74] as well as the work of other authors, in particular T. P. Toropova [17] who studied the case of $m=1.25$, it become clear that with a decrease in the refractive index the elongation of the indicatrix of a polydisperse aerosol increases drastically whereas at small scattering angles φ changes in m have practically no effect on it. The same results were obtained in the work of K. Bullrich, E. Bary, et al. [16]. As an illustration we present a graph (Fig. 44), taken from this work, of the dependence of the relative scattering function on the refractive index ($m=1.50$, 1.40, and 1.33). Realizing that the curve is plotted on a semilogarithmic scale, one can appreciate how drastically the scattering function changes with a change in m at angles $\varphi>20^\circ$ (at angles φ from 0 to 10°, the abscissa axis scale has been stretched out). The effect of fine particles with a 0.04-0.1 μm radius is exceptionally large. The angular dependence of the ratio R_D of the scattering functions, calculated for models with the limits $0.1<r<10$ and $0.04<r<10\,\mu$m, is plotted in Fig. 45 (also taken from [16]); the ratio R_D at large φ reaches almost 0.6 (when $\varphi=120^\circ$) and varies throughout the spectrum.

In view of the difficulties enumerated above, and also because of the fact that detailed calculations appeared relatively recently, very few sky brightness observations, especially at small angular distances from the sun, for the purpose of determining the parameters ν^*, r_1, r_2 and others, have been made.

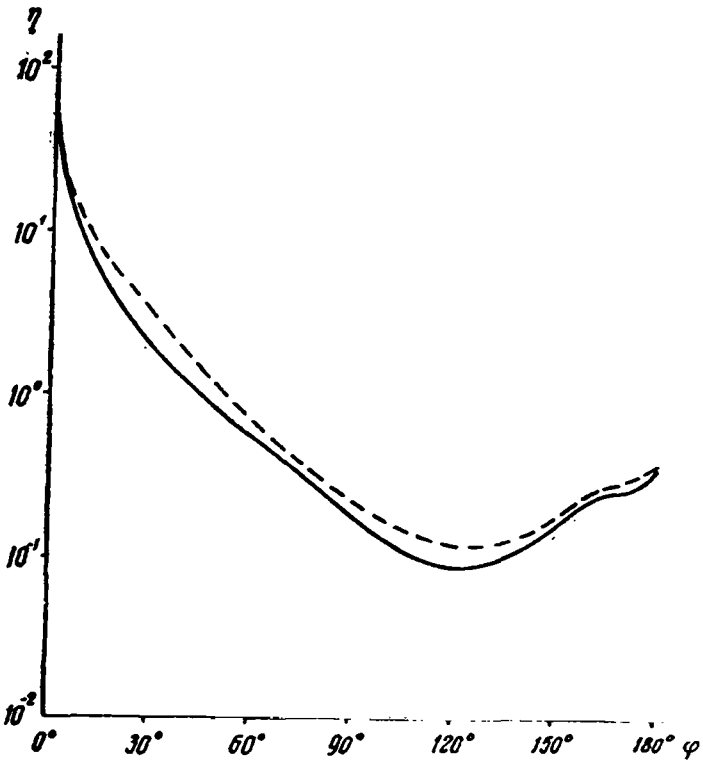

Figure 43. Relative Functions for Light Scattering by Aerosols with Different Numbers of Aitken Particles. Solid line $\eta = \int_{0,1\mu}^{10\mu} \frac{i_1+i_2}{\alpha^{\nu^*+1}}\, d\alpha - \int_{0,2\mu}^{0,3\mu} \frac{i_1+i_2}{\alpha^{\nu^*+1}}\, d\alpha$. Dashed $\eta = \int_{0,1\mu}^{10\mu} \frac{i_1+i_2}{\alpha^{\nu^*+1}}\, d\alpha$ (from data of [16]).

Of the number of recently published papers, one can single out the observations of K. Bullrich, E. Bary and others [16], made on Jungfrau mountain (Switzerland, height of 3500 m above sea level). Data from sky brightness measurements at small φ (from 1 to 15°) are presented in [16] in the form of illustrations for five spectral regions on two days at different solar zenith distances. The authors /71
mention a variation in the curve shape both with a change in $Z_\odot$, and from day to day. The spectral composition of the radiation also changes. Comparison with theory leads to a value close to 3 for the exponent ν^*. This corresponds approximately to the data from observations made in Mainz [50]. The authors say nothing about taking account of the absorption effect in ozone, influncing the radiation spectrum in the region ($0.448<\lambda<0.847$ μm) studied by them. On the other hand it is the spectral dependence itself that is used for determining ν^*. In general it should be noted that direct comparison of sky brightness with theory is not the best method for solving the inverse problem. A comparison with calculations of the scattering indicatrix $\mu_D(\varphi, \lambda)$, which at small φ can be determined with fairly high precision from sky brightness observations, is much more reliable.

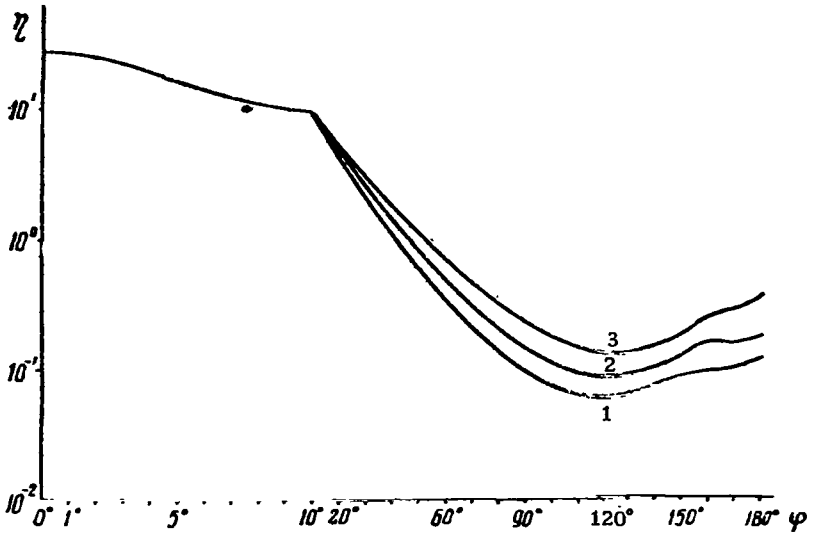

Figure 44. Effect of the Refractive Index m on the Shape of the Indicatrix $\tau_i(\lambda, \varphi) = \int_{0.04\mu}^{3\mu} (i_1 + i_2)\, dn(r)$ for $\lambda = 0.55$ μm. 1—m = 1.33, 2—m = 1.40, 3—m = 1.50.

Quite a large number of observations of transmission, sky brightness and polarization have been made by K. Bullrich, R. Eiden, R. Jaenicke and W. Nowak in the Hawaiian islands. Data from these observations, results of comparing them with theory and an attempt to interpret them are contained in a recently published report [59]. An anomalous behavior of the spectral transmission, caused, as the authors assume, by the presence of particles of a preferential size appearing after eruption of the volcano Agung, is noted. However, no optical effects (for example Bishop rings), characteristic of such conditions, were observed. The Angstrom exponent varied as a function of the spectral region and time of day.

Sky brightness observations at small angular distances from the sun showed that for particles with a radius $r>1$ μm the Junge exponent is $\nu^*>4$ μm and the upper limit of the particle distribution is $r_2 \times 10$ μm. The anomalous behavior of the spectral transmission exerted no effect on sky brightness at small angles φ, because only coarse particles with a radius greater than 1 μm play a significant role in this region. Observations were made at scattering angles of $r_2 \approx 10$ to reveal particles with $r<1$ μm by an optical method. A comparison with theory showed that $\varphi>20°$. The authors concluded that a model with different Junge exponents ν^* for individual particle size intervals characterizes the spectrum more completely. The authors of [59] do not give a detailed description of the method of comparing the theory with the observations. The difficulties of a valid comparison, by which the parameters ν^* can be reliably determined, prevent drawing any definite conclusions with respect to the polarization measurements presented in this same [59].

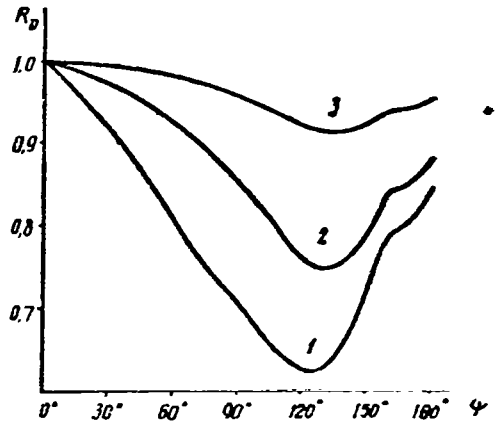

Figure 45. Effect of the Number of Fine Particles on Shape of the Scattering Indicatrix.

$$R_D = \frac{\int_{0.1\mu}^{10\mu} (i_1+i_2)\, dn\,(r)}{\int_{0.04\mu}^{10\mu} (i_1+i_2)\, dn\,(r)}$$

1 — $\lambda = 0.40$ μm, 2 — $\lambda = 0.55$ μm, 3 — $\lambda = 0.85$ μm.

4. Results of Measurements at Small Angular Distances from the Sun

/72

Autumn-Summer Observations.

Sky brightness observations were made by use at the Astrophysical Institute observatory with the equipment described in the first part of this paper. A large number of measurements at small angular distances from the sun ($2° \leqslant \varphi \leqslant 8°$) were made on a photoelectric spectrophotometer. The spectral sky brightness was determined in absolute units (the results have been discussed in the first chapter), as well as the absolute aerosol spectral scattering functions $\mu_D(\varphi)$ and the spectral optical thichnesses $\tau_D = \tau_D' H_D$.

The attempt to solve the inverse problem reduced to a comparison of these data with the analysis results of F. Braun, E. Bary and K. Bullrich [14, 135].

In view of the complexities mentioned above, it was first of all necessary to analyze the results of the calculations themselves in order to see whether a unique solution is possible if it is assumed that the actual aerosol corresponds to one of the analytical models or another.

An examination of the results of theoretical calculations showed the following. When $\nu^*=2.5$ and 3.0, the role of the fine fraction of the aerosol is small in the different models for $2°<\varphi<10°$. Both the relative spectral behavior of the scattering function and the angular dependence for the same Junge exponent vary markedly only with the upper limit of the particle distribution, defined by the radius r_2. Therefore for each value of ν^* it is advisable to isolate three groups of the curves $f_D = f_D(\varphi)$ and $f_D = f_D(\lambda)$, corresponding to the calculations presented in the table of [14] for r_2 equal to 3, 5 and 10 μm. For brevity, on the graphs we designate the different models by the numbers 1 to 6, corresponding to the values of the parameters listed in Table 11.

TABLE XI. Values of the Parameters Assumed for the Calculations

Parameters	Model No. 1	2	3	4	5	6
ν^*	2,5	2,5	2,5	3,0	3,0	3,0
r_2, μm	3	5	10	3	5	10

The angular dependence curves are different for each wavelength λ. When $\lambda=0.4\,\mu$m, the curves corresponding to the different models do not intersect, whereas when $\lambda=0.45\,\mu$m, the angular dependence curves corresponding to models 1, 5 and 6 intersect. A similar parttern is observed when $\lambda=0.55\,\mu$m, and $\lambda=0.65\,\mu$m the curves for models 1 and 5 are close (and intersect at $\varphi\approx 8°$). Thus, for different ν^* values the scattering functions $f_D(\varphi)$, can be very similar, which should be kept in mind when solving the inverse problems.

An examination of the relative shape of the spectral dependence of the $f_D(\lambda)$ function for $\varphi=2°$ showed that models 2 and 6 are characterized by $f_D = f_D(\lambda)$, curves that coincide within the limits of observational accuracy.

Nevertheless, if data are obtained for both the angular and spectral dependence of the scattering functions, then even in the most adverse case it is possible /73
to exclude multivalued solutions and to ascertain what the actual values of ν^* and r_2 are.

However, the values of ν^* and r_2 found by this method characterize only the coarse fraction of the aerosol, determining the sky brightness at small angular distances from the sun. The role of the fine fraction, in particular the Aitken particles, can be clarified through observations of $f_D(\varphi, \lambda)$ at large scattering angles.

The sky brightness observations at large scattering angles, which have been made by many authors and under different conditions, unfortunately do not permit one to reliably isolate the primary aerosol function $f_{1D}(\varphi)$ with any acceptable accuracy.

Because of the reasons cited, an evaluation of the role of fine particles, for those specific conditions under which the observations were made, was made not from the indicatrix at large angles φ, but from the total effect of scattering over all directions which, as is known, determines the value of the aerosol optical thickness τ_D. To isolate τ_D, if the total optical thickness τ_b has been determined, is not difficult in view of the fact that absorption in aerosol is not great.

A comparison of the value of the ratio $\frac{f_D}{\tau_D}$, calculated theoretically and observed, as well as their spectral dependence, seems a rational method to us. The point is that they vary quite a large amount both as a function of ν^* and of the distribution limits [14]. The large or small role of the fine particles for a completely identical relative spectral or angular dependence $f_D=f_D(\bar{\gamma})$ at small φ should exert a direct influence on the value of the ratio $\frac{f_D}{\tau_D}$, then this confirms the fact that the Aitken particles are smaller in reality than assumed in the theoretical model. It should, however, be kept in mind that these too large values can also be explained by the following causes: if there is a departure from Junge's law, associated with the presence or absence of some groups of particles, which has been detected by Fenn [152] and was mentioned above; if the refractive index of the particles is less than 1.50; if pure absorption plays a significant role in the aerosols.

Taking into consideration all that has been said above, it is necessary to consider closely which of these factors can exert, under specific conditions, the most significant effect and which can be neglected.

Let us consider the results of our observations and try to interpret them.

In accordance with available analytical data, for the comparison with theory, the results of measurements at wavelengths close to the tabulated values have been selected, namely: $\lambda=0.410$, 0.447, 0.553 and 0.650 μm. Since the question at hand concerns relative indicatrices, it must be realized that the precision of their determination is not related to the errors of the calibration measurements and can be quite high—about 2-3%. This is not the case for measurements of the spectral dependence of the scattering functions $f_D=f_D(\lambda)$. To obtain the spectral sky brightness, calibration is required. We accomplished this by measuring the brightness of a standard screen, illuminated by perpendicular rays of the sun [33]. Errors in the measurements of the $f_D(\lambda)$ functions reach values of 5-7%. The error in determining the values of f_D/τ_D is especially large because the measurement errors of the scattering functions as well as the optical thicknesses are combined and can amount to about 20% and more, depending on the spectral region. This should be kept in mind when comparing observations with theory since the question of the uniqueness of the solutions often depends primarily on the observational errors. /74

The theoretical curves, corresponding to the relative scattering functions for different aerosol models, are compared with curves from the data of our observations in Fig. 46.

As seen from the figure, the curves of the angular dependence of the relative scattering functions, obtained from observations, often lie below the theoretical for $\nu^*=2.5$. Thus, the aerosol composition during these series of measurements was characterized by a Junge exponent of $\nu^*<2.5$. In order to make a more specific judgment about the value of ν^* we used the data of K. S. Shifrin and E. A. Chayanova [74] who calculated the scattering functions for a Junge exponent of $\nu^*=2$ for the same refractive index of m = 1.5. The calculations in [74] were made for the models with upper particle size limits determined by the quantity $\alpha_2=\frac{2\pi r_2}{\lambda}=150$ and with different lower limits, also specified not by the radius r_1 but by the quantity $\alpha_1=\frac{2\pi r_1}{\lambda}$ (= 0.2, 0.6, 1, 2). Thus, the calculations refer to different values of r_1 and r_2 for different wavelengths. For the upper limits, which also basically determined the scattering functions, starting from the quantity $\alpha_2=\frac{2\pi r_2}{\lambda}=150$ we obtain the following values of the maximum radii r_2 as a function of the wavelength:

λ, μm	0.400	0.450	0.550	0.650
r_2, μm	9.6	10.7	13.1	15.5

The dashed curve plotted in Fig. 46, corresponding to $\nu^*=2$, thus gives the angular dependence at this value of the Junge exponent and at r_2 limits that are different for different wavelengths. The same comments can be made in connection with the value of $\frac{f_D(2^0,\lambda)}{\tau_D}=12{,}3$ determined by us for $\nu^*=2$ from the data of [74].

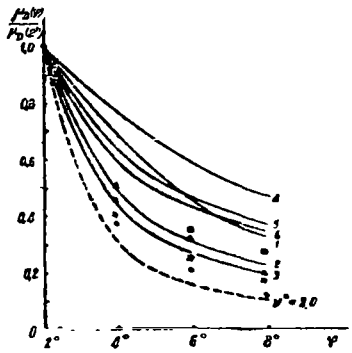

Figure 46. Angular Dependence of the Aerosol Scattering Function for $\lambda=0.55$ μm. 1-6—Data from Calculations: Points—May 6, Crosses-May 12, Triangles-May 15, Squares-Oct. 4, (1965, a.m.).

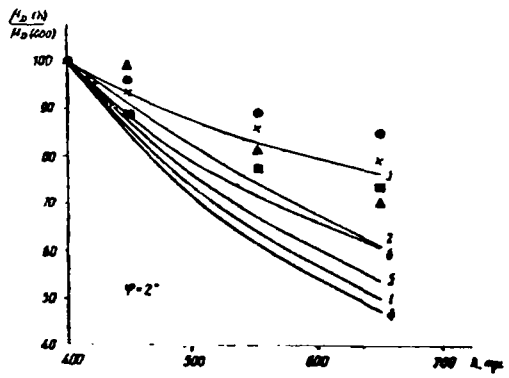

Figure 47. Spectral Dependence of the Aerosol Scattering Function at $\varphi=2^\circ$. Symbols are the Same as in Fig. 46.

The general result of comparing the angular dependence of the observed scattering functions with theory reduces to the following. The Junge exponent ν^* determined from observational data in different spectral regions, was the same within each series. Almost always ν^* does not change with a change in the atmospheric mass during the morning. In 60 series of observations the value of the Junge exponent lies within the interval $2.0<\nu^*<2.5$, while in 28 of them (summer) it was equal to 2.5 and the upper radius limit r_2 was most frequently equal to 10 μm. /75

Let us consider the results of observations of the spectral dependence $f_D=f_D(\lambda)$ at $\varphi=2°$. Of 22 series, half are characterized by smaller wavelength gradients for the scattering functions than the theoretical curves have at $\nu^*=2.5$. As ν^* increases, the gradient should increase. Having no calculated data, one can only state that these series are characterized by values of $\nu^*<2.5$. Let us mention that the observed indicatrices are normalized to the condition $f_D(\lambda=0.41\ \mu m) = 100$. A comparison with theoretical values of $f_D(\lambda)$, normalized to the condition $f_D(\lambda=0.41\ \mu m)=100$, leads to an insignificant error. In exactly the same way, some discrepancy in wavelengths theoretically selected for the observations does not introduce a significant error. The measurement errors amount to 5-7%.

A comparison of observations with theory is depicted in Fig. 47 in which are shown curves of the spectral dependence $f_D(\lambda)$ for different aerosol models and some results of observations. During the day the spectral functions can remain constant within the limits of the measurement errors. Day-to-day variations can reach 30%. The value of ν^* and the upper limit r_2 of the distribution could be determined for 11 series of observations. The model with $\nu^*=2.5$ and $r_2 = 10$ μm fits better than the rest for most of these series. This model, compared with others assumed in the theory, is characterized by having the largest coarse aerosol fraction.

By comparing the values of f_D/τ_D for $\varphi=2°$, determined from the observations, with the theoretical values, one can see that in an overwhelming majority of cases they correspond to a value of ν^* close to 2.0 or lying in the interval $2.0<\nu^*<2.5$, while in this latter case it is more frequently closer to the value $\nu^*=2.0$. It should be taken into consideration that the errors in the observations of $\tau_D(\lambda)$ and in the ratio $\frac{f_D(\lambda)}{\tau_D(\lambda)}$ are very large and, as mentioned above, amount to about 20%.

The major results of a comparison of observations with theory are presented in the summary of Table 12. For each series the values of ν^* and r_2 are listed (in microns) whenever they could be determined. The parameters listed in the table are obtained from measurements of the angular dependence $f_D=f_D(\varphi)$ at different λ, the spectral dependence $f_D=f_D(\lambda)$, the scattering functions at $\varphi=2°$ and from measurements of the ratio $\frac{f_D(\lambda)}{\tau_D(\lambda)}$ at $\varphi=2°$. For 7 of the 20 series the values of the parameter ν^* fall within the limits from 2.0 to 2.5 (according to the data of all three methods of comparison—from $f_D(\varphi)$, $f_D(\lambda)$ and $\frac{f_D}{\tau_D}$); in six cases either the spectral or angular dependence shows that $\nu^*=2.5$, whereas the values of f_D/t_D correspond to $\nu^*=2.0$; four series give a value of $\nu^*=2.5$, both from

$f_D(\varphi)$ and from $f_D(\lambda)$ and the ratio $\frac{f_D}{\tau_D}$ corresponds to a value of $\nu^*=2$. In two series it is established that the spectral and angular dependence are characterized by an exponent $2.0<\nu^*<2.5$, whereas according to $\frac{f_D}{\tau_D}$ — $\nu^*=2$. In one /78
case, all three values of ν^* are equal to 2.5 (June 12, 1965, a.m.). For four series, identical values of $\nu^*=2.5$ are obtained from $f_D(\varphi)$ and $\frac{f_D}{\tau_D}$, with the exception of June 5 when it was ascertained that $2.0<\nu^*<2.5$ on the basis of $f_D(\lambda)$ and $\frac{f_D}{\tau_D}$.

Thus, for the overwhelming majority of the series it is characteristic that the value of ν^*, determined from the scattering functions, is closer to the value $\nu^*=2.5$, whereas by starting from the values of $\frac{f_D}{\tau_D}$ we arrive most frequently at $\nu^*=2,0$. On the basis of this one can draw the following conclusion. The coarse aerosol fraction corresponds approximately to the assumed model with a most probable exponent of $\nu^*=2.5$ and an upper particle radius limit of r_2 = 10 μm. Excessively large values of the quantity $\frac{f_D}{\tau_D}$ can be obtained because of the fact that at large angles φ the aerosol scattering is less than in the model with $\nu^*=2.5$. This effect can be explained by different causes, which we have mentioned above. Let us attempt, however, to isolate the primary ones. A smaller quantity of scattered light at large angles φ cannot be explained by the fact that the refractive index in our locality is less than that assumed in the theory—m = 1.5. Under the dry continental climatic conditions of Central Asia one can rather expect that $m>1.5$. Insofar as pure absorption in aerosols is concerned, for the conditions of our observations this factor plays a small role and it is impossible to explain more than a twofold increase in f_D/τ_D by its effect. One can hardly explain the effect by a departure from a continuous particle distribution—the effect of this factor is insufficient. The apparent cause is the fact that a smaller number of Aitken particles were present in the atmosphere than is assumed in the theoretical Junge models for $\nu^*=2.5$.

A comparison of observed and theoretical values of τ_D leads to approximately /79
the same result: $2.0<\nu^*<2.5$.

The observational data from the year 1965, presented above, were compared with data from 1962. To this end, the scattering functions, observed in 1962 and 1965 in the autumn-summer period at small φ, were approximated by the Van de Hulst formula [13]: $f_D(\lambda, \varphi) = A_\lambda \varphi^{-q_\lambda}$. The quantity q_λ was determined from 111 indicatrices obtained from observations on different days and in different spectral regions.

The q_λ parameters for the theoretical indicatrices were determined in a similar fashion. The results are presented in Fig. 48. The three lower lines represent the spectral dependence of the q_λ values corresponding to a Junge particle distribution with different ν^* and limits of $r_1=0.08$ μm and $r_2=10$ μm [14]. The upper line for $\nu^*=2$ was derived from the results of calculations by K. S. Shifrin and E. A. Chayanova [74]. They did not perform detailed analyses corresponding to different wavelengths and different distribution limits. However,

TABLE XII. Parameters of Polydisperse Aerosol from Theory and Observation Comparison Data

/76

Values to be compared		ν^*	r_2	ν^*	r_2
1		2	3	4	5
		6. V 1965, a. m. m (4,62—3,42)		6. V 1965, a. m. m (1,95—1,70)	
$f_D = f_D(\varphi)$;	λ=0,40 μm	2,0—2,5	—	2,0—2,5	—
»	λ=0,45 μm	2,0—2,5	—	2,0—2,5	—
»	λ=0,55 μm	2,0—2,5	—	2,0—2,5	—
»	λ=0,65 μm	2,0—2,5	—	2,0—2,5	—
$f_D = f_D(\lambda)$;	φ=2°	2,5	5—10	2,5	10
$\frac{f_D}{\tau_D(\lambda)}$;	φ=2°	2,0	—	2,0	—
		6. V 1965, a. m. m (1,66—1,52)		6. V 1965, a. m. m (1,33—1,24)	
$f_D = f_D(\varphi)$;	λ=0,40 μm	2,0—2,5	—	2,0—2,5	—
»	λ=0,45 μm	2,0—2,5	—	2,0—2,5	—
»	λ=0,55 μm	2,0—2,5	—	2,0—2,5	—
»	λ=0,65 μm	2,0—2,5	—	2,0—2,5	—
$f_D = f_D(\lambda)$;	φ=2°	2,5	3—5	2,5	3—5
$\frac{f_D(\lambda)}{\tau_D}$;	φ=2°	3,0	5—10	3,0	5—10
		2,0	—	2,0	—
		12. V 1965, a. m. m (4,64—3,56)		12. V 1965, a. m. m (1,30—1,22)	
$f_D = f_D(\varphi)$;	λ=0,40 μm	2,5	10	2,5	10
»	λ=0,45 μm	2,5	10	2,5	10
»	λ=0,55 μm	2,5	10	2,5	5
»	λ=0,65 μm	2,5	10	2,5	5—10
$f_D = f_D(\lambda)$;	φ=2°	2,5	10	2,5	10
$\frac{f_D(\lambda)}{\tau_D \lambda}$;	φ=2°	2,5	10	2,0	—
		15. V 1965, a. m. m (2,57—2,31)		15. V 1965, a. m. m (1,20—1,19)	
$f_D = f_D(\varphi)$;	λ=0,40 μm	2,5	5—10	2,5	10
»	λ=0,45 μm	2,5	5—10	2,5	10
»	λ=0,55 μm	2,5	5	2,5	10
»	λ=0,65 μm	2,5	5	2,5	10
$f_D = f_D(\lambda)$;	φ=2°	2,5	10	2,5	5—10
$\frac{f_D(\lambda)}{\tau_D(\lambda)}$;	φ=2°	2,0	—	2,0	—
		15. V 1965, a. m. m (1,13—1,11)		5. VI 1965, a. m. m (3,15—2,65)	
$f_D = f_D(\varphi)$;	λ=0,40 μm	2,5	5—10	2,0—2,5	—
»	λ=0,45 μm	2,5	5—10	2,0—2,5	—
»	λ=0,55 μm	2,5	5	2,0—2,5	—
»	λ=0,65 μm	2,5	5	2,0—2,5	—
$f_D = f_D(\lambda)$;	φ=2°	2,5	10	2,0—2,5	—

Table 12 (cont'd) on next page.

TABLE XII. (cont'd).

1		2	3	4	5
$\frac{f_D(\lambda)}{\tau_D(\lambda)}$;	$\varphi=2°$	2,0	—	2,0—2,5	—
		5. VI 1965, a. m. m (2,14—1,76)		5. VI 1965, a. m. m (1,55—1,41)	
$f_D=f_D(\varphi)$;	$\lambda=0,40$ μm	2,0—2,5	—	2,0—2,5	—
»	$\lambda=0,45$ μm	2,0—2,5	—	2,0—2,5	—
»	$\lambda=0,55$ μm	2,0—2,5	—	2,0—2,5	—
»	$\lambda=0,65$ μm	2,0—2,5	—	2,0—2,5	—
$f_D=f_D(\lambda)$;	$\varphi=2°$	2,0—2,5	—	2,0—2,5	—
$\frac{f_D(\lambda)}{\tau_D(\lambda)}$;	$\varphi=2°$	2,0—2,5	—	2,0—2,5	—
		5. VI 1965, a. m. m (1,31—1,25)		7. VII 1965, a. m. m (2,98—2,06)	
$f_D=f_D(\varphi)$;	$\lambda=0,40$ μm	2,0—2,5	—	2,5	10
»	$\lambda=0,45$ μm	2,0—2,5	—	2,5	10
»	$\lambda=0,55$ μm	2,0—2,5	—	2,5	10
»	$\lambda=0,65$ μm	2,0—2,5	—	2,0—2,5	10
$f_D=f_D(\lambda)$;	$\varphi=2°$	2,0—2,5	—	2,0—2,5	—
$\frac{f_D(\lambda)}{\tau_D(\lambda)}$;	$\varphi=2°$	2,0—2,5	—	2,0—2,5	—
		7. VII 1965, a. m. m (1,93—1,71)		7. VII 1965, a. m. m (1,42—1,31)	
$f_D=\varphi_D(\varphi)$;	$\lambda=0,40$ μm	2,0—2,5	—	2,0—2,5	—
»	$\lambda=0,45$ μm	2,0—2,5	—	2,0—2,5	—
»	$\lambda=0,55$ μm	2,0—2,5	—	2,0—2,5	—
»	$\lambda=0,65$ μm	2,5	10	2,0—2,5	—
$f_D=f_D(\lambda)$;	$\varphi=2°$	2,0—2,5	—	2,5	10
$\frac{f_D(\lambda)}{\tau_D(\lambda)}$	$\varphi=2°$	2,0	—	2,0	—
		7. VII 1965, a. m. m (1,10—1,07)		18. VIII 1965, a. m. m (2,97—2,70)	
$f_D=f_D(\varphi)$;	$\lambda=0,40$ μm	2,0—2,5	—	2,0—2,5	—
»	$\lambda=0,45$ μm	2,0—2,5	—	2,0—2,5	—
»	$\lambda=0,55$ μm	2,0—2,5	—	2,0—2,5	—
»	$\lambda=0,65$ μm	2,0—2,5	—	2,5	10
$f_D=f_D(\lambda)$;	$\varphi=2°$	2,0—2,5	—	2,5	5—10
$\frac{f_D(\lambda)}{\tau_D(\lambda)}$;	$\varphi=2°$	2,0	—	2,0	—
		17. IX 1965, a. m. m (3,07—3,70)		17. IX 1965, a. m. m (2,76—2,40)	
$f_D=f_D(\varphi)$;	$\lambda=0,40$ μm	2,0—2,5	—	2,0—2,5	—
»	$\lambda=0,45$ μm	2,0—2,5	—	2,0—2,5	—
»	$\lambda=0,55$ μm	2,0—2,5	—	2,0—2,5	—
»	$\lambda=0,65$ μm	2,0—2,5	—	2,0—2,5	—
$f_D=f_D(\lambda)$;	$\varphi=2°$	2,0—2,5	—	2,0—2,5	—
$\frac{f_D(\lambda)}{\tau_D(\lambda)}r$;	$\varphi=2°$	2,0—2,5	—	2,0	—

Note: Commas represent decimal points.

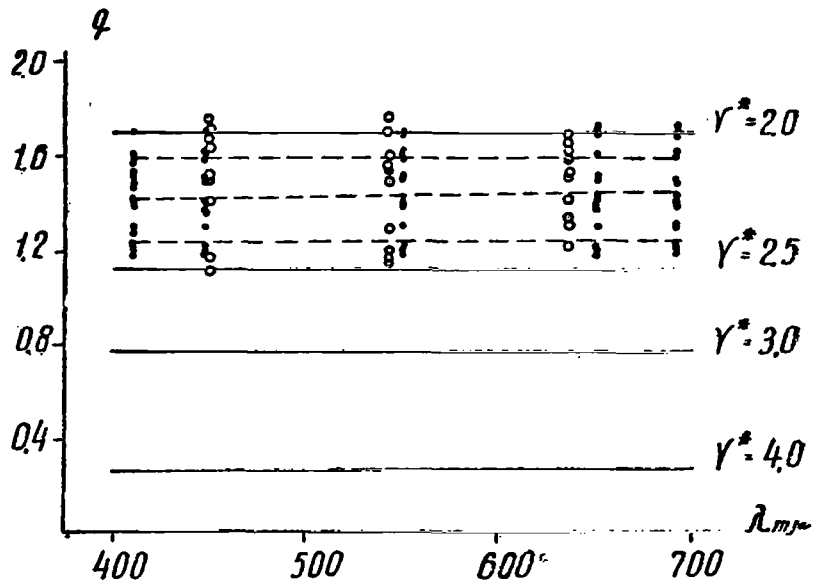

Figure 48. Spectral Dependence of the Exponent in the Van de Hulst Formula.

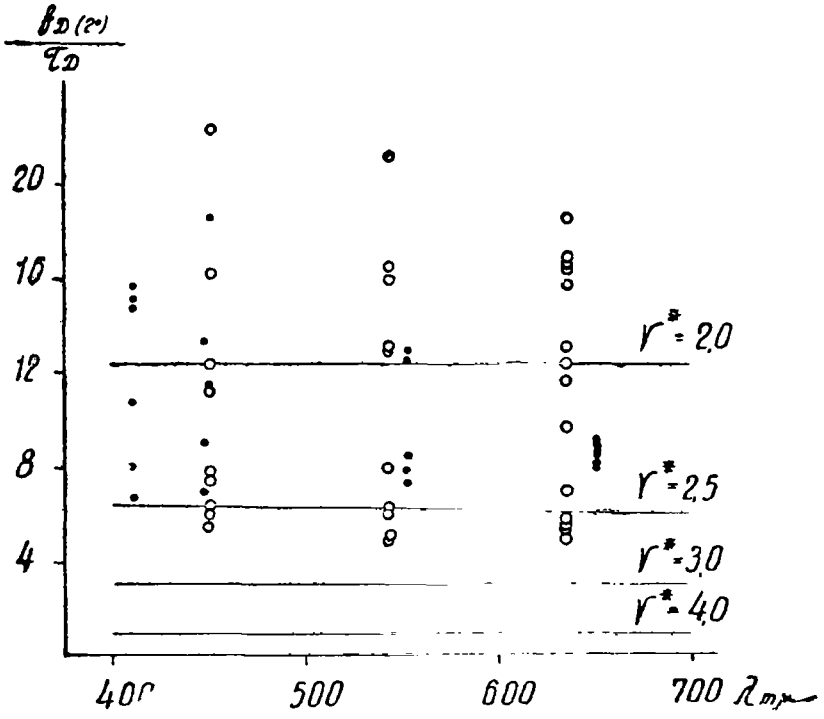

Figure 49. Spectral Dependence of $\frac{f_D(2^\circ)}{\tau_D}$.

the shape of the curve (Fig. 48), corresponding to $\nu^*=2$ is fairly representative. The observational data are denoted in the figure by circles (1962) and by points (1965). The dashed lines depict the observed spectral behavior of q_λ from data of certain selected series.

As seen from the figure, the linear (within the experimental error limits) dependence on q_λ on λ agrees with theory. The values of the parameter ν^* lie primarily within the interval $2<\nu^*<2.5$. The theoretical and observed values of the ratio of $f_D(\lambda, \varphi)$ at $\varphi=2°$ to the aerosol optical thickness τ_D are compared in Fig. 49). The upper line was determined from the data of [74], the lower—from [14] for $\nu^*=2.5$ with $r_1 = 0.08\,\mu m$ and $r_2 = 10\,\mu m$, for $\nu^*=3$ with $r_1 = 0.04\,\mu m$ and $r_2 = 10\,\mu m$, and for $\nu^*=4$ with $r_1 = 0.04\,\mu m$ and $r_2 = 3\,\mu m$. The observation series are denoted by circles (1962) and points (1965). /80

Winter Observations

An analogous comparison of observational data and theoretical calculations [14, 74] for optical thicknesses and scattering functions of an atmosphere aerosol has also been done for winter measurements. The angular and spectral dependences of the scattering functions were compared. For this, both the theoretical and experimental functions were normalized in the following manner: 1) in comparing the angular dependence it was assumed: $\mu_D(10°)=f_D(10°)=100$; 2) in comparing the spectral characteristics—$\mu_D(650\,\mu m) = f_D(650\,\mu m) = 100$. In all cases of good agreement of the normalized functions $f_D(\varphi)$ and $\mu_D(2°)$, the value of $\mu_D(\varphi)$ was systematically found to be greater than the corresponding theoretical value (Fig. 50). A similar situation was also observed in comparing the spectral dependence $\mu_D(\lambda)$ with $f_D(\lambda)$. The curve of the spectral dependence for $\varphi=2°$ agrees better with the model for which ν^* is less than the values of this quantity determined from scattering angles of $\varphi=4°$ and $\varphi=10°$ (Figs. 51, 52).

In 16 of 27 series, the curves $\mu_D = \mu_D(\varphi)$ and $\mu_D = \mu_D(\lambda)$ corresponded to different models or generally did not coincide with any one of the theoretical curves. As a rule the angular dependence $\mu_D(\varphi)$ is described by larger values of ν^*, than the spectral. In 59% of the cases it was found that a Junge aerosol size distribution is not fulfilled. In 41% of the cases it could be stated that the aerosol scattering functions for small angles, observed during winter time, coincide, both in angular and spectral behavior, with the theoretical values calculated for a fully defined model of a polydisperse aerosol (Junge distribution—$\nu^*=2.5-3$). However, even in these cases the value of $\mu_D(2°)$ turns out to be larger than the theoretical (in the long wavelength region this difference is more pronounced), and its wavelength dependence corresponds to the analogous theoretical curve [14] for $\nu^*=2$. This gives a basis for assuming that an especially coarse aerosol fraction, which influenced the sky brightness at very small angles $\varphi\leqslant 2°$ was present in the atmosphere in large amounts during the winter observations. Some difference in the ν^* values for different λ supports this notion (for large λ the ν^* values were smaller). /81

A comparison was also made of the theoretical and experimental values of the ratio of the scattering function $\mu_D(4°)$ to the aerosol optical thickness τ_D As

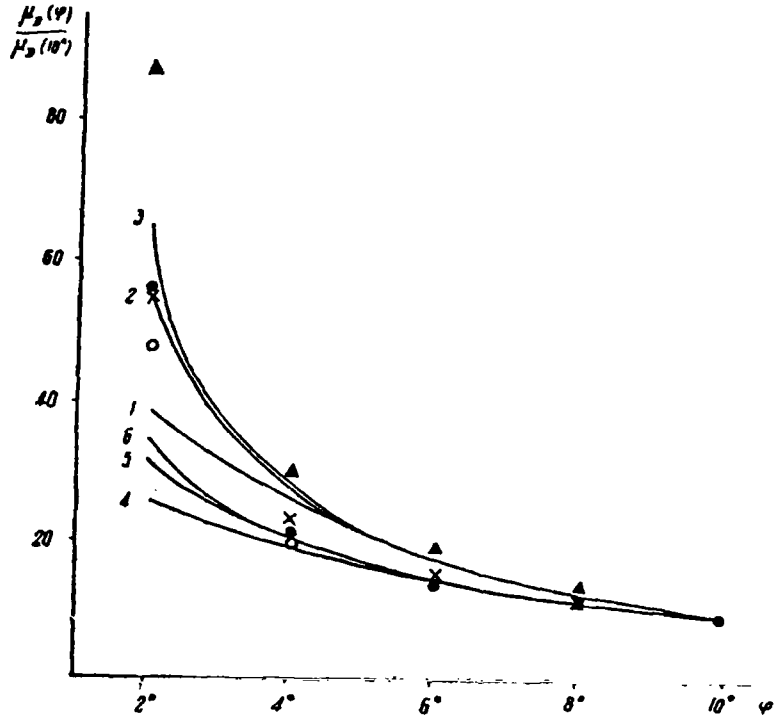

Figure 50. Angular Dependence of the Aerosol Scattering Function for λ 0.55 μm. 1-6—Data from Theoretical Calculations: Points—Dec. 17, 1965, a.m., Crosses—Dec. 17, 1965, p.m., Circles—Dec. 10, 1965, p.m., Triangles—Feb. 11, 1966, a.m.

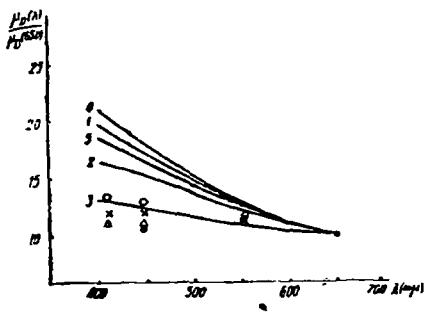

Figure 51. Spectral Dependence of the Aerosol Scattering Function μ_D at $\varphi=2°$. Symbols are the Same as in Fig. 50.

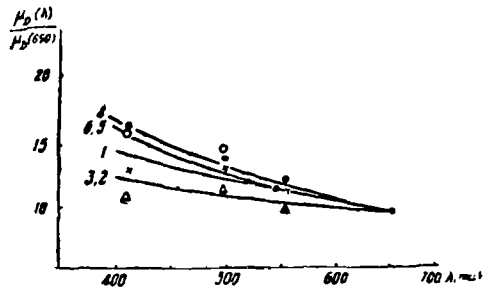

Figure 52. Spectral Dependence of the Aerosol Scattering Function μ_D at $\varphi=4°$. Symbols are the Same as in Fig. 50.

already mentioned above, such a comparison enables one to explain the role of the fine fraction qualitatively, without recourse to measurements at large scattering angles. Such an analysis showed that the experimental values of $\frac{\mu_D}{\tau_D}$ turn out to be too low, compared with the

theoretical values. This can be caused by different reasons, in particular a large number of Aitken nuclei than that assumed in the calculations of [14], and by the fact that the refractive index of the aerosol particles is $m>1.50$.

It is of interest to note that the observed and theoretical data coincide at relatively high turbidities and large values of μ_D (characterized by small values of ν^*). In this regard it is worthwhile to cite the comment of Junge [95] on the fact that departures from the Junge aerosol particle size distribution emerge more markedly at low turbidities.

Let us compare the results of summer and winter observations. As shown previously, the Junge particle size distribution provides a good description of certain optical characteristics of the coarse aerosol fraction on an autumn-summer day. Under winter time conditions, in many cases a Junge distribution is not observed in the real atmosphere. Also characteristic are smaller values of the scattering function at angles of $\varphi \leqslant 10°$ than in the summer and less indicatrix asymmetry γ (the dependence of γ on λ is also different). For a Junge particle distribution in the case of summer observations: $2 \leqslant \nu^* < 2.5$, and for winter: $2.5 \leqslant \nu^* \leqslant 3$ (only the coarse aerosol fraction is involved here). /82

It is of interest to compare the average observed scattering functions $\bar{\mu}_D(\lambda, \varphi)$ and the aerosol optical thickness $\bar{\tau}_D(\lambda)$ with theoretical data for autumn-summer and winter observations. For summer observations, both the angular and the spectral behavior of the average values of the aerosol function $\bar{\mu}_D(\lambda, \varphi)$ are well described by the corresponding theoretical curves, calculated for $\nu^*=2.5$ ($r_2=10$ μm). The values of $\frac{\mu_D}{\tau_D}$, however, are too large compared with $\frac{f_D}{\tau_D}$, corresponding to an exponent of $\nu^*=2.5$. Thus, the average optical parameters of the coarse aerosol fraction are described well by Junge curves for a value of $\nu^*=2.5$. The averaged data also confirm a deficiency of fine particles in the real atmosphere, compared with their number in the models of [14]. An analogous comparison of theoretical and winter experimental data leads to less definite results. Thus, the curves of $\bar{\mu}_D = \bar{\mu}_D(\varphi)$ coincide with the theoretical, calculated for $\nu^*=3$ (the value of $\bar{\mu}_D(2°)$ coincided with the theoretical function f_D (2°) for $\nu^*=2.5$). At the same time the spectral dependence of $\bar{\mu}_D(\lambda)$ at $\varphi=4°$ corresponds to the theoretical calculations at $\nu^*=2.5$ ($r_2=3 \cdot 10^{-4}$ cm). Thus, some discrepancy is observed in the functions $\bar{\mu}_D(\varphi)$ and $\bar{\mu}_D(\lambda)$ (if a Junge particle size distribution is assumed). Even if the curves $\bar{\mu}_D(\varphi)$ and $\bar{\mu}_D(\lambda)$ are satisfactorily described, within the error limits, by the calculations for $2.5<\nu^*<3$, then it is necessary to take account of the unusual problem at $\varphi=2°$, where the values of $\mu_D(2°)$ usually correspond to an exponent of $\nu^*=2.5$ ($r_2=10 \cdot 10^{-4}$ cm). One is obliged to assume the presence, in the winter atmosphere, of a small number of very large particles that have their major effect on the scattering at $\varphi \leqslant 2°$. The lower values of $\bar{\mu}_D / \bar{\tau}_D$, compared with theoretical values of f_D/τ_D, calculated at $\nu^*= 2.5–3$, most likely indicate either a surplus of Aitken nuclei compared with their assumed number [14] or that the refractive index of the real particles is $m>1.50$.

Thus, we see that on the average the summer atmosphere differs from the winter not only in the size of the coarse aerosol fraction (by about a factor of 5-6),

but also in its distribution. The fine particle fraction in the total aerosol mass is also clearly different.

In many cases (especially in winter) the character of the spectral dependence of the scattering functions and the aerosol optical thickness indicates the presence of particles with a preferential size in the atmosphere. It is completely possible that the anomalies in the spectral behavior of μ_D and τ_D observed by us, are explained either by a Gaussian particle size distribution or, as Junge [95] and the authors of [59] assume, by the fact that each aerosol fraction is characterized by a Junge distribution with a different exponent ν^*. Direct measurements of the aerosol particles by Laktionov [139] favor this assumption. However, the theoretical work on calculating one or another optical parameter of a polydisperse aerosol with the particle size distributions mentioned above is still not sufficiently detailed. The calculations of L. Foitzik [19] of the optical parameters of aerosols with a Gaussian particle distribution are insufficiently complete and, therefore, do not permit a detailed analysis of the observational data obtained by us. /83

Observations Under High-Altitude Conditions

In September 1966 we measured the sky brightness at small angular distances from the sun ($\varphi=2—10°$) in the Great Alma-Ata lake area (h = 2800 m above sea level). The observations were made with a photometer with interference light filters (λ_{eff} = 0.405, 0.447, 0.542 and 0.650 μm).

On the basis of the measurement data, the aerosol optical thicknesses τ_D and the scattering functions $\mu_D(\varphi, \lambda)$, were determined, which were compared with the results of theoretical calculations [14, 74].

Let us briefly discuss the general characteristics of the observed aerosol optical parameters (μ_D and τ_D), the data for which are listed in Tables 14, 15. It is interesting that even at an altitude of h = 2800 m, large aureoles were often observed for which the values of μ_D (2°) for $\lambda=0.553$ μm varied from 0.158 to 2.18. The aerosol optical thickness for $\lambda=0.553$ μm varied from day to day within the interval $0.001\leqslant\tau_D\leqslant0.152$. The angular behavior of the scattering function $\mu_D=\mu_D(\varphi)$. is also quite varied. The angular and spectral dependences of the function μ_D and of the values of τ_D are discussed below when the observational data are compared with the calculations made in [14, 74]. The following comparisons were made by us: 1) the values of the angular dependence of the scattering functions, normalized to the condition $\mu_D(2°)=f_D(2°)=100°$; 2) the values of the spectral dependences at $\varphi=2°$, normalized to the condition $\mu_D(0.650\ \mu m)$ = $f_D(0.650\ \mu m)$ =100; c) the values of the ratios of $\mu_D(\lambda)$ and $f_D(\lambda)$ to the optical thicknesses τ (λ) for $\varphi=2°$.

In five of 17 cases the observed angular and spectral dependences of the μ_D functions were described by theoretical curves with ν^* lying in the interval $2=\nu^*<2.5$. For 9 series, the coarse aerosol fraction had a Junge particle size distribution characterized by an exponent $\nu^*=2.5$ and r_2 = 5–10 μm, and on Sept. 12 for two series the distribution could be represented by a model with $\nu^*=3$ and r_2 = 10 μm. We note that the increase in the total number of particles toward midday usually had a small effect on the aerosol distribution.

On Sept. 2, p.m., the character of the spectral dependence of $\mu_D(2°)$ corresponded to the theoretical calculations for $\nu^*=2.5$ and $r_2 = 10\ \mu m$, and the angular dependence of $\mu_D(\varphi)$ can be characterized by a curve with $\nu^*<2$. Obviously, the real aerosol distribution in this case could not be described by the Junge formula. In two series (Sept. 14 with $m_\odot = 4.34$ and Sept. 13 with $m_\odot = 1.60$) and anomalous scattering was observed for $\lambda = 0.542$ apparently caused by the presence in the atmosphere of particles with a preferential size.

A comparison of the values of $\frac{\mu_D}{\tau_D}$ and $\frac{f_D}{\tau_D}$ showed that in some cases the observed values are much too large. This can be caused either by an insufficient number of fine particles or by the fact that the refractive index of the aerosol particles is $m<1.5$. However, under our conditions (the hot continental climate of Central Asis) one can expect that $m>1.5$. At the same time, such large differences between theoretical and observational data (factor of two and more) can hardly be explained by anomalies in the particle distribution [152]. Probably the most acceptable is the conclusion that the number of Aitken nuclei in the models of [14] is too large compared with their number in the area of our observations. It should, however, be mentioned that at a high altitude (h = 2800 m, where $2.5 \leqslant \nu^* \leqslant 3$) the role of the fine particles in light scattering is somewhat greater than at an altitude of h = 1450 m. /84

5. Brightness and Light Polarization of the Daytime Sky at Large Angular Distances from the Sun and the Size Distribution of the Atmosphere Aerosol

Let us consider the question of the effect of a change in the aerosol particle size distribution on the sky brightness and light polarization.

Let us represent the observed brightness indicatrix as the sum of three terms:

$$\mu(\varphi) = \mu_1(\varphi) + \mu_2(\varphi) + \mu_q, \tag{3.19}$$

where μ_1 is the atmosphere scattering indicatrix which, in turn, can be expressed in the form of a sum of Rayleigh $\mu_R(\varphi)$ and aerosol $\mu_D(\varphi)$ components: $\mu_2(\varphi)$ and μ_q are terms produced by multiple scattering and by light reflected from the underlying surface.

The quantities $\mu_2(\varphi)$ and μ_q can be found with the aid of the tables of [23, 24] in which are given the results of a numerical solution of the transport equation for radiant energy in the atmosphere for cases of anisotropic scattering. In calculations of the aerosol components the tables of [14, 79] are used for different polydisperse aerosol models with a refractive index of 1.5 and a Junge particle size distribution law.

The brightness indicatrices $\mu(\varphi)$, calculated for different aerosol models, are listed in Table 13. The limits of the variations of the value of ν^* (from 2 to

3) were selected on the basis of the results of a study of aerosols (see foregoing paragraphs).

From the table it is seen that as the parameter ν^* changes from 2 to 3 in the $\lambda=0.65\ \mu$m region, the difference between the μ values does not exceed 10%. Calculations were not made for $\nu^*=2$ in other spectral regions; however, it is clear that this difference will be even less since with a decrease in wavelength the contribution of aerosol scattering to the total sky brightness will be less. If the accuracy of the $\mu(\varphi)$ measurements amounts to $\sim 5\%$, then even in the case of a perfectly accurate specification of the values of τ_R and τ_D the form of the experimentally determined function, all things being equal, does not enable one to make a judgment concerning the particle distribution of the atmosphere aerosol.

Let us consider the question of the effect of the aerosol particle size distribution function on the light polarization of the daytime sky. To this end, calculations were made of the degree of polarization, for different polydisperse aerosol models, in the solar vertical at an angular distance of $\varphi=90°$ from the sun. In the calculations the following parameter values were assumed: $Z_\odot = 78°$; turbidity factor (for $\lambda=0.55\ \mu$m) T = 1.8: the ν^* value was varied from 2.5 to 4: the radius value varied within the intervals: $0.08 \leqslant r_{max} \leqslant 10\ \mu$m, $0.04 \leqslant r_{min} \leqslant 3.0\ \mu$m The aerosol degree of polarization P_D in this case varied from 0.02 to 0.59.

The results of calculations of the maximum degree of polarization are listed in Table 14. From this it is seen that a fairly broad range of variations in the particle distribution leads to some changes in the maximum polarization of the sky light. The differences in P, as one should expect, increase with an increase in wavelength. /85

Can one draw any conclusion concerning the aerosol particle distribution from the change in degree of polarization? In practice, the question of measurement errors becomes the determining quantity in this case.

The polarization, to a large extent, depends on the optical thickness and the albedo of the underlying surface. In order to estimate how important it is to take these facts into consideration, the following calculations were made. The maximum degree of polarization in the red region of the spectrum at $\lambda=0.65\ \mu$m. where the relative role of the aerosol is quite large, was calculated for two values of the atmosphere transmission coefficient $p+\Delta p$ and $p-\Delta p$ and two values of the albedo of the underlying surface $q-\Delta q$ and $q+\Delta q$, where Δp and Δq are the errors in determining these quantities ($p = 0.875 \pm 0.009$ and $q = 0.20 \pm 0.05$). The results of calculations for T = 2 are shown in Table 15 and refer to a "normal" Junge distribution ($\nu^*=3$; $0.04 \leqslant r \leqslant 10\ \mu$m,) and to two widely differing aerosol models. /86

As seen from Table 15, the changes in the degree of polarization, associated with the shape of the aerosol particle distribution, lie at error values whose magnitudes are determined by the errors in measuring the parameters p and q.

Since the role of aerosol scattering increases with a decrease of the scattering angle φ, then the question of the effect of the aerosol particle size distribution on the sky light polarization at angular distances other than $\varphi=90°$ from the sun

TABLE XIII. Brightness Indicatrices for Different Aerosol Models

λ, μm	0,40		0,45		0,55	
τ_1*	0,6		0,4		0,3	
ν*	2,5	3,0	2,5	3,0	2,5	3,0
$r_1 \cdot 10^{-4}$ см	0,08	0,04	0,08	0,04	0,08	0,04
$r_2 \cdot 10^{-4}$ см	10,0	3,0	10,0	3,0	10,0	3,0
φ^0	μ (φ)					
20	0,257	0,259	0,140	0,140	0,119	0,121
30	0,196	0,201	0,099	0,102	0,078	0,082
50	0,131	0,135	0,060	0,060	0,042	0,044
70	0,095	0,097	0,043	0,043	0,029	0,030
90	0,082	0,083	0,034	0,035	0,022	0,023
110	0,083	0,084	0,033	0,034	0,021	0,022
130	0,089	0,090	0,038	0,038	0,021	0,022
150	0,101	0,102	0,045	0,046	0,024	0,024
	λ=0,65		τ_1=0,2			

ν*	2,0	2,5	3,0
$r_1 \cdot 10^{-4}$ см	0,04	0,08	0,04
$r_2 \cdot 10^{-4}$ см	15,5	10,0	3,0
20	0,0738	0,0793	0,0824
30	0,0471	0,0499	0,0534
50	0,0238	0,0247	0,0265
70	0,0153	0,0156	0,0166
90	0,0118	0,0121	0,0128
110	0,0111	0,0115	0,0121
130	0,0117	0,0120	0,0126
150	0,0138	0,0141	0,0145

*Values of τ_1 are taken from [34].

Note: Commas represent decimal points.

must be considered. Corresponding calculations for the λ=0.55 μm spectral region, turbidity factor of T = 2 and $Z_\odot$=78° are listed in Table 16. From this it is seen that other scattering angles values do not have marked advantages for determining the particle distribution from measurements of the degree of polarization. /87

Let us consider the qeustion of the dependence of the degree of sky light polarization on the refractive index of the particle size distribution with an

TABLE XIV. Values of Maximum Degree of Polarization

λ, μm	ν*	r	P_D	P	λ, μm	ν*	P_D	P
0,40	2,5	r_{max}	0,02	0,69	0,55	2,5	0,09	0,68
		r_{min}	0,11	0,68			0,12	0,68
	3,0	r_{max}	0,10	0,68		3,0	0,21	0,69
		r_{min}	0,26	0,68			0,27	0,69
	4,0	r_{max}	0,29	0,67		4,0	0,46	0,72
		r_{min}	0,54	0,68			0,57	0,74
0,45	2,5	r_{max}	0,05	0,73	0,65	2,5	0,10	0,64
		r_{min}	0,12	0,73			0,13	0,64
	3,0	r_{max}	0,15	0,71		3,0	0,24	0,66
		r_{min}	0,26	0,72			0,27	0,67
	4,0	r_{max}	0,46	0,71		4,0	0,51	0,72
		r_{min}	0,56	0,72			0,59	0,74

TABLE XV. Accuracy of Degree of Polarization Calculations

$0.04 \leq r_{min} \leq 3$ μm

$0.04 \leq r_{norm} \leq 10$ μm

$0.08 \leq r_{max} \leq 10$ μm

ν*	r	p=0,866, q=0,25	p=0,884, q=0,15
2.5	r_{max}	0.43	0.50
3.0	r_{norm}	0.46	0.54
4.0	r_{min}	0.53	0.60

TABLE XVI. Angular Dependence of Degree of Polarization

Z°	ν*=2,5				ν*=3				ν*=4			
	r_{min}		r_{max}		r_{min}		r_{max}		r_{min}		r_{max}	
	q=0	q=0,25	q=0	q=0,25	q=0	q=0,25	q=0	q=0,25	q=0	b=0,25	q=0	q=0,25
50,2	0	0	0	0	0,01	0,01	0,01	0,01	0,02	0,02	0,02	0,02
43,9	0,03	0,03	0,03	0,03	0,04	0,04	0,04	0,04	0,06	0,06	0,06	0,06
32,8	0,12	0,11	0,12	0,11	0,14	0,13	0,13	0,12	0,17	0,16	0,16	0,15
23,0	0,22	0,20	0,22	0,20	0,30	0,28	0,23	0,22	0,28	0,26	0,25	0,23
11,4	0,39	0,35	0,39	0,35	0,42	0,38	0,41	0,37	0,46	0,42	0,44	0,40
0	0,57	0,49	0,57	0,49	0,59	0,51	0,58	0,50	0,64	0,56	0,61	0,53
11,4	0,63	0,56	0,63	0,55	0,64	0,58	0,64	0,57	0,69	0,63	0,67	0,60
23,0	0,58	0,50	0,58	0,50	0,59	0,52	0,59	0,51	0,64	0,56	0,62	0,54
32,8	0,46	0,41	0,46	0,41	0,47	0,42	0,47	0,42	0,51	0,46	0,50	0,44
43,9	0,32	0,28	0,32	0,28	0,33	0,28	0,32	0,28	0,35	0,31	0,34	0,30
50,2	0,22	0,20	0,22	0,20	0,23	0,21	0,23	0,21	0,25	0,23	0,24	0,22
58,6	0,10	0,09	0,10	0,09	0,11	0,10	0,10	0,09	0,13	0,12	0,12	0,11

Note: Commas represent decimal points.

TABLE XVII. Dependence of Degree of Polarization on the Refractive Index

Z°	P			
	$m=1,25$		$m=1,50$	
	$q=0$	$q=0,25$	$q=0$	$q=0,25$
50,2	0,02	0,02	0	0
43,9	0,06	0,05	0,04	0,04
32,8	0,18	0,17	0,13	0,13
23,0	0,30	0,28	0,23	0,22
11,4	0,50	0,44	0,41	0,38
0	0,67	0,57	0,59	0,51
11,4	0,71	0,63	0,65	0,58
23,0	0,64	0,55	0,60	0,52
32,8	0,51	0,45	0,48	0,43
43,9	0,35	0,31	0,33	0,29
50,2	0,26	0,23	0,23	0,21
58,6	0,13	0,12	0,11	0,10

Note: Commas represent decimal points.

exponent of $\nu^*=3$, T. P. Toropova calculated the polarization components of the scattering functions for two types of polydisperse aerosol with a refractive index of 1.25 and 1.50 [17]. The results of calculations of the angular dependence of the degree of polarization in the solar vertical at $Z_\odot = 78^\circ$ on the refractive index are listed in Table 17.

From a comparison of Tables 16 and 17 it is seen that the difference in the values of the degree of polarization is practically the same both as a function of the refractive index and as a function of the shape of the particle distribution. /88

Thus, measurements of the sky light brightness in the visible and ultraviolet spectral regions for a relatively high atmospheric transmission can hardly be used for studying the physical characteristics of an atmospheric aerosol. Polarization studies in the infrared portion of the spectrum, where multiple light scattering in aerosols becomes the dominant factor, are obviously the most promising in this area.

CONCLUSION /89

The question of a more rigorous solution of the direct problem is formulated in this paper on the basis of data from direct observations of day time sky brightness and polarization, and an analysis is made of the possibility of solving the inverse problem.

The proposed analysis methods enable one to determine the brightness and polarization for a large portion of the sky (excluding the region of small angular distances from the sun) with an accuracy that is satisfactory for many practical problems.

The results of investigations of the major atmospheric optical parameters, their variations and interrelationship, presented in this paper, make it possible

to draw conclusions about a variety of optical effects and possible variations of the radiation field during clear weather in the daytime.

With respect to the inverse problem, one can say the following. Serious attempts to determine the aerosol distribution from optical observations of the daytime sky have essentially only now begun. By making measurements at small scattering angles, one can obtain some information about the coarse aerosol fraction. However, starting from brightness and polarization measurements at large scattering angles, it is impossible to draw any definite conclusions about the particle size distribution of an atmospheric aerosol.

REFERENCES

1. Rozenberg, G.V. Usp. Fiz. Nauk. (UFN) 1960, Vol. 71, No. 2. /90
2. Rayleigh. Philos. Mag., 47 (5), 375 (1899).
3. Chandrasekhar, S. Radiative Transfer, Dover 1960.
4. Sekera, Z. Advan. Geophys., Vol. 3, No. 34 (1956).
5. Chandrasekhar, S., and Elbert, D. Trans. Am. Phil. Soc. New Series. Vol. 44, Part 6 (1954).
6. Coulson, K.L., Dave, J.V., and Sekera, Z. Tables Univ. of California Press, Berkeley — Los Angeles, 1960.
7. Dave, J. J. Opt. Soc. Am. Vol. 54, No. 3 (1964).
8. Dave, J., and Furukawa, P. J. of Atmosph. Sciences, Vol. 21, No. 2, (1964).
9. Dave, J., and Furukawa, P. Ibid.
10. Love, A.E. Proc. London Math. Soc., 30, 308 (1899).
11. Mie, G. Ann. Physik, 25, 377 (1908).
12. Shifrin, K.S. (Rasseyaniye sveta v mutnoy srede (Light Scattering in a Turbid Medium), Gostekhizdat, Moscow 1951.
13. Hulst, G. Van de. Light Scattering by Small Particles. Wiley, 1957.
14. Bary, E. de, Braun, B., and Bullrich, K. Tables Related to Light Scattering in a Turbid Atmosphere, Vol. I, II, II. Camb. Res. Lab., Special Reports, 33, AFCRL-65—710 (1), 1965.
15. Shifrin, K. S., and Zel'manovich, I. L. Tablitsy po svetorasseyaniyu (Light Scattering Tables), Vol. I. L., Gidrometeoizdat, 1966.
16. Bullrich, K., Bary, E., de, Danzerk., Eiden, R. and Hanel, G. Scient. Rep., No. 4, AF61 (052) –595 (1966).
17. Toropova, T.P. — Trudy Astrofizich. in-ta AN KazSSR, 1966, Vol. 7.
18. Danzer, K., and Bullrich, K. Appl. Opt., Vol.4, No. 11 (1965).
19. Foitzik, L., Hebermehl, G. and Spänkuch, D. Optik, 23, H. 3 (1965-1966).
20. Ambartsumyan, V.A. — Dokl. AN SSSR , 1944, Vol. 43, No. 3.
21. Sobolev, V. V. Perenos luchistoy energii v atmosferakh zvezd i planet (Radiative Energy Transfer in the Atmospheres of Stars and Planets). M., Gostekhizdat, 1956.
22. Kuznetsov, Ye. S. — Izv. AN SSSR, seriya geofiz. , 1951, No. 4.
23. Feygel'son, Ye. M., Malkevich, M. S., Kogan, S. R., koronatova, G.D., Glazova, K.S., and Kuznetsova, M.A. — Trudy In-ta fiziki atmosfery AN SSSR, 1958, Part. 1, No. 1.
24. Atroshenko, V.S., Glazova, K.S., Malkevich, M.S., and Feygel'son, Ye. M. — Trudy In-ta fiziki atmosfery AN SSSR, 1962, Part. 2, No.3.
25. Shifrin, K. S., and Pyatovskaya, N. P. Tablitsy naklonnoy dalnosti vidimozti i yarskosti dnevnogo neba (Tables of Slant Visibility Range and Daytime Sky Brightness. L., Gidrometeoizdat), 1959.
26. Minin, I. N., and Sobolev, V. V. Kosmicheskiye issledovaniya , 1963, Vol. 1, No. 2; 1964, Vol 2, No. 4.
27. Bary, E. de. Z. f. Met., Vol. 2, No. 11 (1965).

28. Bary, E. de. Appl. Opt., Vol. 3 (1964).
29. Iensen, Ch. Handb. Physik, Vol. 19 (1928).
30. Dorno, C. Verofent. d. Preuss. Meteorol. Inst., Abh. Vol. 6, No. 303 (1919).
31. Krat, V.A. — "Izv. GAO", 1946, Vol. XXII.
32. Pyaskovskaya-Fesenkova, Ye. V. Issledovaniye rasseyaniya sveta v zemnoy atmosfere (Study of Light Scattering in the Earth's Atmosphere). M., Izd-vo AN SSSR, 1957.
33. Livshits, G. Sh. Rasseyaniye sveta v atmosfere, ch. I (Light Scattering in the Atmosphere, Part I. Trudy Astrofizich. in-ta AN KazSSR, Vol. VI, 1965.
34. Kondrat'yev, K. Ya. Solar Radiant Energy. L., Gidrometeoizdat, 1954.
35. Rozenberg, G.V. Twilight. Fizmatgiz, Moscow, 1963.
36. Kondrat'yev, K. Ya., and Burgova, M. P. — Trudy Vsesoyuznogo nauchnogo meteorologicheskogo soveshchaniya, (Trans. of the All-Union Scientific Meteorology Conference), Vol. 6, 1963.
37. Kondrat'yev, K. Ya., Kudryavtseva, L. A., and Manolova, M. P. — "Vestn. LGU, seriya mat., fiz., khim.", 1955, No. 5.
38. Gordon, J. and Church, P. Appl. Opt., Vol. 5, No. 5 (1966). Billeau, R., and Gordon, J. Ibid.
39. Jain, R. Indian J. Pure and Appl. Geoph., Vol. 3, No. 3 (1965).
40. Hoffmeister, Cuno. Veroff. Sterwarte Sonneberg, No. 4 (1966).
41. Pavlov, V. Ye. Dissertation in competition for the Academic Degree of candidate of Physico-Mathematical Sciences, 1966.
42. Krat, V.A. — "Astronomicheskiy zhurnal", 1942, Vol. 19, No. 6.
43. Barteneva, O.D. "Izv. AN SSSR, seriya geofiz.", 1960, No. 12.
44. Sandomirskiy, A.B., Al'tovskaya, N.P., and Trifonov, G.I. — Coll. Sb. Aktinometriya i optika atmosfery (Atmospheric Actinometry and Optics). M., 1964.
45. Mikirov, A. Ye. "Kosmicheskiye issledovaniya", 1965, Vol. 3, No. 2.
46. Rozenberg, G.V., and Nikolayeva-Tereshkova, V.V. — "Izv. AN SSSR, fizika atmosfery i okeana", 1965, Vol. I, No. 4.
47. Sekera, Z. Advan. Geophys., Vol. 3, No. 4 (1956).
48. Roggenkamp, F. Meteorol. Zeitschr., Vol. 50, No. III (1933).
49. Rozenberg, G.V. — "Izv. AN SSSR, seriya geograf. i geofiz.", 1949, Vol. 13.
50. Bullrich, K. Advan. Geophys., Vol. 10 (1964).
51. Driving, A. Ya., Rozenberg, G.V., and Turikova, N.K. Doklad na soveshchanii po aktinom. i atmosf. optike. (Proceedings of conference on Actinometry and Atmospheric Optics; UNF, Vol. 68, No. 2, 1959.
52. Rozenberg, G.V., and Mikhaylin, I.M. — "Dokl. AN SSSR", 1958, Vol. 122, No. 1.
53. Pyaskovskaya-Fesenkova, Ye.V. — "Dokl. AN SSSR", 1958, Vol. 123, No. 6.
54. Pyaskovskaya-Fesenkova, Ye.V. — "Dokl. AN SSSR", 1960, Vol. 134, No. 4.
55. Pyaskovskaya-Fesenkova, Ye.V. — "Izv. AN KazSSR, seriya fiziko-matematicheskikh nauk", 1963, No. 1.
56. Pyaskovskaya-Fesenkova, Ye.V. — Trudy Astrofizicheskogo instituta AN KazSSR, 1966, Vol. 7.
57. Stamov, D.G. Aktinometriya i atmosfernaya optika (Actinometry and Atmospheric Optics. L., 1961.
58. Georgiyevskiy, Yu.S., Driving, A.Ya., Zolotavina, N.V., Rozenberg, G.V., Feygel'son, Ye. M., and Khazanov, V.S. Prozhektornyy luch v atmosfere (Searchlight Beam in the Atmosphere, M., Izd-vo AN SSSR, 1960.
59. Bullrich, K., Eiden, R., Jaenicke, R., and Nowak, W. Mainz. Final Technical report. Contract DA-91-591-EUC-3458 (1966).
60. Fesenkov, V.G. — "Astronomich. Zhurn.", 1960, Vol. 37, No. 5.
61. Nokson, J., and Goody, R. — "Izv. AN SSSR, fizika atmosfery i okeana", 1965, Vol. I, No. 3.

62. Bary, E. de, and Bullrich, K. "Optik", Bd. 21 (1964).
63. Boll, E., Eisner, L., Young, J., and Oetjen, R. JOSA, Vol. 50 (1960).
64. Shifrin, K. S., Minin, I. N., Avaste, O. A., and Pyatovskaya, N. P. Trudy Vsesoyuzn. nauchnogo meteorolog. soveshchaniya (Trans. of All-Union Scientific Meteorology Conference, Vol. VI, L., Gidrometeoizdat, 1963.
65. Jameson, J., et al. (Fizika i tekhnika infrakrasnogo izlucheniya (Infrared Radiation Physics and Techniques. M., Izd-vo "Sovetskoye radio", 1965.
66. Soret, I. Ann. Chim. et Phys., 503 (1888); Arch. Sci. Phys. et Natur., Vol. 20 (1888).
67. Ahlgrimm, F. Tahrb. d. Hamburg. Wis. Austalten., Vol. 32 (1914).
68. Tichanowsky, J. J. Phys. Zeits., Vol. 28, No. 252 (1927).
69. Rozenberg, G. V. — UFN, 1965, Vol. 56, No. 1.
70. Pyaskovskaya-Fesenkova, Ye. V. — "Dokl. AN SSSR", 1960, Vol. 134, No. 4.
71. Bullrich, K. Ber. Deutsch. Wetterdienstes, No. 51 (1958).
72. Dietze, G. Zeitschr. f. Meteorol., Vol. 10, No. 12 (1956).
73. Gehrels, T. JOSA, Vol. 52, No. 10 (1962).
74. Shifrin, K. S., and Chayanova, E. A. — Trudy GGO, No. 170, 1965.
75. Ivanov, A. I., Livshits, G. Sh., and Tashenov, B. T. — Trudy Astrofizicheskogo instituta, Vol. VIII, 1967.
76. Boyko, P. N. — "Izv. Astrofizicheskogo in-ta AN KazSSR", 1959, Vol. 8.
77. Jonson, F. J. of Meteorol., Vol. 11, No. 6 (1954).
78. Yaroslavtsev, I. N. — "Izv. AN SSSR, seriya geofiz.", 1953, No. 1.
79. Feygel'son, Ye. M. — "Izv. AN SSSR, seriya geofiz.", 1958, No. 10.
80. Bary, E. de, and Bullrich, K. Optik, 21, H. 9 (1964).
81. Bary, E. de, and Bullrich, K. Arch. Meteorol. Geophys. Biokl., B. 12 (1963).
82. Bary, E. de, and Bullrich, K. Arch. Meteorol. Geophys. Biokl., B.13 (1963).
83. Bary, E. de, and Bullrich, K. Optik, Vol. 21 (1964).
84. Linke, F., and Boda, K. Met. Ztsch., Vol. 39, No. 161 (1922).
85. Dave, J. JOSA, Vol. 54, No. 3 (1964).
86. Fesenkov, V. G. — Astronomich. zhurn. , 1933, Vol. 10, No. 3.
87. Pavlov, V. Ye. Coll. Sb. Rasseyaniye i polyarizatsiya sveta v zemnoy atmosfere (Light Scattering and Polarization in the Earth's Atmosphere). Alma-Ata, 1962.
88. Pavlov, V. Ye. — Trudy Astrofizich. In-ta AN KazSSR, Vol. 8, 1967.
89. Pavlov, V. Ye. — "Astronomich. zhurn.", 1964, Vol. 41, No. 1.
90. Toropova , T. P., and Pavlov, V. Ye. Trudy Vsesoyuznogo nauchn. meteorologichesk. soveshchaniya (Trans. of All-Union Scientific Meteorology Conference, Vol. VI, 1963.
91. Tashenov, B. T. — Trudy Astrofizich. In-ta AN KazSSR, Vol. 8, 1967.
92. Barteneva, O. D., Dovgyallo, Ye. N., and Polyakova, Ye. A. Eksperimental'nyye issledovaniya opticheskikh svoystv prizemnogo sloya atmosfery (Experimental Studies of the Optical Properties of the Atmosphere Near the Earth's Surface). Trudy GGO, No. 220. Gidrometeoizdat, L., 1967.
93. Livshits, G. Sh., Pavlov, V. Ye., and Milyutin, S. N. — Trudy Astrofizich. In-ta AN KazSSR, Vol. 7, 1966.
94. Toropova, T. P. — "Izv. Astrofizich. In-ta AN KazSSR", 1958, Vol. 6.
95. Junge, C. Khimicheskiy sostav i radioaktivnost' atmosfery (Chemical Composition and Radioactivity of the Atmosphere). M., Izd-vo "Mir", 1965.
96. Pritchard, B., and Elliot, W. JOSA, Vol. 50, No. 3 (1960).
97. Kastrov, V. G. — Trudy TsAO, 1959, No. 32.
98. Sekihara, K. Doklad na mezhdunarodnom simpoziume po issledovaniyu radiatsionnykh protsessov (Report to the International Symposium on Radiation Processes Research). L., 1964.

99. Robinson, G. Arch. Meteorol. Geophys. Biokl., B. 12 (1963).
100. Leopold, R. Report to the International Symposium on Radiation Processes Research. L., 1964.
101. Siendentopf, H. Zeitschr. f. Meteorol. No. T4 (1947).
102. Shifrin, K. S., and Raskin, V. F. Trudy Vsesoyuznogo nauchnogo meteorologicheskogo soveshchaniya (Transactions of All-Union Scientific Meteorology Conference). Vol. 9, M., Gidrometeoizdat, 1963.
103. Shifrin, K. S., and Raskin, V. F. Trudy vtorogo soveshchaniya po aktinometrii i atmosfernoy optike (Transactions of Second Conference on Actinometry and Atmospheric Optics. L., Gidrometeroizdat, 1960.
104. Shifrin, K. S., and Raskin, V. F. — Trudy GGO, No. 109, 1961, p. 155.
105. Shifrin, K. S., and Raskin, V. F. — Trudy GGO, No. 109, 1961, p. 161.
106. Shifrin, K. S., and Golikov, V. I. — Trudy VI mezhvedomstvennoy konferentsii po issledovaniyu oblakov, osadkov i grozovogo elektrichestva (Transactions of 6th Interdepartmental Conference of Cloud, Rainfall and Thunderstorm Electricity Research). M., 1961.
107. Shifrin, K. S., and Perel'man, A. Ya. — "Dokl. AN SSSR", 1964, Vol. 158, No. 3.
108. Shifrin, K. S., and Perel'man, A. Ya. — "Dokl. AN SSSR", 1963, Vol. 151, No. 2.
109. Nolan, P., and Donerty, D. Proc. Roy. Irish Acad., A 53 (1950).
110. Israel, H., and Schulz, L. Meteorol. Ztschr., Vol. 49 (1932).
111. Junge, C. Ann. Meteorol., 1952, Vol. 380 (1952).
112. Coetz, A., and Preining, O. Physics of Precipitation. Monogr. 5. NASJVRC No. 746, Am. Geoph. Un., Wash., No. 164 (1960).
113. May, K. J. Sci. Instr., Vol. 22 (1945).
114. Junge, C. Tellus, Vol. 5, No. 1 (1953).
115. Junge, C. Ber. d. dtsch. Wetterd. US-Zone, Nr. 35 (1952).
116. Junge, C. J. Meteorol., Vol. 12, No. 13 (1955).
117. Molan, P., and Donerty, D. Proc. Roy. Irish Acad., A53, Vol. 163 (1950).
118. Friedlander, S. J. Meteorol., Vol. 17 (1960).
119. Rau. W. Meteorol. Rundschau, Vol. 8 (1952).
120. Junge, C. Ann. Meteorol., Vol. 1 (1952).
121. Eldridge, R. J. Meteorol., No. 14 (1957).
122. Stewart, K. Meteorol. Research, Paper No. 1074, Sc. 111/246, Aer. Ministry, London, 1957.
123. Kuroiwe, D. J. Meteorol., Vol. 13 (1956). Studies on Fog. Ed. T. Heri, Fenne Tr. Co., Japan (1953).
124. Laktionov, A. G. — Trudy Vsesoyuzn. nauchn. meteorolog. soveshchaniya (Transactions of All-Union Scientific Meteorological Conference, Vol. 6, L., Gidrometeoizdat, 1963.
125. Chagnon, C., and Junge, C. J. Meteorol., Vol. 18 (1961).
126. Junge, C. J. Meteorol., Vol. 18 (1961).
127. Junge, C., and Ryan, T. J. Roy. Meteorol. Soc., Vol. 84 (1958).
128. Junge, C., Chagnon, C., and Manson, J. J. Meteorol., Vol. 18 (1961).
129. Buddhue, T. Meteoritic Dust. New Mexico Press, Albuquerque, New Mexico, 1950.
130. Clozier, W. J. Geophys. Research, Vol. 65 (1960).
131. Lassen, L., and Rau, G. Zs. Phys., 1960, No. 504 (1960).
132. Nisikori Kiyesi., Isida Toru, et al. Dempa kenkyuse kikho. Rev., Radio Res. Labs., Vol. 11, No. 54 (1965).
133. Tiocco, G., and Grans, G. J. Atmosph. Sciences, Vol. 21, No. 3 (1964).
134. Ivanov, A. I. — Tr. Astrofizich. instituta, Vol. VIII, 1967.
135. Livshits, G. Sh., and Tashenov, B. T. — "Izv. AN SSSR, fizika atmosf. i okenana", 1967, Vol. III, No. 6.
136. Georgii, H. Meteorol. Rundschau, Vol. 11 (1958).

137. Pasceri, R., and Friedlander, S. J. Atmosph. Sci., Vol. 22, No. 5 (1965).
138. Schmolinskiy, F. Meteorol. Zeit., Bd. 61, No. 6 (1944).
139. Laktionov, A.G. — "Izv. AN SSSR, seriya geofiz.", 1958, No. 3; 1959, No. 11; 1960, Nos. 4, 5, 9.
140. Newkirk, G., and Eddy, Y. J. Atmosph. Science, Vol. 1 (1964).
141. Fenn, R., and Gerber, H. U.S.A.S.R.D.L. Fort Monmouth, New Jersey, Tech. Rep. 2247 (1962).
142. Fenn, R. U.S.A.S.R.D.L. Fort Monmouth, New Jersey, Tech. Rep. 2247 (1962).
143. Deirmendjian, D., and Sekera, Z. JOSA, Vol. 46, No. 8 (1956).
144. Sekihara, K., and Murui, K. Papers in Meteorol. and Geophysics, Vol. 12, No. 1 (1961).
145. Moore, D., and Mason, B.Q. Journ. Roy. Met. Soc., Vol. 80 (1954).
146. Volz, F. Ber. d. Deutsch. Wetterd., Bd. 2, Nr. 13 (1954).
147. Junge, C., Chagnon, C., and Manson, J. J. of Meteor., Vol. 18, No. 1, (1961).
148. Volz, F., and Goody, R. J. Atmosph. Science, Vol. 19 (1962).
149. Giese, R., Bary, E. de, Bullrich, K., and Vinnermann, C. Tabellen der Streufunktionen. (Tables of Scattering Functions) Akademie Verlag, Berlin, 1962.
150. Volz, F. Optik des Dunstes. Handbuch der Geophysik. (Optics of Dust, and Fogs. Handbook of Geophysics) Vol. 8, Borntrager, Berlin, p. 823, (1956).
151. Middleton, W. Gerl. Beitr. Geophys., Vol. 44 (1935).
152. Fenn, R. Beitr. Physik d. Atmosph., Vol. 37 (1964).
153. Gertner, G. Prozrachnost' zamutnennoy atmosfery dlya infrakrasnykh voln (Transmittance of Turbid Atmosphere for Infrared Waves. M.-L., Izd-vo "Gosenergo", 1949.

TABLE 1a. Sky Spectral Brightness B (W/cm^2-sterad-μm) x 10^2

	ψ°														
Z°	0	45	90	135	180	0	45	90	135	180	0	45	90	135	180
1	2	3	4	5	6	7	8	9	10	11	12	13	14	15	16

27.VIII 1965, a. m. λ=0,691 μm; p_b=0,86±0,01; τ_b=0,15
$Z_\odot$=78°,1 $Z_\odot$=70°,4 $Z_\odot$=63°,3

0	0,064	0,064	0,064	0,064	0,064	0,083	0,083	0,083	0,083	0,083	0,112	0,112	0,112	0,112	0,112
15	0,090	0,080	0,064	0,056	0,055	0,120	0,105	0,081	0,066	0,063	0,168	0,141	0,107	0,087	0,084
30	0,140	0,107	0,068	0,055	0,055	0,220	0,105	0,086	0,067	0,064	0,321	0,205	0,112	0,082	0,077
45	0,320	0,166	0,083	0,069	0,072	0,550	0,235	0,100	0,079	0,082	—	0,301	0,127	0,091	0,092
60	—	0,290	0,112	0,099	0,108	—	0,366	0,140	0,114	0,123	—	0,446	0,169	0,126	0,132
75	—	0,540	0,208	0,203	0,215	—	0,549	0,239	0,213	0,239	—	0,657	0,257	0,231	0,249

27.VIII 1965, a. m. λ=0,553 μm; p_b=0,82±0,01; τ_b=0,20
$Z_\odot$=76° $Z_\odot$=68°,6 $Z_\odot$=61°,3

0	0,149	0,149	0,149	0,149	0,149	0,198	0,198	0,198	0,198	0,198	0,248	0,248	0,248	0,248	0,248
15	0,204	0,184	0,153	0,139	0,137	0,281	0,247	0,196	0,169	0,163	0,361	0,313	0,245	0,205	0,195
30	0,320	0,244	0,186	0,144	0,146	0,481	0,345	0,217	0,175	0,170	0,693	0,440	0,260	0,202	0,190
45	0,643	0,356	0,201	0,182	0,192	1,04	0,502	0,247	0,208	0,211	—	0,641	0,300	0,234	0,226
60	—	0,587	0,280	0,266	0,302	—	0,755	0,335	0,297	0,327	—	0,887	0,394	0,322	0,340
75	—	1,01	0,514	0,494	0,570	—	1,19	0,554	0,541	0,614	—	1,30	0,693	0,575	0,635

27.VIII 1965, a. m. λ=0,404 μm; p_b=0,66±0,01; τ_b=0,42
$Z_\odot$=72°,5 $Z_\odot$=65°,8 $Z_\odot$=58°,7

0	0,332	0,332	0,332	0,332	0,332	0,438	0,438	0,438	0,438	0,438	0,546	0,546	0,546	0,546	0,546
5	0,406	0,378	0,331	0,310	0,303	0,579	0,524	0,443	0,402	0,398	0,734	0,660	0,546	0,485	0,462
0	0,610	0,495	0,381	0,353	0,353	0,848	0,669	0,481	0,417	0,408	1,13	0,846	0,582	0,492	0,464
5	1,04	0,681	0,449	0,445	0,463	1,53	0,907	0,558	0,506	0,516	—	1,10	0,656	0,568	0,568
60	—	0,951	0,575	0,606	0,669	—	1,19	0,699	0,688	0,741	—	1,41	0,801	0,747	0,788
75	—	1,28	0,794	0,878	0,993	—	1,56	0,950	1,01	1,12	—	1,71	1,08	1,10	1,20

7.IX 1965, a. m. λ=0,691 μm; p_b=0,86±0,2; τ_b=0,15
$Z_\odot$=76°,1 $Z_\odot$=69°,9 $Z_\odot$=61°,6

0	0,076	0,076	0,076	0,076	0,076	0,091	0,091	0,091	0,091	0,091	0,114	0,114	0,114	0,114	0,114
15	0,111	0,097	0,079	0,069	0,066	0,130	0,111	0,087	0,072	0,069	0,180	0,150	0,113	0,092	0,085
30	0,188	0,133	0,083	0,067	0,064	0,240	0,165	0,096	0,074	0,071	0,366	0,219	0,120	0,086	0,080
45	0,405	0,206	0,101	0,080	0,080	0,588	0,258	0,112	0,086	0,087	—	0,319	0,137	0,095	0,092
60	—	0,353	0,136	0,119	0,130	—	0,399	0,150	0,122	0,133	—	0,455	0,169	0,131	0,136
75	—	0,610	0,230	0,216	0,248	—	0,659	0,260	0,233	0,267	—	0,652	0,271	0,248	0,261

7.IX 1965, a. m.; λ=0,593 μm; p_b=0,80±0,02; τ_b=0,22
$Z_\odot$=74°,4 $Z_\odot$=68°,2 $Z_\odot$=60°,1

0	0,130	0,130	0,130	0,130	0,130	0,155	0,155	0,155	0,155	0,155	0,192	0,192	0,192	0,192	0,192
15	0,179	0,158	0,127	0,111	0,108	0,224	0,192	0,150	0,126	0,120	0,291	0,250	0,188	0,158	0,146
30	0,288	0,211	0,133	0,115	0,109	0,385	0,271	0,162	0,127	0,122	0,558	0,358	0,203	0,148	0,139
45	0,615	0,322	0,166	0,131	0,146	0,844	0,392	0,189	0,149	0,149	—	0,501	0,226	0,167	0,158
60	—	0,517	0,222	0,197	0,217	—	0,593	0,244	0,311	0,225	—	0,684	0,282	0,228	0,236
75	—	0,862	0,364	0,351	0,416	—	0,920	0,398	0,386	0,434	—	0,970	0,418	0,396	0,440

7.IX 1965, a. m. λ=0,495 μm; p_b=0,76±0,02; τ_b=0,28
$Z_\odot$=72°,2 $Z_\odot$=65°,7 $Z_\odot$=58°,2

0	0,258	0,258	0,258	0,258	0,258	0,296	0,296	0,296	0,296	0,296	0,386	0,386	0,386	0,386	0,386
15	0,355	0,320	0,266	0,248	0,234	0,403	0,359	0,280	0,245	0,237	0,557	0,486	0,382	0,318	0,324
30	0,548	0,416	0,284	0,242	0,242	0,678	0,496	0,319	0,258	0,250	0,994	0,679	0,407	0,312	0,290
45	1,04	0,604	0,339	0,299	0,312	1,37	0,713	0,372	0,306	0,314	—	0,918	0,453	0,351	0,342
60	—	0,935	0,456	0,432	0,477	—	1,04	0,479	0,430	0,479	—	1,22	0,569	0,482	0,500
75	—	1,42	0,703	0,723	0,843	—	1,50	0,745	0,745	0,840	—	1,65	0,865	0,816	0,902

TABLE 1a (cont'd)

1	2	3	4	5	6	7	8	9	10	11	12	13	14	15	16

11.IX 1965, a. m. $\lambda=0,691$ μm; $p_b=0,88\pm0,01$; $\tau_b=0,13$
$Z_\odot=76°,7$ $Z_\odot=69°,6$ $Z_\odot=61°,7$

0	0,058	0,058	0,058	0,058	0,058	0,067	0,067	0,067	0,067	0,067	0,084	0,084	0,084	0,084	0,084
15	0,079	0,069	0,055	0,048	0,046	0,099	0,084	0,065	0,054	0,052	0,134	0,111	0,081	0,066	0,062
30	0,131	0,094	0,058	0,047	0,047	0,176	0,120	0,069	0,053	0,050	0,252	0,158	0,085	0,062	0,057
45	0,304	0,148	0,071	0,060	0,064	0,405	0,179	0,081	0,063	0,064	—	0,225	0,098	0,069	0,069
60	—	0,258	0,104	0,092	0,103	—	0,289	0,113	0,094	0,102	—	0,325	0,126	0,101	0,106
75	—	0,488	0,179	0,174	0,202	—	0,484	0,193	0,181	0,209	—	0,495	0,214	0,195	0,212

11.IX 1965 a. m. $\lambda=0,650$ μm; $p_b=0,88\pm0,01$; $\tau_b=0,13$
$Z_\odot=74°,8$ $Z_\odot=67°,7$ $Z_\odot=59°,8$

0	0,079	0,079	0,079	0,079	0,079	0,093	0,093	0,093	0,093	0,093	0,114	0,114	0,114	0,114	0,114
15	0,112	0,099	0,079	0,069	0,066	0,138	0,121	0,093	0,078	0,074	0,179	0,150	0,111	0,087	0,085
30	0,192	0,136	0,083	0,069	0,069	0,246	0,169	0,100	0,076	0,072	0,339	0,216	0,118	0,087	0,080
45	0,406	0,206	0,101	0,084	0,089	0,578	0,252	0,115	0,089	0,093	—	0,313	0,134	0,100	0,096
60	—	0,354	0,143	0,129	0,145	—	0,393	0,155	0,132	0,146	—	0,433	0,169	0,138	0,142
75	—	0,632	0,249	0,245	0,285	—	0,658	0,278	0,257	0,291	—	0,652	0,300	0,271	0,292

11.IX 1965 a. m. $\lambda=0,447$ μm; $p_b=0,74\pm0,01$; $\tau_b=0,30$
$Z_\odot=72°,4$ $Z_\odot=65°,5$ $Z_\odot=57°,2$

0	0,324	0,324	0,324	0,324	0,324	0,390	0,390	0,390	0,390	0,390	0,506	0,506	0,506	0,506	0,506
15	0,418	0,386	0,331	0,309	0,301	0,530	0,480	0,400	0,350	0,340	0,710	0,630	0,510	0,440	0,410
30	0,632	0,502	0,363	0,321	0,326	0,840	0,630	0,430	0,360	0,360	1,170	0,840	0,540	0,420	0,400
45	1,11	0,694	0,435	0,414	0,435	1,52	0,870	0,500	0,450	0,460	—	1,09	0,610	0,500	0,490
60	—	1,03	0,579	0,589	0,662	—	1,240	0,660	0,630	0,690	—	1,49	0,770	0,690	0,730
75	—	1,60	0,870	0,958	1,10	—	1,79	1,00	1,04	1,18	—	1,98	1,13	1,14	1,26

TABLE 1b. Sky Spectral Brightness B (W/cm^2-sterad-un) x 10^2

Z°	ψ°											
	34	64	94	124	154	176	30	60	90	120	120	150
	12.VI 1964, a. m. $\lambda=0,340$ μm; $p_b=0,481$; $\tau_b=0,73$											
	$Z_\odot=44°,1$						$Z_\odot=41°,5$					
0	0,59	0,59	0,59	0,59	0,59	0,59	0,64	0,64	0,64	0,64	0,64	0,64
10	0,64	0,60	0,58	0,53	0,51	0,50	0,74	0,70	0,64	0,60	0,58	0,57
20	0,75	0,64	0,57	0,52	0,49	0,49	0,87	0,76	0,64	0,58	0,55	0,55
30	0,86	0,76	0,58	0,55	0,49	0,48	1,00	0,83	0,67	0,58	0,55	0,53
40	0,95	0,74	0,61	0,54	0,52	0,51	1,09	0,84	0,69	0,60	0,57	0,56
50	1,02	0,79	0,65	0,60	0,58	0,57	1,13	0,88	0,72	0,64	0,62	0,61
60	1,05	0,84	0,71	0,66	0,66	0,67	1,16	0,93	0,78	0,71	0,70	0,71

Z°	ψ°											
	15	45	75	105	135	165	2	32	62	92	122	152
	$Z_\odot=31°,2$						$Z_\odot=26°,4$					
0	0,78	0,78	0,78	0,78	0,78	0,78	0,88	0,88	0,88	0,88	0,88	0,88
10	0,96	0,89	0,81	0,76	0,70	0,68	1,16	1,07	0,94	0,86	0,79	0,76
20	1,31	0,96	0,81	0,72	0,66	0,63	2,12	1,18	0,95	0,82	0,74	0,71
30	1,56	1,03	0,85	0,72	0,67	0,63	2,13	1,26	0,94	0,84	0,74	0,69
40	1,35	1,02	0,85	0,73	0,66	0,62	1,34	1,18	0,97	0,82	0,74	0,68
50	1,31	1,06	0,87	0,77	0,70	0,67	1,28	1,16	0,97	0,85	0,76	0,72
60	1,24	1,08	0,91	0,79	0,75	0,72	1,25	1,15	0,98	0,85	0,78	0,75

Note: Commas represent decimal points.

TABLE 2a. Sky Spectral Brightness at Small Angular Distances from Sun, $\varphi < 10°$ (autumn-summer observations)

φ	Date	6.V 1965, a. m.			12.V 1965, a. m.			15.V 1965, a. m.			5.VI 1965, a. m.			7.VI 1965, a. m.		
	λ, μm	$m_{\odot}$ = 2,90	$m_{\odot}$ = 2,00	$m_{\odot}$ = 1,40	$m_{\odot}$ = 2,90	$m_{\odot}$ = 2,00	$m_{\odot}$ = 1,40	$m_{\odot}$ = 2,90	$m_{\odot}$ = 2,00	$m_{\odot}$ = 1,40	$m_{\odot}$ = 2,90	$m_{\odot}$ = 2,00	$m_{\odot}$ = 1,40	$m_{\odot}$ = 2,90	$m_{\odot}$ = 2,00	$m_{\odot}$ = 1,40
1	2	3	4	5	6	7	8	9	10	11	12	13	14	15	16	17
2°	0,730	63,6	47,1	40,5	34,8	—	—	51,4	45,2	47,6	49,6	39,6	27,1	19,3	22,3	18,9
	0,691	75,8	53,6	44,2	35,6	25,2	29,5	53,0	44,6	—	51,6	31,4	26,7	23,6	20,7	19,9
	0,650	90,6	65,1	52,9	36,1	25,6	30,3	58,4	49,0	54,2	47,5	40,8	26,9	26,4	23,1	21,5
	0,553	81,2	65,5	56,5	33,4	31,6	31,7	70,6	63,3	70,9	58,5	50,2	33,7	26,7	26,2	24,9
	0,520	75,8	65,0	58,0	45,9	33,5	45,0	74,2	66,8	77,3	57,9	49,9	36,5	25,9	28,0	26,5
	0,495	85,0	73,6	67,0	44,5	32,2	45,1	78,1	73,6	79,5	57,3	49,3	36,2	28,2	30,5	28,3
	0,470	76,1	73,7	65,3	41,2	30,9	48,4	58,0	73,9	60,9	54,4	48,4	38,2	30,8	31,6	30,6
	0,447	63,0	71,5	65,3	38,5	29,4	47,6	73,5	67,1	79,4	54,1	46,7	34,2	25,7	28,8	27,8
	0,423	45,7	55,1	57,2	30,0	24,6	27,3	59,0	62,6	71,2	44,9	38,6	31,5	21,0	21,9	23,1
	0,410	38,1	52,4	63,7	27,5	19 4	33,5	45,4	47,6	58,4	44,3	36,1	30,3	17,4	22,0	21,5
4°	0,730	24,1	19,7	16,9	14,1	9,61	—	29,9	23,6	23,1	18,0	14,4	9,41	7,80	8,80	8,70
	0,691	29,1	21,2	17,8	15,0	10,4	13,4	31,1	23,5	27,1	19,1	11,1	9,40	6,40	8,80	7,40
	0,650	31,8	24,1	19,2	15,7	11,3	14,6	35,8	28,7	30,7	17,8	15,8	10,2	14,1	10,4	9,00
	0,553	30,3	24,7	21,6	13,9	13,6	18,4	38,8	33,4	36,4	21,7	17,4	12,0	11,4	10,5	9,30
	0,520	28,4	24,6	22,2	19,2	14,2	19,3	39,9	34,9	39,3	21,4	16,5	12,3	11,4	11,1	9,70
	0,495	30,0	33,4	24,2	19,1	14,4	17,5	43,1	37,6	41,1	21,4	17,2	13,3	12,4	12,5	10,8
	0,470	28,2	27,5	24,7	17,5	13,9	21,6	35,5	35,1	41,7	20,2	16,2	12,7	11,5	13,2	11,5
	0,447	24,3	27,1	24,6	16,1	12,8	22,5	36,8	35,3	41,0	21,7	16,8	14,4	11,8	12,0	10,9
	0,423	16,7	21,1	19,9	13,6	11,2	19,3	31,9	31,6	37,2	14,0	14,6	11,5	9,80	8,00	9,20
	0,410	12,4	19,7	19,0	10,8	9,70	16,2	25,4	24,1	32,4	12,7	13,7	11,4	9,40	9,20	9,00

Note: Commas represent decimal points.

TABLE 2a (cont'd)

1	2	3	4	5	6	7	8	9	10	11	12	13	14	15	16	17
6°	0,730	12,7	11,0	8,54	8,98	6,74	8,49	20,5	17,0	16,5	10,2	8,20	5,42	5,83	4,39	3,84
	0,691	14,8	11,9	9,34	9,37	6,97	8,54	20,7	15,6	17,4	10,2	6,02	5,33	6,44	4,68	4,42
	0,650	17,1	14,0	11,5	9,65	7,22	9,70	22,0	17,4	17,9	8,70	7,79	5,50	7,25	5,74	4,66
	0,553	17,0	12,9	11,3	9,70	9,77	13,1	24,3	21,6	21,9	11,0	9,27	7,09	7,11	6,57	5,58
	0,520	16,5	13,2	11,6	12,6	11,0	13,6	21,2	21,5	22,7	12,2	8,82	7,53	9,04	7,14	5,95
	0,495	17,9	13,1	13,2	12,4	9,80	10,3	24,7	22,6	22,9	11,1	9,36	7,76	7,88	7,82	6,28
	0,470	15,9	14,1	12,9	11,3	9,30	14,4	17,7	21,7	23,1	7,90	8,97	7,86	8,66	8,26	7,06
	0,447	15,2	13,4	12,8	11,0	9,44	14,3	21,1	19,4	22,8	10,5	9,34	8,06	7,89	7,40	6,25
	0,423	12,6	10,9	10,4	8,99	8,58	12,2	13,2	17,8	21,0	10,5	8,11	6,99	6,48	5,89	5,60
	0,410	11,0	11,3	10,5	8,32	8,64	11,2	13,4	12,1	17,2	9,94	7,85	6,64	5,89	5,34	3,57
8°	0,730	9,01	7,09	5,63	6,54	5,06	—	14,5	11,7	11,1	6,89	5,01	3,51	6,33	3,84	2,64
	0,691	9,60	7,79	6,10	6,99	5,39	6,69	15,0	11,0	12,6	7,11	3,98	3,54	4,92	3,83	3,13
	0,650	10,8	8,24	6,70	7,70	5,86	7,27	16,3	13,0	13,6	6,99	5,52	3,88	5,96	4,42	3,52
	0,553	10,1	8,56	7,20	6,60	7,12	8,63	16,6	12,9	15,7	8,17	6,57	4,86	5,66	4,63	3,80
	0,520	9,92	8,62	7,40	9,79	7,73	9,37	16,4	13,7	14,4	7,50	8,12	5,03	5,53	5,05	4,11
	0,495	11,0	9,30	8,20	9,80	7,70	9,30	17,4	15,0	15,2	7,66	6,90	5,42	6,37	5,74	4,53
	0,470	10,5	9,15	8,50	9,30	7,70	9,80	12,8	14,3	15,3	7,13	6,55	5,44	6,90	5,95	5,01
	0,447	9,79	9,24	10,7	8,87	7,72	10,1	14,6	13,7	15,8	7,62	7,04	5,82	6,14	6,37	4,94
	0,423	7,31	7,03	6,70	7,65	6,71	8,37	12,4	12,2	14,3	6,27	5,92	5,26	5,57	4,74	4,21
	0,410	6,62	6,04	6,80	6,50	5,90	7,00	10,0	8,12	12,0	6,00	5,49	5,05	5,28	5,45	4,65

Note: Commas represent decimal points.

TABLE 2b. Sky Spectral Brightness at Small Angular Distances from Sun, $\varphi \leq 10$ (winter observations)

φ	Date	17.XII 1965, a.m.	17.XII 1965, p.m.	18. XII 1965	11. II 1966	14. II 1966
	λ, μm	$m_\odot = 2{,}00$	$m_\odot = 2{,}00$	$m_\odot = 2{,}00$	$m_\odot = 2{,}00$	$m_\odot = 2{,}00$
1	2	3	4	5	6	7
2°	0,772	6,55	11,8	—	17,7	2,91
	0,691	7,50	14,7	4,38	21,1	3,60
	0,650	8,50	16,8	4,54	22,9	4,08
	0,617	—	17,8	4,74	24,1	4,27
	0,593	9,10	18,5	4 74	24,7	4,38
	0,553	9,80	19,4	5,07	27,3	5,12
	0,520	10,0	20,7	5,18	27,1	5,24
	0,495	9,52	21,2	4,82	26,3	5,35
	0,470	9,79	22,5	6,84	27,4	5,73
	0,447	8,82	19,2	5,84	24,2	4,90
	0,423	7,66	16,0	4,27	17,1	4,27
	0,410	7,73	16,4	4,84	18,6	4,44
4°	0,772	2,50	4,67	—	6,62	1,50
	0,691	2,94	5,97	2,08	8,07	2,00
	0,650	3,31	6,67	2,16	8,88	2,38
	0,617	—	7,61	2,41	9,38	2,64
	0,593	3,86	8,06	2,56	9,70	2,79
	0,553	4,00	8,46	2,76	10,4	3,28
	0,520	4,16	8,92	2,91	10,9	3,43
	0,495	4,23	9,52	2,84	11,3	3,64
	0,470	4,47	9,92	3,88	11,7	3,94
	0,447	4,23	9,23	3,62	10,7	3,53
	0,423	3,73	7,85	2,82	8,35	3,24
	0,410	3,92	7,93	3,24	8,13	3,64
6°	0,772	1,63	3,04	—	4,23	1,37
	0,691	1,96	3,71	1,51	5,10	1,77
	0,650	2,30	4,34	1,75	5,76	2,20
	0,617	—	4,95	2,05	5,90	2,53
	0,593	2,70	5,32	2,02	5,97	2,54
	0,553	2,88	5,82	2,28	6,61	3,05
	0,520	3,13	6,43	2,43	6,87	2,82
	0,495	3,18	6,70	2,38	6,94	3,41
	0,470	3,45	7,21	3,33	7,39	3,73
	0,447	3,24	6,66	3,12	6,54	3,27
	0,423	3,11	6,12	2,54	6,03	2,96
	0,410	3,14	5,67	2,91	5,57	3,31
8°	0,772	1,26	2,26	—	2,98	1,24
	0,691	1,60	2,92	1,36	3,62	1,64
	0,650	1,83	3,43	1,53	3,91	1,98
	0,617	—	3,88	1,77	4,12	2,23
	0,593	2,25	4,33	1,78	4,33	2,36
	0,553	2,45	4,68	2,03	4,79	2,80
	0,520	2,66	5,18	2,18	4,93	2,91
	0,495	2,78	5,59	2,18	5,12	3,14
	0,470	2,99	5,98	2,87	5,39	3,42
	0,447	2,92	5,90	2,81	5,05	3,10
	0,423	2,59	5,09	2,18	4,20	2,72
	0,410	2,76	5,07	2,64	4,37	3,16
10°	0,772	1,06	1,88	—	2,23	1,15
	0,691	1,38	2,44	1,21	2,70	1,53
	0,650	1,64	2,93	1,38	2,98	1,88
	0,617	—	3,34	1,65	3,21	2,12
	0,593	1,95	3,59	1,63	3,26	2,18
	0,553	2,14	4,00	1,85	3,67	2,46
	0,520	2,39	4,45	1,94	3,93	2,72
	0,495	2,40	4,76	1,92	4,00	2,86
	0,470	2,68	5,11	2,58	4,31	3,14
	0,447	2,51	4,90	2,59	3,80	2,78
	0,423	2,44	4,47	2,03	3,41	2,54
	0,410	2,61	4,57	2,39	3,24	2,81

Note: Commas represent decimal points.

TABLE 3. Data from Calculations (upper and lower lines) and Observations (middle line) of the Sky Spectral Brightness B (W/cm^2-sterad-μm)

Z°	Ψ°				
	0	45	90	135	180
1	2	3	4	5	6
27. VIII 1965; λ=0,533 μm; p_b=0,82±0,01 $Z_\odot$=60°					
0	0,00281	0,00281	0,00281	0,00281	0,00281
	0,00248	0,00248	0,00248	0,00248	0,00248
	0,00211	0,00211	0,00211	0,00211	0,00211
15	0,00417	0,00366	0,00284	0,00248	0,00227
	0,00361	0,00313	0,00245	0,00205	0,00195
	0,00302	0,00266	0,00214	0,00188	0,00172
30	0,00695	0,00470	0,00275	0,00212	0,00201
	0,00693	0,00440	0,00260	0,00202	0,00190
	0,00486	0,00343	0,00214	0,00163	0,00157
45	—	0,00639	0,00308	0,00241	0,00241
	—	0,00641	0,00300	0,00234	0,00226
	—	0,00456	0,00242	0,00195	0,00197
60	—	0,00849	0,00397	0,00346	0,00360
	—	0,00887	0,00394	0,00322	0,00340
	—	0,00616	0,00311	0,00281	0,00300
75	—	0,0120	0,00605	0,00591	0,00648
	—	0,0130	0,00693	0,00575	0,00635
	—	0,00924	0,00491	0,00489	0,00557
11.IX 1965, a.m. λ=0,600 μm; p_b=0,88±0,01; $Z_\odot$=59°,8					
0	0,00158	0,00158	0,00158	0,00158	0,00158
	0,00114	0,00114	0,00114	0,00114	0,00114
	0,00107	0,00107	0,00107	0,00107	0,00107
15	0,00246	0,00212	0,00158	0,00134	0,00149
	0,00179	0,00150	0,00111	0,00087	0,00085
	0,00164	0,00143	0,00109	0,00095	0,00086
30	0,00448	0,00292	0,00157	0,00112	0,00104
	0,00339	0,00216	0,00118	0,00087	0,00080
	0,00290	0,00197	0,00114	0,00081	0,00075
45	—	0,00402	0,00174	0,00131	0,00131
	—	0,00313	0,00134	0,00100	0,00096
	—	0,00268	0,00128	0,00098	0,00100
60	—	0,00542	0,00275	0,00187	0,00189
	—	0,00433	0,00169	0,00138	0,00142
	—	0,00376	0,00172	0,00148	0,00156
75	—	0,00782	0,00350	0,00320	0,00350
	—	0,00652	0,00300	0,00271	0,00292
	—	0,00554	0,00290	0,00268	0,00302
6.IX 1965, a.m. λ=0,593 μm; p_b=0,79±0,01; $Z_\odot$=59°,1					
0	0,00279	0,00279	0,00279	0,00279	0,00279
	0,00200	0,00200	0,00200	0,00200	0,00200
	0,00203	0,00203	0,00203	0,00203	0,00203
15	0,00441	0,00370	0,00279	0,00237	0,00213
	0,00312	0,00263	0,00194	0,00157	0,00148
	0,00303	0,00262	0,00200	0,00171	0,00155

Note: Commas represent decimal points.

TABLE 3 (cont'd)

1	2	3	4	5	6
30	0,00767	0,00495	0,00266	0,00196	0,00182
	0,00600	0,00382	0,00210	0,00142	0,00140
	0,00536	0,00347	0,00196	0,00143	0,00134
45	—	0,00636	0,00296	0,00218	0,00215
	—	0,00505	0,00231	0,00166	0,00161
	—	0,00479	0,00217	0,00162	0,00162
60	—	0,00899	0,00370	0,00304	0,00312
	—	0,00739	0,00290	0,00228	0,00235
	—	0,00632	0,00277	0,00232	0,00239
75	—	0,0122	0,00542	0,00507	0,00542
	—	0,0103	0,00466	0,00417	0,00450
	—	0,00917	0,00427	0,00396	0,00430

TABLE 4. Comparison of Theoretical Sky Brightness Values B_t (upper line) and Observed (lower line) B_o in the Ultraviolet Spectral Region B (W/cm^2-sterad-μm)

$Z°$	$\psi°$									
	0	20	40	60	80	100	120	140	160	180
	30.VII 1965, a.m. λ=0,34 μm ; p_b=0,492; $Z_\odot$=41,5°									
0	0,0062	0,0062	0,0062	0,0062	0,0062	0,0062	0,0062	0,0062	0,0062	0,0062
	0,0066	0,0066	0,0066	0,0066	0,0066	0,0066	0,0066	0,0066	0,0066	0,0066
10	0,0071	0,0071	0,0068	0,0066	0,0064	0,0062	0,0060	0,0059	0,0057	0,0057
	0,0072	0,0071	0,0069	0,0064	0,0063	0,0061	0,0059	0,0056	0,0054	0,0055
20	0,0082	0,0080	0,0076	0,0070	0,0065	0,0060	0,0056	0,0054	0,0053	0,0052
	0,0094	0,0081	0,0072	0,0070	0,0063	0,0063	0,0057	0,0056	0,0053	0,0053
30	0,0103	0,0095	0,0085	0,0076	0,0068	0,0062	0,0057	0,0054	0,0052	0,0051
	0,0121	0,0094	0,0089	0,0078	0,0073	0,0065	0,0051	0,0053	0,0054	0,0057
40	—	0,0101	0,0090	0,0078	0,0069	0,0062	0,0057	0,0053	0,0052	0,0052
	—	0,0117	0,0099	0,0083	0,0074	0,0063	0,0062	0,0062	0,0058	0,0056
50	0,0127	0,0110	0,0095	0,0082	0,0072	0,0064	0,0059	0,0056	0,0056	0,0056
	0,0145	0,0118	0,0093	0,0088	0,0077	0,0070	0,0064	0,0052	0,0063	0,0060
60	0,0121	0,0113	0,0101	0,0083	0,0077	0,0069	0,0065	0,0064	0,0064	0,0065
	0,0140	0,0116	0,0107	0,0083	0,0076	0,0071	0,0071	0,0069	0,0070	0,0070
70	0,0122	0,0116	0,0105	0,0093	0,0081	0,0075	0,0074	0,0076	0,0078	0,0079
	0,0121	0,0110	0,0099	0,0088	0,0075	0,0077	0,0073	0,0074	0,0074	0,0078

Note: Commas represent decimal points.

TABLE 5a. Absolute Brightness Indicatrix Measurement Conditions

Series No.	Date	λ, μm	P_b	$m_\odot$	Underlying surface
1	7.VI 1962, a. m.	0,634	0,87	4,37	Grass covering
2	"	0,542	0,81	4,08	"
3	"	0,450	0,76	5,12	"
4	20.VI 1962, a. m.	0,542	0,86	4,54	"
5	"	0,634	0,91	4,08	"
6	29.VI 1962, a. m.	0,634	0,89	4,72	"
7	"	0,542	0,84	4,22	"
8	"	0,450	0,77	5,60	"
9	30.VI 1962, a. m.	0,634	0,91	4,72	"
10	"	0,542	0,86	4,08	"
11	4.VIII 1962, a. m.	0,634	0,88	3,82	"
12	"	0,542	0,84	3,48	"
13	"	0,450	0,75	4,72	"
14	17.VIII 1962, a. m.	0,634	0,90	3,30	"
15	"	0,450	0,75	4,44	"
16	23.VIII 1962, a. m.	0,450	—	2,16	"
17	24.VIII 1962, a. m.	0,634	0,90	4,13	"
18	"	0,542	0,84	3,30	"
19	"	0,450	0,76	3,63	"
20	8.IX 1962, a. m.	0,634	0,88	2,65	"
21	2.IX 1962, a. m.	0,542	0,83	3,49	"
22	"	0,450	0,75	3,00	"
23	9.VIII 1962, a. m.	0,634	0,90	4,54	"
24	"	0,542	0,85	3,94	"
25	"	0,450	0,77	5,12	"
26	17.IX 1962, a. m.	0,634	0,90	4,91	"
27	"	0,542	0,85	3,63	"
28	"	0,450	0,78	4,13	"
29	30.VII 1965, a. m.	0,340	0,492	3,18	"
30	7.IX 1965, a. m.	0,340	0,37	4,58	"
31	"	"	"	2,64	"
32	12.IX 1965, a. m.	0,340	0,45	3,73	"
33	14.XI 1966, a. m.	0,312	0,27	2,38	Snow covering
34	"	0,334	0,43	2,34	"
35	"	0,358	0,56	2,28	"
36	"	0,377	0,62	2,22	"

TABLE 5b. Absolute Brightness Indicatrices*

1		2		3		4	
φ°	$\mu(\varphi)$	φ°	$\mu(\varphi)$	φ°	$\mu(\varphi)$	φ°	$\mu(\varphi)$
1	2	3	4	5	6	7	8
2,0	0,52	2,0	0,59	2,0	0,64	1,9	0,22
2,5	0,40	2,5	0,47	2,5	0,52	2,6	0,151
3,0	0,33	3,0	0,38	3,0	0,46	2,9	0,129
3,5	0,28	3,5	0,32	3,5	0,36	3,6	0,103
4,0	0,24	4,0	0,28	4,0	0,31	3,9	0,096
5,9	0,152	5,8	0,167	5,9	0,21	5,8	0,070
10	0,076	10	0,084	10	0,119	10	0,050
15	0,053	15	0,063	15	0,094	15	0,042
20	0,038	19	0,048	20	0,077	20	0,037
29	0,025	29	0,035	29	0,060	29	0,030
39	0,0181	39	0,026	39	0,050	39	0,024
49	0,0135	48	0,020	49	0,041	49	0,0192
58	0,0107	58	0,0166	59	0,036	58	0,0158
68	0,0087	68	0,0140	69	0,031	68	0,0132
78	0,0080	77	0,0125	78	0,027	78	0,0117
87	0,0068	87	0,0114	88	0,027	87	0,0107
97	0,0068	96	0,0114	97	0,026	97	0,0098

*The series number, information about which is contained in Table 5a, is designated at the top of the columns.

Note: Commas represent decimal points.

TABLE 5b (cont'd)

/102

1	2	3	4	5	6	7	8
106	0,0068	106	0,0114	107	0,026	106	0,0098
116	0,0069	114	0,0116	116	0,027	116	0,0107
125	0,0073	123	0,0120	125	0,030	124	0,0111
133	0,0076	132	0,0130	134	0,031	133	0,0120
141	0,0080	140	0,0140	144	0,033	141	0,0128
148	0,0083	146	0,0145	150	0,035	148	0,0132
154	0,0083	152	0,0145	158	0,036	155	0,0137

5		6		7		8	
φ°	μ(φ)	φ°	μ(φ)	φ°	μ(φ)	φ°	μ(φ)
1,9	0,20	1,9	0,28	1,9	0,31	1,9	0,38
2,6	0,131	2,6	0,197	2,6	0,22	2,6	0,28
2,9	0,109	2,9	0,173	2,9	0,196	2,9	0,25
3,6	0,088	3,6	0,129	3,6	0,155	3,6	0,20
3,9	0,080	3,9	0,124	3,9	0,142	3,9	0,182
5,8	0,054	5,9	0,077	5,9	0,088	5,8	0,131
10	0,036	10	0,049	10	0,054	10	0,083
15	0,028	15	0,030	15	0,039	15	0,071
19	0,024	20	0,024	19	0,033	20	0,063
29	0,0196	29	0,0177	29	0,026	30	0,053
39	0,0156	39	0,0137	39	0,021	40	0,043
48	0,0123	49	0,0108	48	0,0164	49	0,036
58	0,0097	58	0,0091	58	0,0137	59	0,031
67	0,0081	68	0,0074	68	0,0116	69	0,028
77	0,0069	78	0,0062	77	0,0100	79	0,025
86	0,0061	87	0,0055	86	0,0092	88	0,024
96	0,0055	97	0,0053	96	0,0089	98	0,024
105	0,0057	106	0,0053	105	0,0089	108	0,024
114	0,0059	116	0,0055	115	0,0094	117	0,025
122	0,0062	124	0,0059	123	0,0097	126	0,027
131	0,0065	133	0,0062	132	0,0106	136	0,028
138	0,0068	141	0,0066	140	0,0113	144	0,031
145	0,0071	148	0,0068	146	0,0119	152	0,031
152	0,0074	156	0,0068	153	0,0119	160	0,032

9		10		11		12	
φ°	μ(φ)	φ°	μ(φ)	φ°	μ(φ)	φ°	μ(φ)
1,9	0,196	1,9	0,23	1,9	1,07	1,9	1,03
2,6	0,126	2,6	0,153	2,6	0,69	2,6	0,66
2,9	0,111	2,9	0,135	2,9	0,57	2,9	0,55
3,6	0,089	3,6	0,108	3,6	0,40	3,6	0,39
3,9	0,079	3,9	0,099	3,9	0,35	3,9	0,33
5,8	0,052	5,8	0,067	5,8	0,171	—	—
10	0,033	10	0,045	10	0,069	—	—
15	0,024	15	0,035	15	0,048	15	0,053
20	0,0197	19	0,030	19	0,035	19	0,046
29	0,0149	29	0,024	29	0,024	29	0,036
39	0,0118	39	0,0197	39	0,0184	38	0,029
49	0,0087	48	0,0163	48	0,0153	48	0,023
58	0,0080	58	0,0132	57	0,0122	57	0,0192
68	0,0067	68	0,0118	67	0,0101	67	0,0166
78	0,0058	77	0,0105	76	0,0087	76	0,0144
87	0,0053	87	0,0094	86	0,0077	86	0,0131
97	0,0050	96	0,0093	96	0,0073	95	0,0131
106	0,0050	105	0,0093	105	0,0073	104	0,0125

Note: Commas represent decimal points.

TABLE 5b (cont'd)

1	2	3	4	5	6	7	8
116	0,0053	115	0,0097	114	0,0073	112	0,0129
124	0,0055	123	0,0102	122	0,0074	121	0,0132
133	0,0060	132	0,0110	130	0,0077	129	0,0139
141	0,0065	140	0,0115	138	0,0081	136	0,0147
148	0,0068	146	0,0123	144	0,0086	142	0,0150
156	0,0070	152	0,0126	150	0,0091	147	0,0153

13		14		15		16	
φ°	$\mu(\varphi)$	φ°	$\mu(\varphi)$	φ°	$\mu(\varphi)$	φ°	$\mu(\varphi)$
1,9	1,24	1,9	0,67	1,9	1,64	1,9	1,79
2,6	0,78	2,6	0,43	2,6	1,00	2,6	1,07
2,9	0,64	2,9	0,35	2,9	0,79	2,9	0,83
3,6	0,46	3,6	0,25	3,6	0,56	3,6	0,60
3,9	0,40	3,9	0,22	3,9	0,47	3,9	0,53
5,8	0,22	5,7	0,104	5,8	0,23	5,3	0,27
10	0,122	10	0,043	10	0,124	9,0	0,168
15	0,088	14	0,034	15	0,093	13	0,124
20	0,078	19	0,025	20	0,079	18	0,100
29	0,063	29	0,0184	29	0,063	27	0,077
39	0,053	38	0,0144	39	0,052	35	0,061
49	0,045	48	0,0116	49	0,044	44	0,050
58	0,039	57	0,0095	58	0,038	53	0,041
68	0,034	66	0,0081	68	0,033	61	0,036
78	0,033	76	0,0069	78	0,031	70	0,031
87	0,029	85	0,0064	87	0,030	78	0,028
97	0,029	94	0,0061	97	0,029	86	0,026
106	0,029	103	0,0060	106	0,029	93	0,025
116	0,030	111	0,0061	116	0,030	100	0,026
124	0,031	120	0,0062	124	0,032	107	0,026
133	0,032	127	0,0065	133	0,033	113	0,027
141	0,035	134	0,0068	141	0,036	118	0,027
149	0,037	140	0,0071	148	0,037	123	0,027
156	0,037	145	0,0072	154	0,037	125	0,028

17		18		19		20	
φ°	$\mu(\varphi)$	φ°	$\mu(\varphi)$	φ°	$\mu(\varphi)$	φ°	$\mu(\varphi)$
1,9	0,80	1,9	—	1,9	0,91	1 9	0,79
2,6	0,50	2,6	0,52	2,6	0,59	2,6	0,55
2,9	0,42	2,9	0,43	2,9	0,49	2 9	0,46
3,6	0,30	3,6	0,32	3,6	0,36	3,6	0,32
3,9	0,26	3,9	0,28	3,9	0,31	3,9	0,28
5,9	0,128	5,7	0,195	5,8	0,180	5,7	0,158
10	0,058	10	0,078	10	0,107	—	—
15	0,038	14	0,050	15	0,084	14	0,050
19	0,029	19	0,041	19	0,073	18	0,038
29	0,020	29	0,031	29	0,060	28	0,028
39	0,0160	38	0,025	39	0,051	37	0,021
48	0,0132	48	0,020	48	0,042	46	0,0171
58	0,0107	57	0,0170	58	0,037	55	0,0139
68	0 0094	66	0,0146	67	0,033	64	0,0119
77	0,0080	76	0,0130	77	0,030	73	0,0103
87	0,0073	85	0,0117	86	0,028	82	0,0095

Note: Commas represent decimal points.

TABLE 5b (cont'd)

1	2	3	4	5	6	7	8
96	0,0068	95	0,0112	96	0,028	90	0,0087
105	0,0068	103	0,0112	105	0,028	98	0,0082
114	0,0070	111	0,0115	114	0,029	106	0,0082
123	0,0073	120	0,0122	122	0,030	114	0,0084
132	0,0077	127	0,0129	130	0,032	121	0,0084
140	0,0080	135	0,0134	138	0,033	126	0,0087
146	0,0085	140	0,0143	144	0,034	131	0,0087
152	0,0086	145	0,0144	148	0,035	136	0,0087

21		22		23		24	
φ°	μ(φ)	φ°	μ(φ)	φ°	μ(φ)	φ°	μ(φ)
1,9	1,02	1,9	1,06	1,9	0,39	1,9	0,45
2,6	0,63	2,6	0,66	2,6	0,26	2,6	0,29
2,9	0,52	2,9	0,54	2,9	0,22	2,9	0,25
3,6	0,37	3,6	0,39	—	—	3,6	0,189
3,9	0,32	3,9	0,35	3,9	0,149	3,9	0,170
5,8	0,169	5,7	0,21	5,8	0,085	5,8	0,098
10	0,088	9	0,128	10	0,047	10	0,060
14	0,064	14	0,104	—	—	14	0,043
19	0,053	19	0,089	20	0,026	19	0,037
29	0,041	28	0,072	30	0,0197	29	0,032
38	0,033	38	0,060	39	0,0156	39	0,025
48	0,026	47	0,050	49	0,0123	48	0,020
57	0,021	56	0,042	58	0,0099	58	0,0166
67	0,0178	65	0,037	68	0,0082	67	0,0141
76	0,0158	74	0,034	78	0,0073	77	0,0125
86	0,0141	83	0,031	87	0,0064	86	0,0114
95	0,0133	92	0,030	97	0,0065	96	0,0111
104	0,0132	101	0,031	106	0,0062	105	0,0112
112	0,0137	109	0,031	116	0,0063	114	0,0117
121	0,0142	117	0,034	124	0,0067	122	0,0122
129	1,0150	124	0,034	133	0,0070	130	0,0129
136	0,0157	130	0,035	141	0,0075	138	0,0139
142	0,0161	136	0,036	148	0,0077	144	9,0143
147	0,0161	141	0,037	155	0,0079	151	0,0146

25		26		27		28	
φ°	μ(φ)	φ°	μ(φ)	φ°	μ(φ)	φ°	μ(φ)
1,9	0,52	1,9	1,04	1,9	1,07	1,9	1,26
2,6	0,35	2,6	0,69	2,6	0,71	2,6	0,83
2,9	0,29	2,9	0,58	2,9	0,58	2,9	0,70
3,6	0,23	3,6	0,42	3,6	0,43	3,6	0,52
3,9	0 21	3,9	0,37	3,9	0,36	3,9	0,46
5,8	0,138	5,8	0,178	5,8	0,178	5,8	0,22
10	0,097	10	0,065	10	0,073	10	0,127
15	0,080	15	0,044	14	0,051	15	0,077
20	0,072	20	0,032	19	0,038	19	0,072
29	0,059	29	0,022	29	0,029	29	0,060
39	0,048	39	0,0172	39	0,023	39	0,051
49	0,040	49	0,0135	48	0,0189	48	0,044
59	0,034	59	0,0113	58	0,0159	58	0,040
69	0,030	68	0,0094	67	0,0139	68	0,036
78	0,028	78	0,0082	77	0,0120	77	0,033

Note: Commas represent decimal points.

TABLE 5b (cont'd)

1	2	3	4	5	6	7	8
88	0,026	88	0,0075	86	0,0112	87	0,032
98	0,026	97	0,0072	96	0,0108	96	0,032
107	0,026	107	0,0073	105	0,0108	105	0,032
117	0,028	116	0,0075	114	0,0112	114	0,033
126	0,030	125	0,0078	122	0,0119	123	0,035
135	0,031	134	0,0083	130	0,0126	134	0,037
144	0,033	143	0,0087	138	0,0134	140	0,039
151	0,035	150	0,0091	144	0 0139	146	0,040
158	0,036	157	0,0093	148	0,0141	152	0,041

29		30		31		32	
φ°	μ(φ)	φ°	μ(φ)	φ°	μ(φ)	φ°	μ(φ)
2	1,16	2	1,60	2	1.70	2	1,20
3	0,55	3	0,98	3	0,96	3	0,71
4	0,39	4	0,70	4	0,63	4	0,55
5	0,34	5	0,57	5	0,51	5	0,46
6	0,29	6	0,50	6	0,43	6	0,41
7	0,27	7	0,46	7	0,40	7	0,38
8	0,26	8	0,42	8	0,36	8	0,37
9	0,24	10	0,40	9	0,34	10	0,34
—	—	15	0,35	14	0,30	14	0,30
20	0,20	20	0,33	19	0,26	19	0,27
—	—	29	0,29	28	0,23	29	0,24
40	0,162	39	0,26	37	0,196	39	0,21
—	—	49	0,23	46	0,172	48	0,189
60	0,136	58	0,21	55	0,160	58	0,171
—	—	68	0,195	64	0,144	67	0,162
80	0,118	78	0,190	73	0,136	77	0,152
90	0,115	88	0,181	82	0,131	86	0,149
100	0,114	97	0,181	90	0,128	95	0,147
—	—	106	0,184	99	0 128	104	0,149
—	—	115	0,190	107	0,131	113	0,154
120	0,118	124	0,195	114	0,135	122	0,162
—	—	133	0,20	121	0,139	130	0,167
140	0,127	141	0,21	127	0,144	137	0,173
—	—	148	0,22	132	0,147	143	0,179
—	—	155	0,22	135	0,150	149	0,181

33		34		35		36	
φ°	μ(φ)	φ°	μ(φ)	φ°	μ(φ)	φ°	μ(φ)
2	0,48	2	0,40	2	0,31	2	0,29
3	0,40	3	0,32	3	0,25	3	0,22
4	0,34	4	0,29	4	0,22	4	0,183
6	0,33	6	0,26	6	0,190	6	0,156
10	0,30	10	0,23	10	0,158	10	0,129
15	0,28	15	0,21	15	0,141	15	0,115
20	0,26	20	0,20	20	0,131	20	0,104
40	0,23	40	0,171	40	0,107	40	0,082
60	0,20	60	0,146	60	0,091	60	0,069
80	0,182	80	0,133	80	0,083	80	0,061
90	0,182	90	0,132	90	0,081	90	0,060
100	0,182	100	0,133	100	0,081	100	0,060
110	0,188	110	0,136	110	0,085	110	0,062
120	0,194	120	0,143	120	0,088	120	0,065
125	0,194	125	0,146	125	0,091	125	0,067

Note: Commas represent decimal points.

TABLE 6. Total (weighted) μ and Aerosol μ_D Scattering Functions at Small Angular Distances from Sun, $\varphi < 10°$ (autumn–summer observations)

Date	$m_\odot$	φ	2°		4°		6°		8°		10°	
		λ, μm	μ	μ_D	μ	μ_D	μ	μ_D	μ	μ_D	μ	μ_D
1	2	3	4	5	6	7	8	9	10	11	12	13
6. V 1965, a. m.	1,95—1,52	0,730	1,93	1,93	0,77	0,77	0,43	0,43	0,276	0,273	—	—
		0,691	2,10	2,10	0,78	0,78	0,43	0,43	0,276	0,272	—	—
		0,650	2,28	2,28	0,82	0,82	0,47	0,47	0,281	0,276	—	—
		0,593	2,31	2,30	0,85	0,84	0,47	0,46	0,289	0,279	—	—
		0,553	2,30	2,29	0,86	0,85	0,46	0,45	0,294	0,281	—	—
		0,520	2,30	2,29	0,88	0,86	0,47	0,45	0,299	0,282	—	—
		0,495	2,44	2,42	0,91	0,89	0,49	0,47	0,305	0,284	—	—
		0,470	2,53	2,50	0,97	0,94	0,49	0,46	0,316	0,288	—	—
		0,447	2,76	2,73	1,03	1,00	0,51	0,48	0,322	0,289	—	—
		0,423	2,71	2,67	1,02	0,98	0,52	0,48	0,330	0,284	—	—
		0,410	2,79	2,74	1,09	1,04	0,50	0,46	0,327	0,274	—	—
	4,62—3,42	0,730	2,18	2,18	0,85	0,85	0,48	0,48	0,320	0,317	—	—
		0,691	2,18	2,18	0,85	0,85	0,48	0,48	0,318	0,314	—	—
		0,650	2,39	2,39	0,85	0,85	0,48	0,48	0,305	0,300	—	—
		0,593	2,47	2,46	0,91	0,90	0,51	0,50	0,520	0,310	—	—
		0,553	2,52	2,51	0,94	0,93	0,54	0,53	0,330	0,317	—	—
		0,520	2,57	2,55	0,95	0,93	0,51	0,49	0,340	0,323	—	—
		0,495	2,70	2,68	1,00	0,88	0,53	0,51	0,348	0,327	—	—
		0,470	2,83	2,80	1,03	1,00	0,54	0,51	0,360	0,332	—	—
		0,447	2,90	2,87	1,04	1,01	0,59	0,56	0,385	0,352	—	—
		0,423	2,94	2,90	1,07	1,03	0,61	0,57	0,428	0,382	—	—
		0,410	3,26	3,21	1,14	1,09	0,66	0,61	0,461	0,408	—	—
12. V 1965, a. m.	4,64—3,56	0,730	0,93	0,93	0,38	0,38	0,238	0,235	0,184	0,181	—	—
		0,691	0,93	0,93	0,38	0,38	0,240	0,236	0,186	0,182	—	—
		0,650	0,99	0,99	0,40	0,40	0,257	0,252	0,202	0,197	—	—
		0,593	1,04	1,03	0,42	0,41	0,273	0,263	0,206	0,196	—	—
		0,553	1,08	1,07	0,44	0,43	0,288	0,275	0,212	0,199	—	—
		0,520	1,10	1,08	0,45	0,43	0,292	0,275	0,230	0,213	—	—
		0,495	1,14	1,12	0,47	0,45	0,301	0,280	0,245	0,224	—	—
		0,470	1,20	1,17	0,48	0,46	0,315	0,287	0,260	0,222	—	—
		0,447	1,20	1,17	0,49	0,46	0,331	0,298	0,274	0,241	—	—
		0,423	1,20	1,16	0,52	0,47	0,356	0,310	0,282	0,236	—	—
		0,410	1,30	1,25	0,51	0,46	0,374	0,321	0,294	0,241	—	—
15. V 1965, a. m.	2,57—2,31	0,730	1,80	1,80	1,00	1,00	0,69	0,69	0,50	0,50	—	—
		0,691	1,80	1,80	1,04	1,04	0,70	0,70	0,50	0,50	—	—
		0,650	1,97	1,97	1,11	1,11	0,73	0,73	0,52	0,52	—	—
		0,593	2,17	2,16	1,21	1,20	0,78	0,77	0,54	0,53	—	—
		0,553	2,35	2,34	1,26	1,25	0,80	0,79	9,54	0,53	—	—
		0,520	2,52	2,50	1,37	1,35	0,82	0,80	0,54	0,52	—	—
		0,495	2,58	2,56	1,39	1,37	0,82	0,80	0,56	0,54	—	—
		0,470	2,86	2,83	1,49	1,46	0,84	0,81	0,57	0,54	—	—
		0,447	3,14	3,11	1,56	1,53	0,90	0,87	0,61	0,58	—	—
		0,423	2,94	2,90	1,47	1,43	0,86	0,82	0,59	0,55	—	—
		0,410	3,17	3,12	1,46	1,41	0,97	0,92	0,63	0,58	—	—
5. VI 1965, a. m.	3,65—3,15	0,730	1,32	1,32	0,48	0,48	0,270	0,267	0,170	0,167	—	—
		0,691	1,31	1,31	0,47	0,47	0,266	0,262	0,168	0,164	—	—
		0,650	1,36	1,36	0,48	0,43	0,262	0,263	0,175	0,170	—	—
		0,593	1,43	1,42	0,50	0,49	0,270	0,260	0,184	0,174	—	—
		0,553	1,46	1,45	0,50	0,49	0,268	0,255	0,191	0,178	—	—
		0,520	1,46	1,44	0,50	0,48	0,270	0,253	0,193	0,176	—	—

Note: Commas represent decimal points.

TABLE 6 (cont'd)

1	2	3	4	5	6	7	8	9	10	11	12	13
8. VI 1965, a.m.	3,65—3,15	0,495	1,52	1,50	0,50	0,48	0,282	0,261	0,204	0,183	—	—
		0,470	1,58	1,55	0,52	0,49	0,288	0,260	0,211	0,183	—	—
		0,447	1,50	1,47	0,54	0,51	0,304	0,270	0,222	0,189	—	—
		0,423	1,55	1,50	0,55	0,50	0,323	0,277	0,232	0,186	—	—
		0,410	1,54	1,49	0,54	0,49	0,326	0,273	0,215	0,162	—	—
7. VI 1965, a.m.	2,98—2,60	0,730	0,50	0,50	0,220	0,217	0,136	0,133	0,102	0,099	—	—
		0,691	0,49	0,49	0,221	0,217	0,136	0,132	0,100	0,096	—	—
		0,650	0,52	0,52	0,236	0,231	0,144	0,139	0,108	0,103	—	—
		0,593	0,56	0,55	0,247	0,237	0,154	0,144	0,117	0,107	—	—
		0,553	0,59	0,58	0,257	0,244	0,162	0,149	0,123	0,110	—	—
		0,520	0,58	0,57	0,259	0,242	0,172	0,155	0,124	0,107	—	—
		0,495	0,62	0,60	0,274	0,253	0,175	0,154	0,140	0,119	—	—
		0,470	0,65	0,62	0,271	0,243	0,181	0,153	0,141	0,113	—	—
		0,447	0,64	0,61	0,287	0,254	0,191	0,158	0,148	0,115	—	—
		0,423	0,67	0,62	0,293	0,247	0,206	0,160	0,168	0,122	—	—
		0,410	0,69	0,64	0,318	0,265	0,209	0,156	0,175	0,122	—	—
17. IX 1965, a.m.	3,70—3,07	0,730	0,75	0,75	0,258	0,255	0,137	0,134	0,090	0,087	0,070	0,067
		0,691	0,77	0,77	0,265	0,261	0,140	0,136	0,095	0,091	0,072	0,068
		0,650	0,81	0,81	0,272	0,267	0,143	0,138	0,098	0,093	0,075	0,070
		0,593	0,83	0,82	0,290	0,280	0,153	0,143	0,110	0,100	0,085	0,075
		0,553	0,84	0,83	0,279	0,266	0,156	0,143	0,110	0,097	0,093	0,080
		0,520	0,86	0,85	0,285	0,268	0,164	0,147	0,119	0,102	0,100	0,083
		0,495	0,89	0,87	0,305	0,284	0,170	0,149	0,130	0,109	0,110	0,089
		0,470	0,91	0,88	0,308	0,280	0,180	0,152	0,140	0,112	0,121	0,093
		0,447	0,96	0,93	0,320	0,287	0,198	0,165	0,158	0,125	0,135	0,102
		0,423	0,99	0,94	0,338	0,292	0,215	0,169	0,161	0,115	0,150	0,104
		0,410	0,97	0,92	0,346	0,294	0,221	0,169	0,174	0,122	0,154	0,102
4. X 1965, a.m.	3,20—2,45	0,730	0,162	0,159	0,065	0,062	0,050	0,047	0,039	0,036	0,036	0,033
		0,691	0,168	0,164	0,068	0,064	0,050	0,046	0,042	0,038	0,037	0,033
		0,650	0,174	0,169	0,074	0,069	0,056	0,051	0,046	0,041	0,040	0,035
		0,593	0,177	0,168	0,081	0,072	0,061	0,052	0,052	0,043	0,046	0,037
		0,553	0,189	0,168	0,088	0,076	0,071	0,059	0,059	0,047	0,054	0,042
		0,520	0,190	0,174	0,095	0,080	0,077	0,061	0,067	0,051	0,060	0,044
		0,495	0,204	0,184	0,106	0,086	0,084	0,064	0,074	0,054	0,065	0,045
		0,470	0,206	0,181	0,111	0,086	0,088	0,063	0,078	0,053	0,070	0,045
		0,447	0,212	0,182	0,119	0,089	0,097	0,067	0,088	0,058	0,077	0,047
		0,423	0,228	0,186	0,132	0,090	0,108	0,066	0,098	0,056	0,087	0,045
		0,410	0,236	0,189	0,136	0,090	0,115	0,068	0,104	0,057	0,096	0,049

TABLE 7. Total (weighted) μ and Aerosol μ_D Scattering Functions at Small Angular Distances from Sun, $\varphi \leqslant 10°$ (winter observations)

Date	$m_\odot$	φ	2°		4°		6°		8°		10°	
		λ, μm	μ	μ_D	μ	μ_D	μ	μ_D	μ	μ_D	μ	μ_D
1	2	3	4	5	6	7	8	9	10	11	12	13
7. XII 1965, a.m.	3,06—2,64	0,772	0,105	0,102	0,046	0,043	0,038	0,035	0,034	0,031	0,031	0,028
		0,691	0,115	0,111	0,058	0,054	0,046	0,042	0,041	0,037	0,038	0,034
		0,650	0,115	0,109	0,031	0,055	0,054	0,048	0,049	0,043	0,044	0,038
		0,617	0,120	0,112	0,037	0,059	0,059	0,051	0,052	0,044	0,049	0,041
		0,593	0,118	0,109	0,073	0,034	0,033	0,054	0,059	0,050	0,050	0,041
		0,553	0,139	0,127	0,083	0,071	0,076	0,034	0,037	0,055	0,060	0,048

Note: Commas represent decimal points.

TABLE 7 (cont'd)

1	2	3	4	5	6	7	8	9	10	11	12	13
7. XII 1965, a.m.	3,08—2,64	0,520	0,148	0,132	0,093	0,077	0,082	0,066	0,076	0,060	0,068	0,052
		0,495	0,152	0,131	0,097	0,076	0,089	0,068	0,083	0,062	0,075	0,054
		0,470	0,158	0,132	0,106	0,080	0,094	0,068	0,088	0,062	0,078	0,052
		0,447	0,167	0,132	0,118	0,083	0,102	0,067	0,098	0,063	0,085	0,050
		0,423	0,192	0,146	0,125	0,079	0,117	0,071	0,110	0,064	0,100	0,054
		0,410	0,198	0,146	0,138	0,086	0,126	0,074	0,118	0,066	0,111	0,059
13. XII 1965, a.m.	3,84—3,18	0,772	0,110	0,107	0,048	0,045	0,038	0,035	0,033	0,030	0,030	0,027
		0,691	0,108	0,104	0,056	0,052	0,046	0,042	0,041	0,037	0,037	0,033
		0,650	0,113	0,107	0,062	0,056	0,051	0,045	0,046	0,040	0,041	0,035
		0,617	0,118	0,110	0,067	0,059	0,056	0,048	0,050	0,042	0,045	0,037
		0,593	0,118	0,109	0,071	0,062	0,058	0,049	0,053	0,044	0,047	0,038
		0,553	0,134	0,122	0,082	0,070	0,068	0,056	0,062	0,050	0,057	0,045
		0,520	0,144	0,128	0,089	0,073	0,075	0,059	0,069	0,053	0,064	0,048
		0,495	0,145	0,124	0,084	0,073	0,079	0,058	0,074	0,053	0,065	0,044
		0,470	0,155	0,129	0,099	0,073	0,086	0,060	0,079	0,053	0,071	0,045
		0,447	0,160	0,125	0,110	0,075	0,096	0,061	0,090	0,055	0,085	0,050
		0,423	0,171	0,125	0,120	0,074	0,106	0,060	0,100	0,054	0,095	0,049
		0,410	0,162	0,110	0,128	0,076	0,112	0,060	0,105	0,053	0,098	0,046
17. XII 1965, a.m.	3,99—3,26	0,772	0,197	0,194	0,075	0,072	0,049	0,046	0,038	0,035	0,032	0,029
		0,730	0,203	0,199	0,078	0,074	0,052	0,048	0,041	0,037	0,036	0,032
		0,691	0,207	0,203	0,081	0,078	0,054	0,050	0,044	0,040	0,038	0,034
		0,650	0,218	0,210	0,085	0,077	0,059	0,051	0,046	0,039	0,042	0,034
		0,593	0,219	0,210	0,093	0,087	0,065	0,056	0,054	0,045	0,047	0,038
		0,553	0,247	0,235	0,101	0,089	0,073	0,061	0,062	0,050	0,054	0,042
		0,520	0,260	0,244	0,108	0,092	0,081	0,065	0,069	0,063	0,062	0,046
		0,495	0,252	0,231	0,111	0,090	0,083	0,062	0,073	0,052	0,063	0,042
		0,470	0,252	0,226	0,115	0,089	0,089	0,063	0,077	0,051	0,069	0,043
		0,447	0,253	0,218	0,121	0,086	0,093	0,058	0,084	0,049	0,072	0,037
		0,423	0,271	0,225	0,132	0,086	0,110	0,064	0,092	0,046	0,086	0,040
		0,410	0,281	0,229	0,142	0,090	0,114	0,062	0,100	0,048	0,095	0,043
10. I 1966, a.m.	3,76—2,85	0,772	0,179	0,176	0,086	0,083	0,064	0,061	0,052	0,049	0,045	0,042
		0,691	0,184	0,180	0,099	0,095	0,074	0,070	0,060	0,056	0,052	0,048
		0,650	0,200	0,194	0,108	0,102	0,092	0,076	0,068	0,062	0,059	0,053
		0,617	0,213	0,205	0,116	0,108	0,089	0,081	0,078	0,065	0,064	0,056
		0,593	0,214	0,205	0,124	0,115	0,091	0,082	0,076	0,067	0,062	0,053
		0,553	0,239	0,227	0,136	0,124	0,105	0,093	0,087	0,075	0,073	0,061
		0,520	0,260	0,244	0,147	0,131	0,115	0,099	0,095	0,080	0,079	0,063
		0,495	0,268	0,247	0,154	0,133	0,119	0,098	0,101	0,080	0,088	0,067
		0,470	0,276	0,250	0,166	0,140	0,128	0,102	0,110	0,084	0,098	0,072
		0,447	0,286	0,251	0,176	0,141	0,135	0,100	0,118	0,083	0,102	0,067
		0,423	0,298	0,252	0,180	0,134	0,146	0,100	0,129	0,083	0,115	0,069
		0,410	0,313	0,261	0,196	0,144	0,158	0,106	0,142	0,090	0,125	0,073
13. I 1966, a.m.	4,37—3,70	0,772	0,080	0,077	0,036	0,033	0,030	0,027	0,028	0,025	0,027	0,024
		0,691	0,080	0,076	0,043	0,039	0,037	0,033	0,036	0,032	0,032	0,028
		0,650	0,085	0,079	0,049	0,043	0,043	0,037	0,042	0,036	0,031	0,025
		0,617	0,090	0,082	0,054	0,046	0,047	0,039	0,043	0,035	0,040	0,032
		0,593	0,091	0,082	0,057	0,048	0,049	0,040	0,047	0,038	0,042	0,033
		0,553	0,103	0,091	0,067	0,055	0,060	0,048	0,055	0,043	0,051	0,039
		0,520	0,112	0,096	0,074	0,058	0,066	0,050	0,062	0,046	0,057	0,041
		0,495	0,117	0,096	0,074	0,053	0,068	0,047	0,065	0,044	0,060	0,039
		0,470	0,125	0,099	0,087	0,061	0,078	0,052	0,074	0,048	0,069	0,043
		0,447	0,129	0,094	0,095	0,060	0,085	0,050	0,082	0,047	0,075	0,040
		0,423	0,140	0,094	0,106	0,060	0,099	0,053	0,093	0,047	0,087	0,041
		0,410	0,147	0,095	0,118	0,066	0,108	0,056	0,096	0,044	0,095	0,043

Note: Commas represent decimal points.

TABLE 7 (cont'd)

1	2	3	4	5	6	7	8	9	10	11	12	13
11. II 1966, a.m.	4,25—8,18	0,772	0,560	0,56	0,209	0,206	0,134	0,131	0,094	0,091	0,070	0,067
		0,691	0,600	0,60	0,230	0,226	0,146	0,142	0,103	0,099	0,077	0,073
		0,650	0,630	0,62	0,244	0,238	0,158	0,152	0,108	0,102	0,082	0,076
		0,617	0,660	0,65	0,256	0,248	0,162	0,154	0,113	0,105	0,088	0,080
		0,593	0,660	0,65	0,259	0,249	0,160	0,150	0,116	0,106	0,087	0,077
		0,553	0,730	0,72	0,276	0,263	0,176	0,163	0,128	0,115	0,098	0,085
		0,520	0,740	0,72	0,296	0,278	0,187	0,169	0,134	0,116	0,107	0,089
		0,495	0,700	0,68	0,300	0,277	0,186	0,162	0,136	0,113	0,106	0,083
		0,470	0,720	0,69	0,307	0,279	0,194	0,166	0,142	0,114	0,113	0,085
		0,447	0,720	0,68	0,320	0,283	0,195	0,158	0,150	0,113	0,113	0,076
		0,423	0,660	0,61	0,322	0,278	0,233	0,184	0,162	0,113	0,132	0,083
		0,410	0,740	0,68	0,324	0,269	0,222	0,167	0,174	0,119	0,129	0,074
14. II 1966, a.m.	4,55—8,38	0,772	0,091	0,088	0,047	0,044	0,043	0,040	0,039	0,036	0,036	0,033
		0,691	0,108	0,104	0,060	0,056	0,053	0,049	0,049	0,045	0,046	0,042
		0,650	0,113	0,107	0,066	0,060	0,061	0,055	0,055	0,049	0,052	0,046
		0,617	0,115	0,107	0,071	0,063	0,068	0,060	0,060	0,052	0,057	0,049
		0,593	0,119	0,110	0,076	0,067	0,069	0,064	0,060	0,055	0,059	0,050
		0,553	0,137	0,125	0,088	0,076	0,082	0,070	0,075	0,063	0,066	0,054
		0,520	0,150	0,134	0,098	0,082	0,092	0,076	0 083	0,067	0,078	0,062
		0,495	0,146	0,125	0,100	0,079	0,093	0,072	0,086	0,065	0,078	0,057
		0,470	0,154	0,128	0,106	0,080	0,100	0,074	0,092	0,066	0,084	0,058
		0,447	0,155	0,120	0,112	0,077	0,103	0,068	0,098	0,063	0,088	0,053
		0,423	0,169	0,123	0,128	0,082	0,117	0,071	0,107	0,061	0,100	0,054
		0,410	0,168	0,116	0,138	0,086	0,126	0,074	0,120	0,068	0,107	0,055

TABLE 8. Optical Thickness of Atmospheric Haze (τ_h)

Date	Haze No.	λ, μm											
		0,735	0,691	0,650	0,593	0,553	0,520	0,495	0,470	0,447	0,423	0,410	$\pm\Delta\tau_a$
15. V 1965, a.m.	1	0,03	0,03	0,03	0,04	0,03	0,02	0,04	0,06	0,05	0,05	0,06	0,01
»	2	0,03	0,03	0,03	0,03	0,04	0,04	0,04	0,04	0,04	0,05	0,06	0,01
»	3	0,12	0,12	0,12	0,13	0,15	0,15	0,15	0,14	0,14	0,20	0,28	0,01
7. VI 1965, a.m.	1	0,03	0,04	0,03	0,04	0,04	0,05	0,03	0,10	0,12	0,08	0,02	0,01
»	2	0,03	0,03	0,03	0,04	0,04	0,06	0,05	0,13	0,11	0,10	0,06	0,01
18. VIII 1965, a.m.	1	0,040	0,040	0,040	0,035	0,035	0,030	0,030	0,040	0,040	0,050	0,050	0,005
18. IX 1965, a.m.	1	0,08	0,08	0,08	0,08	0,12	0,10	0,14	0,14	0,14	0,16	0,12	0,01
20. IX 1965, a.m.	1	—	0,07	0,09	0,09	0,07	0,06	0,07	0,12	0,14	0,18	0,15	0,01
»	2	—	0,010	0,015	0,020	0,035	0,030	0,030	0,035	0,055	0,020	0,005	0,005
18. X 1965, a.m.	1	0,015	0,020	0,020	0,025	0,020	0,020	0,020	0,015	0,025	0,025	0,020	0,005
8. X 1965, a.m.	1	0,045	0,040	0,040	0,025	0,020	0,030	0,030	0,040	0,020	0,020	0,020	0,005
9. X 1965, a.m.	1	0,050	0,030	0,030	0,010	0,020	0,015	0,030	0,060	0,030	0,040	0,020	0,005

Note: Commas represent decimal points.

TABLE 8 (cont'd)

Date	Haze No.	λ, μm													
		0,772	0,730	0,691	0,650	0,617	0,593	0,553	0,520	0,508	0,495	0,470	0,447	0,423	0,410	$\pm\Delta\tau_h$
28. XII 1964, a.m.	1	—	0,06	0,06	0,05	—	0,06	0,05	0,05	—	0,04	0,05	0,06	0,09	—	0,01
4. I 1965, a.m.	1	—	0,05	0,05	0,03	—	0,02	0,04	—	0,05	—	0,05	0,04	0,04	—	0,01
•	2	—	0,04	0,03	0,03	—	0,03	0,05	—	0,05	—	0,08	0,08	0,08	—	0,01
•	1	—	0,020	0,020	0,020	—	0,030	0,030	—	0,030	—	0,030	0,030	0,040	—	0,005
7. I 1965, a.m.	2	—	0,020	0,020	0,020	—	0,020	0,020	—	0,030	—	0,030	0,030	0,040	—	0,005
•	3	—	0,030	0,020	0,020	—	0,020	0,020	—	0,040	—	0,040	0,040	0,020	—	0,005
13. XII 1965 a.m.	1	0,025	—	0,030	0,025	0,030	0,040	0,040	0,050	—	0,050	0,055	0,050	0,065	0,070	0,005
17. XII 1965, a.m.	1	0,015	—	0,015	0,005	—	0,000	0,010	0,000	—	0,025	0,025	0,035	0,030	0,020	0,005
17. XII 1965, p.m.	1	0,020	—	0,025	0,020	0,015	0,030	0,035	0,025	—	0,035	0,040	0,040	0,025	0,025	0,005
13. I 1966, a.m.	1	0,035	—	0,040	0,030	0,035	0,035	0,035	0,050	—	0,050	0,030	0,060	0,060	0,060	0,005

TABLE 9. Atmospheric Haze Scattering Functions at $\varphi=2°$ $\mu_h(2°)$

Date	$m_\odot$	λ, μm											
		0,735	0,691	0,650	0,593	0,553	0,520	0,497	0,470	0,447	0,423	0,410	$\pm\Delta\mu_h$
1	2	3	4	5	6	7	8	9	10	11	12	13	14
6. V 1965, a.m.	Leaving 2,05	0,38	0,41	0,39	0,44	0,46	0,41	0,40	0,40	0,37	0,36	0,36	0,05
•	Arriving 1,50	0,25	0,24	0,27	0,28	0,32	0,33	0,31	0,27	0,28	0,27	0,25	0,05
12. V 1965, a.m.	Arriving 1,30	—	0,44	0,47	—	0,63	0,70	0,62	0,81	0,78	0,72	0,66	0,05
•	Arriving 1,44	—	0,21	0,21	—	0,26	0,30	0,35	0,28	0,33	0,51	0,55	0,05
•	Leaving 2,02	—	0,07	0,08	—	0,05	0,06	0,10	0,08	0,12	0,10	0,11	0,05
•	Arriving 1,74	—	0,08	0,10	—	0,08	0,06	0,08	0,08	0,07	0,27	0,56	0,05
15. V 1965, a.m.	Leaving 2,20	0,11	0,12	0,12	0,21	0,23	0,31	0,40	0,46	0,55	0,68	0,71	0,05
•	Arriving 1,70	0,55	0,59	0,64	0,71	0,30	0,93	0,95	0,99	1,12	1,18	0,23	0,05
15. VI 1965 a.m.	Leaving 2,18	0,20	0,21	0,26	0,24	0,27	0,33	0,32	0,33	0,33	0,35	0,37	0,05
•	Arriving 1,41	0,56	0,57	0,60	0,63	0,64	0,73	0,71	0,76	0,83	0,86	0,93	0,05

Note: Commas represent decimal points.

TABLE 9 (cont'd)

1	2	3	4	5	6	7	8	9	10	11	12	13	14
18. VIII 1965, a.m.	Arriving 2,31	0,03	0,03	0,03	0,03	0,04	0,04	0,02	0,03	0,03	0,02	0,00	0,01
17. IX 1965, a.m.	Leaving 2,76	0,06	0,07	0,07	0,07	0,05	0,07	0,08	0,08	0,08	0,09	0,14	0,02
•	Arriving 1,57	0,10	0,07	0,05	0,05	0,08	0,06	0,05	0,02	0,01	0,05	0,04	0,02
•	Arriving 1,45	0,12	0,15	0,17	0,15	0,12	0,17	0,17	0,20	0,21	0,12	0,13	0,02
•	Arriving 1,39	0,09	0,09	0,07	0,10	0,09	0,07	0,10	0,09	0,07	0,19	0,15	0,02

Date	$m_{\odot}$	λ, μm											
		0,772	0,691	0,650	0,617	0,593	0,553	0,520	0,495	0,470	0,447	0,423	0,410	$\pm\Delta\mu_h$
5. I 1965, p.m.	Arriving 2,64	—	0,007	0,004	—	0,004	0,008	0,009	0,010	0,000	0,006	0,000	—	0,001
•	Leaving 2,86	—	0,002	0,004	—	0,004	0,005	0,008	0,004	0,008	0,006	0,004	—	0,001
•	Arriving 5,72	—	0,0022	0,0024	—	0,0028	0,0032	0,0031	0,0050	0,0140	0,0020	0,020	—	0,0008
7. XII 1965, a.m.	Arriving 2,43	0,019	0,020	0,018	0,020	0,028	0,033	0,037	0,034	0,041	0,033	0,044	0,047	0,005
•	Arriving 2,60	0,018	0,015	0,013	0,013	0 018	0,014	0,018	0,018	0,009	0,006	0,020	0,034	0,005
•	Arriving 3,05	0,016	0,017	0,018	0,018	0,013	0,18	0,011	0,022	0,017	0,020	0,033	0,015	0,005
7. XII 1965, p.m.	Leaving 5,79	0,015	0,013	0,013	0,013	0,018	0,017	0,017	0,022	0,032	0,007	0,010	0,032	0,005
10. XII 1965, p.m.	Leaving 3,28	0,070	0,090	0,090	0,090	0,008	0,09	0,080	0,090	0,110	0,110	0,010	0,130	0,010
13. XII 1965, a.m.	Arriving 2,75	0,016	0,017	0,017	0,017	0,017	0,014	0,019	0,014	0,013	0,020	0,011	0,023	0,005
•	Arriving 2,65	0 050	0,046	0,051	0,055	0,049	0,059	0,055	0,053	0,062	0,044	0,052	0,059	0,005
•	Leaving 2,58	0,022	0,018	0,024	0,025	0,019	0,022	0,021	0,023	0,023	0,014	0,027	0,025	0,005
•	Arriving 2,52	0,071	0,087	0,071	0,059	0,071	0,077	0,090	0,085	0,098	0,090	0,107	0,116	0,008

Note: Commas represent decimal points.

TABLE 10. Average Values and Range of Measurements of Transmission Coefficient and Optical Thickness

Period of observations	λ, μm 0,455	0,546	0,636
1949-1961 r.	0,503<0,748<0,813	0,533<0,815<0,883	0,743<0,857<0,923
	(0,687>0,290>0,207)	(0,627>0,204>0,124)	(0,080>0,154>0,297)
Winter during this same period	0,766<0,789<0,813	0,813<0,856<0,879	0,891<0,897<0,904
	(0,266>0,236>0,207)	(0,207>0,155>0,128)	(0.115>0,108>0,101)
Spring	0,503<0,726<0,789	0,533<0,780<0,859	0,820<0,819<0,883
	(0,687>0,320>0,263)	(0,629>0,248>0,151)	(0,198>0,163>0,124)
Summer	0,655<0,728<0,791	0,718<0,799<0,871	0,815<0,844<0,891
	(0,423>0,317>0,234)	(0,331>0,224>0,138)	(0,204>0,159>0,115)
Autumn	0,545<0,754<0,785	0,617<0,821<0,883	0,743<0,864<0,920
	(0,606>0,282>0,242)	(0,482>0,197>0,182)	(0,297>0,146>0,923)
Forenoon	0,721<0,768<0,802	0,778<0,837<0,883	0,805<0,875<0,920
	(0,327>0,263>0,220)	(0,251>0,177>0,124)	(0,216>0,133>0,083)
Afternoon	0,503<0,724<0,813	0,533<0,796<0,876	0,558<0,841<0,917
	(0,697>0,322>0,207)	(0,629>0,228>0,132)	(0,583>0,173>0,086)

TABLE 11. Results of the Determination of the Transmission Coefficient p_b by the Bouguer Method, from the Sky Brightness at the Point $\varphi=2°$ (line $\lg(B/m_\odot)$) p_0 for Different Instability Factors $\varkappa$

λ, μm	6. V 1965, a. m.					12. V 1965, a. m.					15. V 1965, a. m.				
	p_b	p_o	Δp_{avg}	p_{avg}	$\varkappa$%	p_b	p_o	Δp_{avg}	p_{avg}	$\varkappa$%	p_b	p_o	Δp_{avg}	p_{avg}	$\varkappa$%
Autumn-summer observations															
0,735	0,772	0,802	0,015	0,785	1,9	0,813	0,851	0,019	0,832	2,3	0,759	0,741	0,009	0,750	1,2
0,691	0,791	0,804	0,006	0,798	0,8	0,851	0,841	0,005	0,846	0,6	0,759	0,741	0,009	0,758	1,2
0,650	0,791	0,794	0,002	0,792	0,3	0,832	0,822	0,005	0,827	0,6	0,711	0,733	0,006	0,746	0,5
0,593	0,768	0,778	0,005	0,773	0,6	0,817	0,800	0,008	0,808	1,0	0,740	0,726	0,007	0,733	1,0
0,553	0,721	0,741	0,010	0,731	1,4	0,794	0,759	0,018	0,776	2,3	0,708	0,692	0,008	0,700	1,1
0,520	0,709	0,724	0,012	0,712	1,7	0,776	0,780	0,002	0,778	0,3	0,692	0,676	0,008	0,684	1,2
0,495	0,708	0,724	0,008	0,716	1,1	0,741	0,759	0,009	0,750	1,2	0,692	0,676	0,008	0,684	1,2
0,470	0,676	0,687	0,003	0,682	0,9	0,708	0,741	0,016	0,724	2,2	0,661	0,646	0,008	0,653	1,2
0,447	0,661	0,668	0,004	0,664	0,6	0,682	0,716	0,017	0,699	2,5	0,631	0,631	0,000	0,631	0,0
0,429	0,631	0,621	0,005	0,623	0,8	0,661	0,631	0,015	0,646	2,3	0,603	0,631	0,014	0,617	2,3
0,410	0,631	0,609	0,016	0,616	2,6	0,646	0,617	0,014	0,632	2,2	0,592	0,550	0,021	0,571	3,5
	28. XII 1964, a. m.					4. I 1965, a. m.					4. 1965, p. m.				
Winter observations															
0,735	0,906	0,875	0,016	0,890	1,8	0,906	0,897	0,004	0,902	0,4	0,902	0,794	0,050	0,848	5,9
0,691	0,904	0,881	0,014	0,892	1,6	0,891	0,873	0,009	0,882	1,0	0,902	0,794	0,050	0,848	5,9
0,650	0,885	0,849	0,018	0,867	2,1	0,875	0,873	0,001	0,874	0,0	0,885	0,809	0,038	0,847	4,5
0,593	0,832	0,782	0,025	0,807	3,1	0,847	0,828	0,010	0,840	1,2	0,855	0,755	0,050	0,805	6,3
0,553	0,832	0,794	0,019	0,813	2,3	0,778	0,828	0,025	0,000	3,1	0,832	0,745	0,044	0,788	5,6
0,520	0,832	0,805	0,014	0,818	1,7	—	—	—	—	—	—	—	—	—	—
0,508	—	—	—	—	—	0,738	0,817	0,040	0,780	5,1	0,818	0,745	0,036	0,782	4,6
0,495	0,826	0,789	0,018	0,808	2,2	—	—	—	—	—	—	—	—	—	—
0,470	0,776	0,785	0,004	0,780	0,5	0,728	0,783	0,035	0,756	7,3	0,763	0,741	0,021	0,762	2,8
0,447	0,773	0,736	0,018	0,754	2,4	0,708	0,762	0,054	0,735	7,4	0,757	0,708	0,024	0,732	3,3
0,423	0,736	0,692	0,022	0,714	3,1	0,736	0,723	0,006	0,730	0,8	0,736	0,698	0,019	0,717	2,6

Note: Commas represent decimal points.

TABLE 12. Total Optical Density D of Atmosphere and Its Aerosol Component D_D

Date	λ, μm	0,735	0,730	0,691	0,650	0,593	0,553	0,520	0,495	0,470	0,447	0,423	0,410
Autumn-summer observations													
6. V 1965, a. m.	D	0,105	—	0,098	0,101	0,112	0,136	0,148	0,145	0,166	0,178	0,203	0,210
	D_D	0,082	—	0,079	0,073	0,076	0,086	0,083	0,085	0,098	0,095	0,099	0,092
	ΔD_D	0,020	—	0,004	0,004	0,004	0,008	0,008	0,006	0,005	0,004	0,004	0,013
12. V 1965, a. m.	D	0,080	—	0,073	0,082	0,093	0,110	0,110	0,125	0,140	0,156	0,190	0,199
	D_D	0,057	—	0,054	0,054	0,057	0,060	0,055	0,055	0,072	0,073	0,086	0,081
	ΔD_D	0,021	—	0,004	0,001	0,005	0,012	0,004	0,006	0,013	0,013	0,013	0,008
15. V 1965, a. m.	D	0,125	—	0,120	0,127	0,135	0,155	0,165	0,165	0,185	0,200	0,210	0,243
	D_D	0,102	—	0,101	0,099	0,104	0,105	0,110	0,105	0,117	0,117	0,106	0,125
	ΔD_D	0,005	—	0,002	0,006	0,005	0,002	0,010	0,006	0,007	0,012	0,025	0,040
5. VI 1965, a. m.	D	0,031	—	0,070	0,095	0,086	0,100	0,101	0,115	0,132	0,127	0,140	0,128
	D_D	0,038	—	0,051	0,067	0,050	0,050	0,046	0,055	0,064	0,044	0,036	0,010
	ΔD_D	0,004	—	0,002	0,006	0,002	0,002	0,010	0,006	0,007	0,012	0,025	0,040
7. VI 1965 a. m.	D	0,052	—	0,046	0,056	0,059	0,085	0,083	0,092	0,088	0,116	0,130	—
	D_D	0,029	—	0,027	0,028	0,033	0,035	0,028	0,032	0,020	0,033	0,026	—
	ΔD_D	0,015	—	0,010	0,008	0,010	0,012	0,016	0,016	0,016	0,044	0,018	—
18. VIII 1965, a. m.	D	—	0,168	0,155	0,165	0,182	0,191	0,200	0,228	0,231	0,256	0,282	0,301
	D_D	—	0,155	0,138	0,142	0,145	0,148	0,150	0,170	0,163	0,173	0,178	0,183
	ΔD_D	—	0,008	0,008	0,012	0,014	0,004	0,004	0,016	0,016	0,007	0,007	0,004

Date	λ, μm	0,730	0,691	0,650	0,593	0,553	0,520	0,508	0,495	0,470	0,447	0,423
Winter observations												
28. XII 1964 a. m.	D	0,051	0,050	0,032	0,093	0,090	0,087	—	0,093	0,108	0,123	0,146
	D_D	0,038	0,031	0,034	0,048	0,040	0,032	—	0,033	0,040	0,040	0,042
	ΔD_D	0,010	0,006	0,010	0,016	0,012	0,008	—	0,012	0,003	0,012	0,012
4. I 1965 a. m.	D	0,045	0,054	0,058	0,076	0,097	—	0,108	—	0,121	0,134	0,137
	D_D	0,032	0,035	0,030	0,041	0,047	—	0,053	—	0,059	0,051	0,033
	ΔD_D	0,003	0,006	0,002	0,007	0,012	—	0,022	—	0,033	0,029	0,004
4. I 1965 p. m.	D	0,072	0,072	0,072	0,094	0,103	—	0,107	—	0,118	0,136	0,144
	D_D	0,060	0,057	0,054	0,068	0,038	—	0,058	—	0,051	0,053	0,040
	ΔD_D	0,025	0,025	0,020	0,026	0,021	—	0,011	—	0,012	0,012	0,012
5. I 1965 p. m.	D	0,056	0,056	0,069	0,085	0,100	—	0,094	—	0,120	0,128	0,157
	D_D	0,044	0,041	0,051	0,059	0,065	—	0,045	—	0,053	0,045	0,053
	ΔD_D	0,024	0,024	0,025	0,050	0,026	—	0,016	—	0,027	0,023	0,030
6. I 1965 a. m.	D	0,029	0,050	0,052	0,068	0,079	—	0,096	—	0,112	0,119	0,136
	D_D	0,016	0,031	0,024	0,023	0,029	—	0,041	—	0,044	0,036	0,032
	ΔD_D	0,004	0,005	0,006	0,005	0,010	—	0,011	—	0,009	0,005	0,012
7. I 1965 a. m.	D	0,051	0,046	0,071	0,076	0,092	—	0,099	—	0,128	0,134	0,149
	D_D	0,038	0,027	00043	0,041	0,042	—	0,044	—	0,060	0,051	0,045
	ΔD_D	0,012	0,014	0,015	0,010	0,016	—	0,003	—	0,006	0,003	0,002

Note: Commas represent decimal points.

TABLE 13. Comparison of Atmosphere Transmission Coefficient Values, Determined by the Bouguer Method p_b on a Stable Day, and from the Sky Brightness p_o

Date	λ, μm	p_b	p_o	Nature of underlying surface
23.IX 1952	0,546	0,869	0,871	Grass covering
3.VII 1952	0,577	0,875	0,872	"
19.XI 1952	0,636	0,922	0,927	Snow covering
29.XI 1952	0,636	0,912	0,923	"
10.XI 1960	0,564	0,880	0,882	"
7.VI 1962	0,634	0,874	0,887	Grass covering
"	0,542	0,823	0,838	"
"	0,450	0,762	0,777	"
29.VI 1962	0,634	0,894	0,905	"
"	0,542	0,839	0,839	"
"	0,450	0,778	0,785	"
30.VI 1962	0,634	0,908	0,906	"
"	0,542	0,855	0,868	"
8.IX 1962	0,542	0,828	0,824	"
"	0,450	0,752	0,746	"
9.IX 1962	0,634	0,900	0,892	"
"	0,542	0,836	0,840	"
"	0,450	0,771	0,770	"
17.IX 1962	0,634	0,881	0,886	"
"	0,542	0,837	0,837	"
"	0,450	0,780	0,778	"
20.XII 1962	0,542	0,880	0,871	Snow covering
3.XII 1962	0,542	0,890	0,890	"
9.X 1965	0,410	0,708	0,706	"
10.X 1965	0,410	0,735	0,707	"
2.IX 1966	0,405	0,759	0,773	Grass covering
	0,450	0,832	0,844	"
	0,542	0,900	0,894	"
	0,650	0,940	0,951	"
13.IX 1966, a. m.	0,405	0,588	0,600	"
	0,450	0,668	0,685	"
	0,542	0,776	0,780	"
	0,650	0,802	0,820	"
13.IX 1966, p. m.	0,405	0,714	0,724	"
	0,450	0,794	0,794	"
	0,542	0,845	0,853	"
	0,650	0,879	0,904	"
14.IX 1966	0,405	0,689	0,708	"
	0,450	0,759	0,783	"
	0,542	0,841	0,834	"
	0,650	0,867	0,881	"
15.IX 1966	0,405	0,664	0,641	"
	0,450	0,733	0,723	"
	0,542	0,809	0,784	"
	0,650	0,838	0,827	"
29.XI 1965	0,404	0,660	0,665	Snow covering
	0,495	0,794	0,781	"
	0,593	0,851	0,869	"
	0,691	0,873	0,893	"

Note: Commas represent decimal points.

TABLE 14. Total (μ) and Aerosol (μ_D) Scattering Functions for Small $\varphi < 10°$ (h = 2800 m above sea level)

Date	$m_\odot$	λ, μm	$\varphi°$ 2° μ	2° μ_D	4° μ	4° μ_D	6° μ	6° μ_D	8° μ	8° μ_D	10° μ	10° μ_D
2.IX 1966, a. m.	3,68—2,58	0,650	0,226	0,222	0,072	0,068	0,036	0,032	0,021	0,017	0,018	0,014
		0,542	0,249	0,240	0,100	0,091	0,058	0,049	0,046	0,037	0,038	0,029
		0,450	0,275	0,255	0,117	0,097	0,079	0,059	0,065	0,045	0,57	0,037
		0,405	0,293	0,264	0,138	0,109	0,099	0,070	0,084	0,055	0,078	0,049
12.IX1966, a. m.	4,81—2,60	0,650	0,126	0,122	0,078	0,074	0,057	0,053	0,045	0,041	0,037	0,033
		0,542	0,158	0,149	0,100	0,091	0,072	0,063	0,058	0,049	0,048	0,039
		0,450	0,202	0,182	0,123	0,103	0,092	0,072	0,079	0,059	0,067	0,047
		0,405	0,246	0,217	0,154	0,125	0,117	0,088	0,098	0,069	0,087	0,058
13.IX 1966, a. m.	4,28—3,01	0,650	0,350	0,350	0,169	0,165	0,101	0,097	0,068	0,064	0,052	0,048
		0,542	0,410	0,400	0,194	0,185	0,114	0,105	0,080	0,071	0,062	0,053
		0,450	0,490	0,470	0,223	0,203	0,138	0,118	0,101	0,081	0,083	0,063
		0,405	0,520	0,490	0,242	0,213	0,157	0,128	0,122	0,093	0,105	0,076
14.IX 1966, a. m.	4,54—2,84	0,650	0,40	0,40	0,207	0,203	0,124	0,120	0,082	0,078	0,062	0,058
		0,542	0,56	0,55	0,218	0,209	0,145	0,136	0,096	0,087	0,073	0,064
		0,450	0,54	0,52	0,251	0,231	0,157	0,137	0,114	0,094	0,092	0,072
		0,405	0,62	0,58	0,285	0,256	0,185	0,156	0,141	0,112	0,119	0,090
15.IX 1966, a. m.	4,45—2,81	0,650	1,44	1,44	0,60	0,60	0,331	0,327	0,209	0,205	0,151	0,147
		0,542	1,67	1,68	0,69	0,68	0,365	0,356	0,237	0,228	0,172	0,163
		0,450	1,86	1,84	0,70	0,68	0,381	0,361	0,251	0,231	0,189	0,169
		0,405	2,00	1,97	0,74	0,71	0,400	0,371	0,277	0,248	0,215	0,186

TABLE 15. Total Optical Density D of Atmosphere and Its Aerosol Component D_D (h = 2800 m above sea level)

λ, μm	2.IX 1966, a. m. D	2.IX 1966, a. m. D_D	13.IX 1966, a. m. D	13.IX 1966, a. m. D_D	13.IX 1966, p. m. D	13.IX 1966, p. m. D_D	14.IX 1966, a. m. D	14.IX 1966, a. m. D_D	15.IX 1966, a. m. D	15.IX 1966, a. m. D_D
0,650	0,027	0,001	0,056	0,030	0,096	0,070	0,062	0,036	0,077	0,051
0,542	0,046	0,001	0,073	0,028	0,111	0,066	0,075	0,030	0,092	0,048
0,450	0,080	0,008	0,100	0,028	0,175	0,103	0,120	0,048	0,135	0,063
0,405	0,120	0,012	0,146	0,038	0,231	0,123	0,162	0,054	0,178	0,070

Note: Commas represent decimal points.